11

Arrays

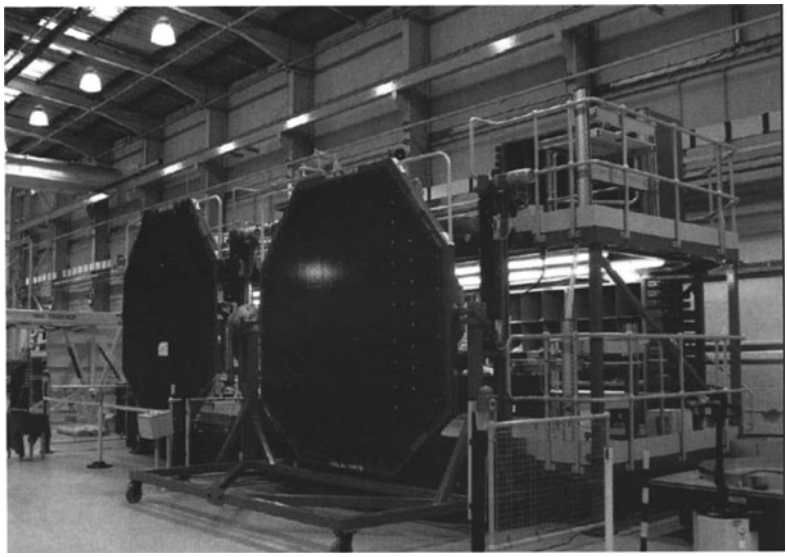

The two array faces of the SAMPSON naval multifunction phased array radar, developed by AMS (photo: AMS).

11.1 INTRODUCTION

Array antennas are used in a large number of applications, such as radioastronomy, space and terrestrial telecommunications - but undoubtedly it is radar that has played the most important role in their development.

A first aspect of interest is electronic scanning. Due to their large inertia, mechanically-steered radar antennas have time constants of the order of a second. This means a waste of valuable time when pointing at multiple successive targets. It is obvious that such an inertia is incompatible with the time constants of the operating electronic circuits which are often of the order of a microsecond or less.

In contrast, a system which can steer the beam without inertia allows the radar to exploit its full possibilities. So the beam of a surveillance radar scanning the horizon can pause to check an occasional detection. Equally, an electronically-scanned

tracking radar can track multiple targets, looking successively at each with no waste of time. Finally, a single radar may simultaneously carry out both surveillance and tracking functions by properly scheduling the various tasks according to the operational scenario.

A second operational aspect is that of 'electromagnetic imaging'. The signal environment of antennas, both in radar and other applications, is generally very complex. This complexity is steadily increasing, so that in general there will be a multiplicity of useful signals coming from various directions with various frequencies and polarizations, as well as natural or deliberate unwanted signals (jammers), multipath, and so on.

The identification, selection and representation of these signals in space and time are the problem of imaging.

Array antennas with appropriate processing allow this to be done. In effect, the elements which make up the array provide spatial samples of the incident field. Thus, it is possible to analyse the field in amplitude, phase and polarization by temporal sampling and spectral analysis, frequently using digital processing techniques. All this relates to the domain of *signal processing antennas* which will be further considered in Chapter 14.

Firstly, let us consider the more classical aspects of array antennas in terms of electronic scanning.

11.1.1 Phased arrays

A process, known for many years, allows electronic scanning to be obtained with phased arrays. This consists of feeding a set of radiating elements regularly disposed on a plane (planar array) by means of phase shifters, in such a way that the phase variations along the array follow an arithmetical progression whose increment is the phase shift between two adjacent elements. Thus, this array generates a plane wave whose direction depends on this phase difference. During the early 1960s, reliable phase shifters were developed which allowed these antennas to be realized in practice.

At the same time, the digital computer became the ideal control and programming tool for these phase shifters. Present-day phase shifters are almost all of the digital type, but the quantized nature of the phase differences imposes certain limitations on the array performances, which will be examined later (§11.5).

11.1.2 Bandwidth - use of delay lines - subarrays

Strictly speaking, delay lines should be used rather than phase shifters. Consider a set of N antenna elements whose phase centres are located at different points $A_0, \ldots A_n, \ldots A_{N-1}$. Consider a wavefront incident from the direction of the unit vector $\mathbf{u}$

(Fig. 11.1). This reaches the element A_n with a time advance τ_n with respect to the element A_0, measured by the distance A_0A_n projected onto **u**

$$\tau_n = \frac{\mathbf{A_0A_n}.\mathbf{u}}{c} \tag{11.1}$$

where c is the velocity of propagation.

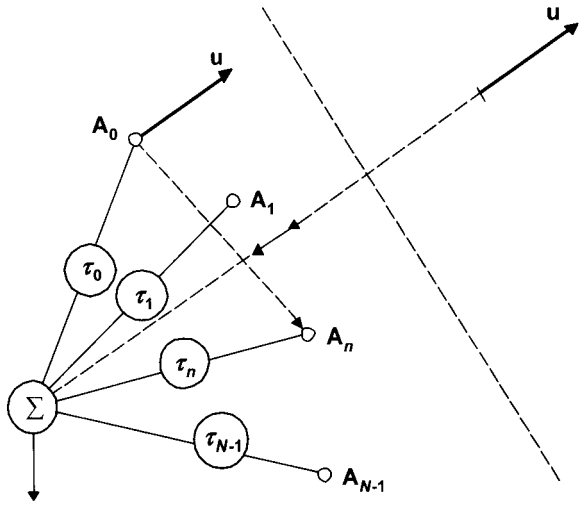

Fig. 11.1 Delay-line array.

If these elements are connected to a common receiver by lines of equal length, and if each line includes a delay which exactly compensates the time advance τ_n, the individual signals add *coherently*. The resulting signal is then a maximum. Correspondingly, on transmit the elements generate a wavefront in the direction **u**.

In which cases can we replace these delay lines by phase shifters? When the frequency bandwidth is sufficiently narrow. The signal delayed by τ_n may be written in complex form

$$\exp\left[j2\pi f\left(t-\tau_n\right)\right]=\exp\left[j\left(2\pi ft-\varphi_n\right)\right] \tag{11.2}$$

with

$$\varphi_n = 2\pi f\tau_n = \frac{2\tau}{\lambda}\mathbf{A_0A_n}.\mathbf{u} \tag{11.3}$$

If the phase remains constant over the frequency range of operation, distortion of the radiated wave may result, and in particular, a pointing error (§11.3.4).

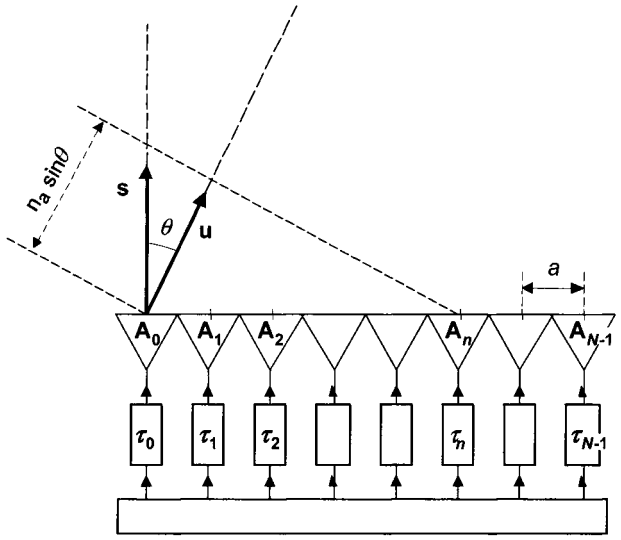

Fig. 11.2 Linear delay-line array.

Comment: In the case of large arrays of large bandwidth, to avoid having to provide each element with a delay line (too expensive), we can divide the array into *phased* subarrays interconnected with delay lines. The pointing error is then avoided, however the sidelobes may be adversely affected (Exercise 11.2).

11.1.3 Active arrays

The phase shifters or delay lines mentioned so far are assumed to be passive. They are thus perfectly linear but some losses inevitably result. Increasingly these components are combined with amplifiers in so-called 'active array modules'. The properties of such modules and arrays are treated in §11.8. We give here only some general characteristics.

Active arrays in transmission

When a phased array is fed by a single transmitter, the connections between transmitter and radiating elements result in significant losses. The feeder lines, the rotating joint (if used) and the phase shifters alone often dissipate more than half of the power of the transmitter.

The development of solid state transmitters now allows us to shift the 'transmission' function into modules which feed the radiating elements directly with

no transmission loss. Another advantage is that these modules generally use transistors, which do not require high voltages and stable regulated power supplies, such as would be the case with tube transmitters.

Also, in the case of failure of some modules, the system can continue to operate with slightly reduced performance; the operating reliability is thus improved. This property is sometimes known as *graceful degradation.*

Finally, the phase shifters associated with each radiating element may operate at *low power level* if they are placed at the *input* of the amplifier. The low power phase shifters are often more accurate, faster and more reliable than the high power phase shifters used with conventional techniques.

All these advantages explain the increasing development of active arrays in transmission.

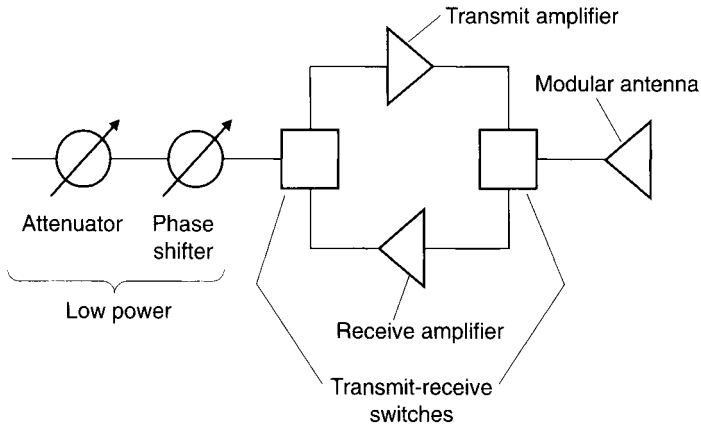

Fig. 11.3 Example of an active array module.

Active arrays on receive

In a 'passive' phased array on receive, the transmission losses that we have mentioned are still present, reducing the signal-to-noise ratio of the received signals. Nevertheless, with certain radar equipment the operational range is limited by the external noise or clutter, and so the external signal-to-noise ratio is not affected by this attenuation.

However, the main benefit of active modules on receive lies in the possibility to control the amplitude and phase weighting (and eventually, the polarization) of the signals received by each element of the array. In fact, passive phased arrays only

allow us to control the phase of such signals. Use of variable attenuation would increase losses in an undesirable way. On the other hand, with active modules, it is possible to control the amplitude without affecting the internal signal-to-noise ratio, provided that the attenuator is placed after the amplification stage.

This amplitude control allows us to modify arbitrarily the form of the receiving pattern, in particular the sidelobe level and position of nulls. This possibility is exploited in adaptive antennas where the weights are adaptively controlled. This is the domain of *signal processing antennas* (§14.5).

Transmitting-receiving active arrays

Of course, the transmitting and receiving functions may be combined in the same module, but then it becomes relatively complex. The development of active arrays is limited by the cost of the antenna which may involve several thousands of modules. The significant advance in the development of monolithic microwave integrated circuits (MMICs) using gallium arsenide (GaAs) has allowed the realization of operational equipment using active arrays.

11.2 GENERAL STRUCTURE OF A PHASED ARRAY (EXAMPLES)

11.2.1 General structure

A 'passive' phased array may take on very different forms, but always includes all of the parts described below (Fig. 11.4). Considering the antenna on transmit, we find successively:

- a feed network or power splitter distributing energy to the different elements of the array by means of phase shifters according to a desired amplitude function. This amplitude function does not vary with the scan angle (except for adaptive arrays and spatial filtering (§14.7));
- the set of phase shifters;
- a computer which calculates the phases for the required pointing direction and a driver that controls the phase shifters (providing control voltages/currents to diode or ferrite phase shifters);
- the set of array elements;
- in some cases, a complementary focusing system (reflector or lens).

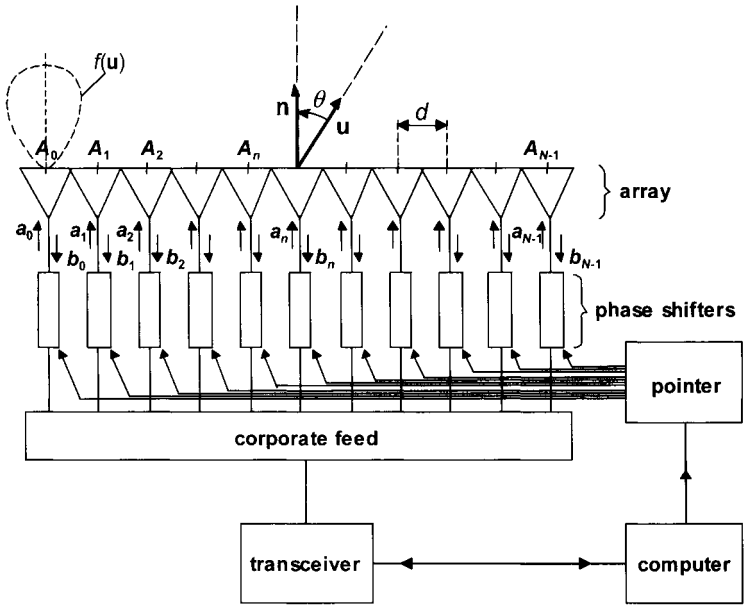

Fig. 11.4 General structure of a phased array.

Feed network - comment

We shall see that due to mutual coupling, the elements have a reflection coefficient which varies with the beam pointing angle ('active' reflection coefficient (§11.4.3)). Therefore, they reflect back a set of signals to the splitter outputs. If these elements are not *individually impedance-matched and isolated*, these signals are reflected once more toward the elements with uncontrolled phases and amplitudes that result in a parasitic radiation pattern which is superimposed on the required pattern. This condition, as we shall see later, plays an important role in the design of feed networks where it is often necessary to use directional couplers and matched loads.

Phase shifter structures

There are several different types of phase shifter that may be used.

Switched line phase shifter: This consists of a number of sections employing two-way switching between different line lengths to achieve a digitally controllable phase shift, as shown in Fig. 11.5.

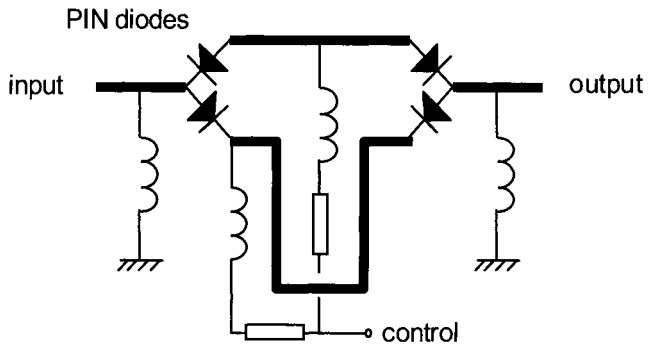

Fig. 11.5 Switched-line phase shifter.

The switching elements are usually PIN diodes, although FETs may also be used. PIN diodes behave as resistors to RF signals, where the resistance is controlled by the dc current. Typically, a forward-biased diode would have a resistance of a few ohms and a reverse-biased diode would have a resistance of 10 - 100 kΩ. The dc bias may be applied through an inductor - with a high reactance compared to 50 Ω at the operating frequency - to avoid any effect on the ac performance.

This type of phase shifter is widely used because it allows digital control of the phase shift and is easy to incorporate in a microprocessor-controlled system. However, it can tend to be lossy - the insertion loss of each phase shifting section being around 0.5 dB - and relatively expensive, because of the number of PIN diodes that are required.

Phase shifter resolution is dependent on the number of sections, or bits, n, according to $\Delta\phi = 2\pi/2^n$. The accuracy of a phase shifter using line lengths is limited by the signal bandwidth, Δf, since the phase shift is only precise at one frequency. In the worst case, when a phase shift of 2π is introduced, its accuracy is $\Delta\phi_e = 2\pi\Delta f / f_c$. An expression for the usable bandwidth of an n-bit phase shifter can be obtained by equating $\Delta\phi_e$ to the resolution $\Delta\phi$, giving a usable fractional bandwidth of

$$\frac{\Delta f}{f_c} = \frac{1}{2^n} \tag{11.4}$$

It is clear that this type of phase shifter is only suitable for relatively narrow-band applications. (Note: although setting the *delays* appropriately would give very broadband performance, the phase shifter sets the phase shifts modulo-2π, thus limiting the bandwidth as discussed above). A more broadband phase shifter could be produced by using all-pass filter networks in place of the line lengths. These filters are designed to produce broadband phase shifts with little attenuation.

Phase shifter performance is specified in terms of:

- accuracy (number of bits, accuracy of each phase increment);
- frequency stability (this type of phase shifter is relatively insensitive to changes in temperature);
- insertion loss;
- impedance match, reproducibility, cost.

Usually, phase shifters have 2 to 5 bits. Their accuracy is of the order of half a bit and their insertion losses range typically from 1 to 2 dB.

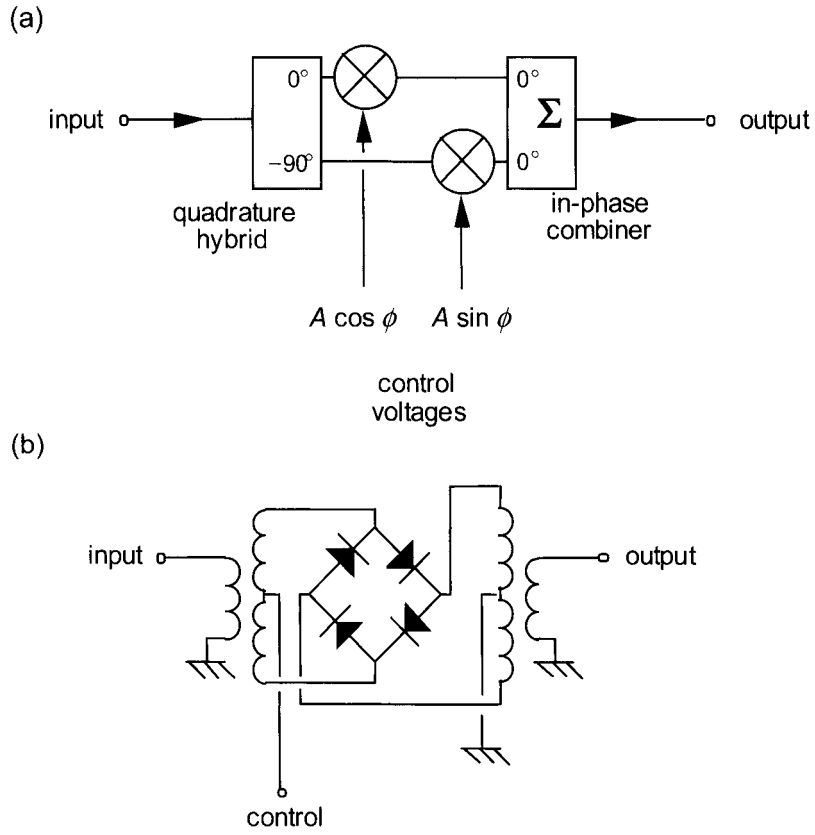

Fig. 11.6 (a) Vector modulator phase shifter; (b) Quad PIN diode attenuator.

Vector modulator: The vector modulator (Fig. 11.6a) is able to control both the phase and amplitude of a signal. It uses the weighted combination of an in-phase (I) and quadrature (Q) phase shifted signal to introduce a phase shift variable over a $\pm\pi$ range. To enable the device to work in all four quadrants the attenuator elements must be bipolar, that is they pass the signal either uninverted or inverted depending on the polarity of the control voltage. Quad PIN diode attenuators are available commercially for this purpose (Fig. 11.6b), though their attenuation-vs-current characteristic is non-linear, and in some applications may need to be linearized by (for example) a digital lookup table and digital-to-analogue converter.

Denoting the input signal by $V_{\text{in}}\cos\omega t$, the signals emerging from the 0° and −90° ports of the quadrature hybrid are $\left(V_{in}/\sqrt{2}\right)\cos\omega t$ and $\left(V_{in}/\sqrt{2}\right)\sin\omega t$, respectively. These signals are then weighted by factors of $A\cos\phi$ and $A\sin\phi$ respectively and are combined in a reactive combiner. The output signal is therefore

$$V_{\text{out}} = \frac{V_{\text{in}}}{\sqrt{2}}\left[\frac{\cos\omega t}{\sqrt{2}}A\cos\phi + \frac{\sin\omega t}{\sqrt{2}}A\sin\phi\right] = \frac{AV_{\text{in}}}{2}\cos(\omega t - \phi) \qquad (11.5)$$

If A is held constant so that the weighting factors are $\cos\phi$ and $\sin\phi$, the vector modulator acts as a constant-amplitude phase shifter. The theoretical insertion loss is 6 dB and in practice it is likely to be slightly higher (nearer 8 or 9 dB) because of the finite minimum attenuation of the attenuators. This may be quite a severe disadvantage in many phased array applications, often restricting the use of vector modulators to IF stages rather than at the antenna elements themselves. The bandwidth, however, is usually quite good, being limited to typically an octave by the quadrature hybrid. The ability of the vector modulator to control the signal amplitude as well as phase makes them particularly useful in adaptive arrays, as discussed in §14.7.

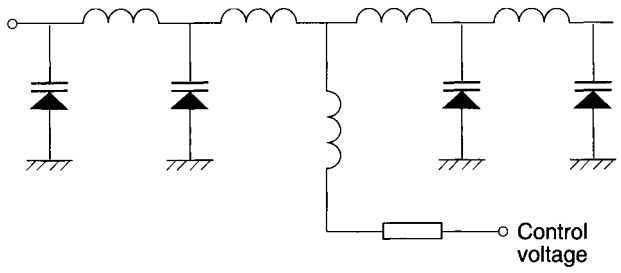

Fig. 11.7 Varactor phase shifter.

Varactor-controlled phase shifter: Fig. 11.7 shows another phase shifter configuration, consisting of a filter containing varactors in place of the usual capacitor elements. The filter is of the 'all-pass' type, producing a broadband phase shift with little attenuation, the phase shift being varied by changing the bias on the varactors. This type of phase shifter is capable of a reasonably low insertion loss, but is highly non-linear because of the response of the varactors and also because of the non-linear relationship between their capacitance and the insertion phase shift.

11.2.2 Examples of array structures

Corporate feed

This is composed of a set of successive power dividers. These are either directional couplers or magic tees whose unused outputs on transmit are terminated by matched loads. This precaution is necessary to satisfy the matching and isolation conditions defined in the preceding section (Fig. 11.8).

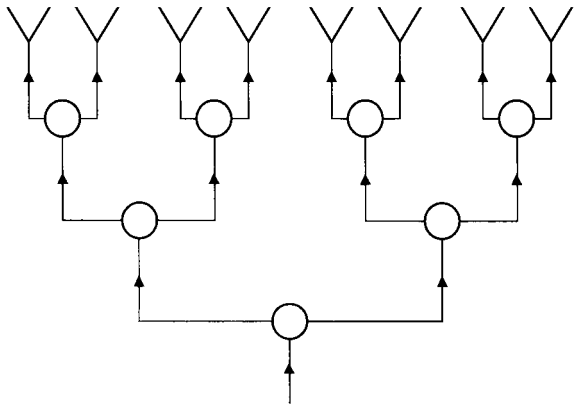

Fig. 11.8 Corporate feed.

Advantages:

- planar symmetric aperiodic structure.

Disadvantages:

- structural complexity;

- losses (this disadvantage does not occur with an active array (§11.8));
- difficulty in obtaining the optimum amplitude weighting function, particularly if the sum and the difference channels are desired simultaneously (see monopulse antennas §10.3.4).

Small planar arrays can easily be realized using printed circuit lines, incorporating the phase shifters, or in some cases using the radiation elements themselves (printed dipoles).

This is a good technique for realizing subarrays combined with intermediate active modules and/or delay lines.

Feed network with waveguides and directional couplers (Fig. 11.9)

The energy distribution is obtained from a central guide whose energy is tapped by means of scaled directional couplers. It is an example of a Blass Matrix (§11.7.4, Fig. 11.24).

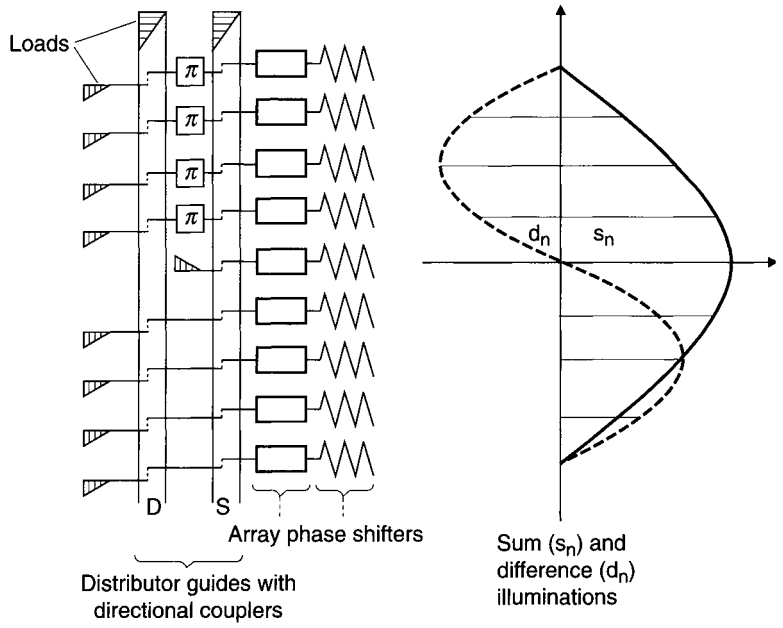

Fig. 11.9 Phased array feed with waveguides and directional couplers.

Advantages:

- Although the preceding corporate feed network distributes the signal in a widening surface, the present feed network has a quasi-linear structure and due to that it can be rather small (this is particularly attractive for high frequencies). In addition, the use of directional couplers ensures the absorption of reflected waves by the couplers (§11.2.2).

Disadvantages:

- frequency sensitivity of the phase function (this may sometimes be applied deliberately) (§11.6);
- many different coupling coefficients for the directional couplers;
- asymmetrical structure, which is generally not suitable for tracking antennas.

If a difference channel is desired, the structure is complicated since it requires its a separate feed guide and a second set of directional couplers giving the desired antisymmetric distribution. The orthogonality of the sum and difference distributions leads to isolation between the two guides, however interactions may occur, and the adjustment should be made with great care (see §11.7.4: Blass matrices).

Feed network using a lens between two parallel planes

A primary element radiates between two parallel planes (with occasionally a sum and a difference channel). An array of elements correctly arranged between two planes (preferably on the arc of a circle) collects the primary energy with amplitude distribution functions controlled by the primary patterns. The collected waves pass through the phase shifters before being radiated (see §11.7.5: Rotman lens, Fig. 11.26).

Advantages:

- relatively simple structure;
- easy adjustment by altering the directivity or the position of the primary element, which is not difficult to adjust;
- symmetrical structure with a large bandwidth.

Disadvantages:

- bulky.

'Disk' feed network

Consider two parallel planes limited by a circle of diameter D and centre O. A central primary element is able to transmit a radial wave propagating between these two planes (Fig. 11.10).

The energy available is collected by means of couplers (preferably directional couplers) placed on concentric circles. It is then phase shifted to compensate for the phase shift produced during the propagation of the radial wave (the phase shift is proportional to the radius), and, on the other hand, to define the correct phase gradient to produce the desired orientation of the beam.

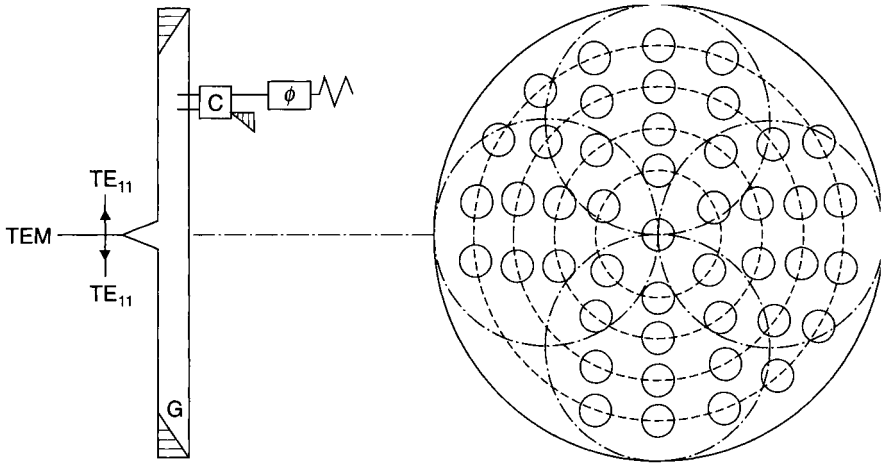

Fig. 11.10 Disk feed network for a planar array.

It is possible, by means of a multimode element, to generate illuminations corresponding to the sum and difference patterns of a monopulse antenna. A circular guide propagating the radial TM_{01} mode will give a TEM wave with an electric field perpendicular to the walls, suitable for an illumination of the 'sum' type. The same guide propagating the TE_{11} mode at vertical or horizontal polarization will generate antisymmetric illuminations in these same planes, and will produce patterns of the 'elevation difference' and 'azimuth difference' types.

Advantages:

- planar structure, longitudinally compact;
- its symmetry makes it suitable for tracking antennas.

Disadvantages:

- the array is fed by a travelling wave, so its phase is a function of frequency. The controlling computer should take into account the frequency to determine the correct phase.

Electronic phased lens

The lens is composed of two arrays (internal and external). The primary element radiates in free space and defines the illumination functions of the lens whose phase shifters are located between the input and output arrays. A spherical input face allows the Abbe condition to be satisfied (§9.7.2), and to use several primary elements simultaneously, permitting electronic scanning of several beams at the same time (§11.7.5: Rotman lens).

Advantages:

- simple feed;
- easy adjustment of the feed by altering only the primary elements;
- symmetrical structure.

Disadvantages:

- difficult access to phase shifters for assembly, maintenance and replacement;
- two arrays are necessary.

Phased reflector array

A 2-D array is illuminated by a primary element which may be non axially-symmetric. The collected waves pass through short-circuited phase shifters that reflect them toward the array with phase shifts $2\phi_k$, where ϕ_k is the differential phase shift corresponding to the transmission of the phase shifter number k. The phases ϕ_k transform the spherical wave from the primary element into a plane wave in the desired direction.

Advantages:

- simple feed, a single array;
- easy adjustment by means of the primary element;
- easy access to the phase shifters.

Disadvantages:

- The matching condition of the feed network of §11.2.1 is difficult to realize.

The interelement coupling between produces an 'active' reflection coefficient (§11.4.3) that reflects part of the primary wave without the correct phase shift. This energy produces a parasitic pattern called the 'primary pattern image' which degrades the angular accuracy and increases the sidelobes. All the advantages of this structure can only be obtained if the matching of the array to the incident and emergent spherical primary waves is carefully thought out. Note that the relative importance of these phenomena decreases as the array becomes larger.

11.3 LINEAR ARRAY THEORY[1]

11.3.1 Basic equation - array factor

The properties of linear arrays can simply be expressed and can easily be extrapolated to the cases of planar arrays (particularly when structures and illuminations are 'separable').

Consider a set of N identical elements whose phase centres A_0, A_1, ... A_{N-1} are aligned along an axis (Fig. 11.4). The spacing between two adjacent phase centres or 'interelement spacing' of the array, plays an important role with respect to the properties of the array. The elements are assumed to be fed by a matched feed network according to an illumination function defined in amplitude and phase by a set of complex numbers

$$a_0, a_1, \ldots\ldots a_n \ldots\ldots a_{N-1}$$

Suppose that each element, the others being present and connected to matched loads, possesses the same pattern $\mathbf{f(u)}$. Due to the principle of linear superposition and the

[1] Hansen, R.C. (ed), *Microwave Scanning Antennas*, Vol. II, Academic Press, New York, 1964, (reprinted by Peninsula Publishing, Los Altos, USA, 1985).

translation theorem (§3.1.2), the pattern of the overall array is obtained by summing the element patterns, taking into account their excitation amplitude and their position with respect to a chosen reference point, for instance the point A_0,

$$\mathbf{F}(\mathbf{u}) = \sum_{n=0}^{N-1} a_n \mathbf{f}(\mathbf{u}) \exp\left(j\frac{2\pi}{\lambda} \mathbf{A}_0\mathbf{A}_n.\mathbf{u} \right) \tag{11.6}$$

$$\mathbf{F}(\mathbf{u}) = \mathbf{f}(\mathbf{u}) R(\mathbf{u}) \tag{11.7}$$

where $R(\mathbf{u})$ is the array factor, which depends only on the spacing and on the illumination function. If θ is the angle between the direction $\mathbf{u}$ and the normal to the array $\mathbf{n}$, we can write

$$\mathbf{A}_0\mathbf{A}_n.\mathbf{u} = nd\sin\theta \tag{11.8}$$

Setting

$$\tau = \sin\theta, \qquad \frac{d}{\lambda} = \Delta v$$

we find

$$R(\mathbf{u}) = \sum_{0}^{N-1} a_n \exp(j2\pi n \Delta v \tau) \tag{11.9}$$

11.3.2 Uniform illumination and constant phase gradient

In this case we can write

$$a_n = \exp(-jn\varphi) \tag{11.10}$$

The array factor then takes the form

$$R(\mathbf{u}) = \sum_{0}^{N-1} \exp\left[jn(2\pi\tau\Delta v - \varphi) \right] \tag{11.11}$$

Setting

$$x = \exp\left[j(2\pi\tau\Delta v - \varphi) \right]$$

we have

$$R(\mathbf{u}) = \sum_{0}^{N-1} x^n = \frac{x^N - 1}{x - 1} = x^{(N-1)/2} \frac{\left(x^{N/2} - x^{-N/2} \right)}{\left(x^{1/2} - x^{-1/2} \right)}$$

Taking out the constant amplitude factor

$$Nx^{(N-1)/2}$$

we have

$$R(\mathbf{u}) = \frac{\sin\left[N\left(\pi\Delta\nu\tau - \frac{\varphi}{2}\right)\right]}{N\sin\left(\pi\Delta\nu\tau - \frac{\varphi}{2}\right)} \tag{11.12}$$

This is a periodic function, and is plotted in Figs. 11.11 and 11.12. It is defined for any value of τ, even for $|\tau| > 1$, which can be interpreted as imaginary, or 'invisible' space (§13.2.2). It passes through a maximum ±1 each time the denominator and numerator are simultaneously equal to zero, that is to say

$$\pi\Delta\nu\tau - \frac{\varphi}{2} = k\pi \quad (k = \text{integer}) \tag{11.13}$$

A maximum is obtained for the direction τ_0 such that

$$\pi\Delta\nu\tau_0 - \frac{\varphi}{2} = 0 \tag{11.14}$$

Thus, a pointing direction τ_0 is obtained with the phase gradient

$$\varphi = 2\pi\Delta\nu\tau_0 = 2\pi\frac{d}{\lambda}\sin\theta_0 \tag{11.15}$$

According to equation (11.13) two consecutive maxima are separated by an interval $\Delta\tau$ such that

$$\Delta\nu\Delta\tau = 1 \tag{11.16}$$

or

$$\Delta\tau = \frac{\lambda}{d} \tag{11.17}$$

These results show an important property of uniformly-spaced arrays, namely the existence of several 'grating lobes' periodically located at intervals inversely proportional to the element spacing. These lobes are in general undesirable because they are sources of losses and directional ambiguity (sometimes they are called ambiguity lobes by analogy with temporal signals). To avoid them, or to separate them sufficiently, we should use a small interelement spacing, for example, for $d = \lambda/2$, $\Delta\tau = 2$, and the grating lobes lie outside the domain $(-1, +1)$ of the real directions. The polarity of the grating lobes depends on the parity of N.

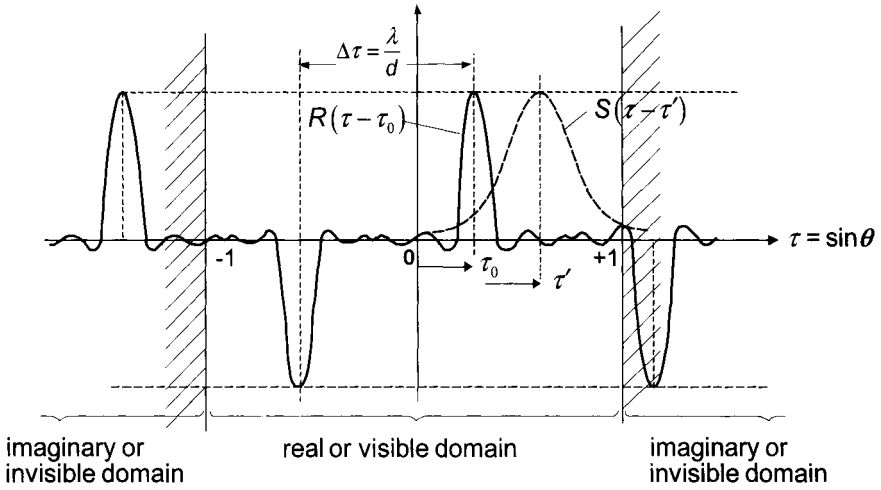

Fig. 11.11 Array factor, even illumination.

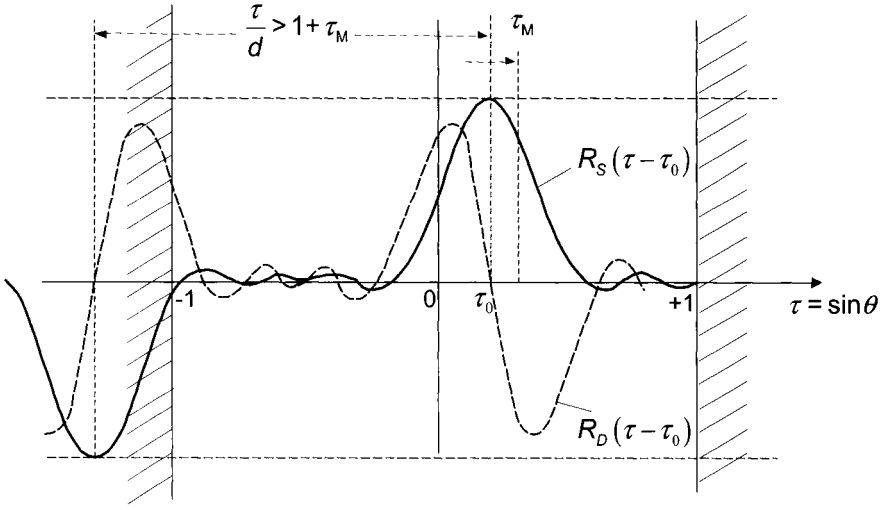

Fig. 11.12 Array factor, odd illumination.

In terms of the pointing direction τ_0 (equation (11.14)), the array factor can be written

$$R_{\tau_0}(\tau) = R(\tau - \tau_0) = \frac{\sin\left[\pi N \Delta\nu(\tau - \tau_0)\right]}{N \sin\left[\pi \Delta\nu(\tau - \tau_0)\right]} \tag{11.18}$$

The phase difference produces a shift of the array factor in τ space. This result corresponds to that known in the time domain, according to which a linear phase slope as a function of frequency does not modify the signal shape, but produces an temporal advance or delay.

Comment: Dispersivity in terms of frequency of an array antenna. Equation (11.15) shows that if the phase gradient φ remains constant as the frequency (and therefore the wavelength) varies, this results in a variation of the pointing direction. A frequency deviation *df* produces an angular error which can be obtained by differentiating equation (11.15).

$$d\varphi = 0$$

then

$$d\theta = -\tan\theta \frac{df}{f} \tag{11.19}$$

11.3.3 Half-power beamwidth

If we take the angle θ as variable instead of $\sin\tau$, the array factor undergoes a distortion as a function of the pointing angle θ_0. In particular, the half-power beamwidth (3 dB width) of the main lobe is increased. This is defined by the condition

$$R = \frac{\sin\left[\pi N \Delta\nu(\sin\theta - \sin\theta_0)\right]}{N \sin\left[\pi \Delta\nu(\sin\theta - \sin\theta_0)\right]} = \frac{1}{\sqrt{2}} \tag{11.20}$$

where

$$\theta = \theta_0 + \frac{\theta_{3\text{dB}}}{2}$$

This is approximately obtained for

$$\pi N \Delta\nu \left[\sin\left(\theta_0 + \frac{\theta_{3\text{ dB}}}{2} \right) - \sin\theta_0 \right] = \frac{\pi}{2} \tag{11.21}$$

from which we obtain

$$\theta_{3\,\mathrm{dB}} \approx \frac{1}{\pi \Delta \nu \cos\theta_0} = \frac{\lambda}{Nd\cos\theta_0} = \frac{\lambda/L}{\cos\theta_0} \tag{11.22}$$

where $L = Nd$ is the total length of the array.

Therefore we have, in the scanning plane, a broadening of the beam by a factor $\cos\theta_0$. Note that for θ close to $\pi/2$ (*endfire arrays*), another approximation may be made, which gives

$$\theta_{3\,\mathrm{dB}} \approx 2\sqrt{\frac{\lambda}{L}} \tag{11.23}$$

11.3.4 Spectral bandwidth available on a phased array

According to a general rule, the available frequency bandwidth is limited to the frequency shift which scans the pointing direction within the 3 dB beamwidth. Comparing equations 11.19 and 11.22 gives

$$\frac{df}{f} = \frac{1}{\sin\theta_0}\frac{\lambda}{L}$$

or

$$df = \frac{1}{\sin\theta_0}\frac{c}{L}$$

where c is the velocity of propagation. This result shows that the available bandwidth does not depend on the centre frequency, but does depend on the array length L. As a general rule, this bandwidth can be considered as the *inverse* of the time required by the radiation to traverse the aperture of the array.

As mentioned in §11.1.2, this frequency sensitivity can be avoided by dividing the array into *phased* subarrays interconnected with delay lines, but at the cost of grating sidelobes. This topic is the subject of exercise 11.2.

11.3.5 Condition to prevent grating lobes from occurring in the scanning region

Consider an array aimed at scanning over a range of angles $\pm\tau_{\mathrm{M}}$ ($\tau_{\mathrm{M}} = \sin\theta_{\mathrm{M}}$). The lack of grating lobe implies that at the scanning end ($\tau = \tau_{\mathrm{M}}$), the closest grating lobe is still in the 'imaginary' domain, in a direction $\tau < -1$, and that the spacing between the lobes $\Delta\tau = 1/\Delta\nu$ is such that

$$\frac{1}{\Delta\nu} > 1 + \tau_{\mathrm{M}} \tag{11.24}$$

from which the element spacing condition is obtained

$$\frac{d}{\lambda} < \frac{1}{1+\sin\theta_M} \tag{11.25}$$

Example:

$$\theta_M = 30°; \qquad \sin\theta_M = \frac{1}{2}; \qquad \frac{d}{\lambda} < \frac{2}{3}$$

This factor is important in array design. The reduction of the element spacing leads to various drawbacks: increased mutual coupling, increase of the total number of elements (and of phase shifters) for a given aperture (dimension which determines the gain), thus increasing the cost. Therefore, a tradeoff has to be found to best meet the requirements.

11.3.6 Effect of weighting the array illumination function

The illuminations considered so far have been of constant amplitude. The corresponding patterns possess quite high close-in sidelobes, of the order of –13 dB. To reduce them, we introduce an amplitude taper by decreasing the relative level of excitation of the elements at the edges. This reduces to a multiplication of the preceding illuminations by a continuous function; let this be $s(\nu)$, whose Fourier transform is $S(\tau)$. According to the convolution theorem, the pattern obtained is the convolution of the preceding pattern with the pattern $S(\tau)$ (Figs. 11.11, 11.12).

This means that each lobe of the array resembles to a certain extent the pattern $S(\theta)$ with close sidelobes more or less improved. The pattern is defined by the function

$$R_S(\tau-\tau_0) = \int_{-\infty}^{\infty} R(\tau'-\tau_0)S(\tau'-\tau)d\tau' \tag{11.26}$$

Application: difference pattern

For tracking antennas, the Δ pattern, which has a null in the pointing direction and two main lobes of opposite phase on either side, is frequently used. Such a pattern is obtained with an antisymmetric weighing function of the array illumination, so that $d(\nu) = d(-\nu)$. Its Fourier transform $D(\tau)$ is also antisymmetric. The convolution of the latter with the pattern $R(\tau-\tau_0)$ leads to a periodic pattern $R_D(\tau-\tau_0)$ composed of a set of anti-symmetric lobe pairs resembling the pattern $D(\tau)$ (Figs. 11.11, 11.12). The particular form of the pattern, its slope in the vicinity of the nulls, and its close-in sidelobes, are determined by the form of the weighing function $d(\nu)$.

11.3.7 Effect of element directivity

Since the pattern of an array F is the product of the pattern $f(\mathbf{u})$ of an element in the presence of the others with the array factor $R(\mathbf{u})$, we see that a first effect of the element directivity is to weight the occasional 'grating lobe' level (Fig. 11.13). We have here

$$F(\tau) = f(\tau)R(\tau - \tau_0)$$

Another important effect is to control the gain variations of the main lobe during scanning. It is desired that $f(\mathbf{u})$ should vary by only a small amount in the useful scanning region, and that it should be minimum outside this region to minimize the grating lobes. If the element spacing is large, such lobes may exist. In other respects, it is possible to influence the element pattern by the choice of element, and by introducing, if necessary, mutual coupling with the neighbouring elements. If the element spacing is small, the choice of the element does not have a large influence on the element pattern, which is almost entirely controlled by the usual couplings between the elements.

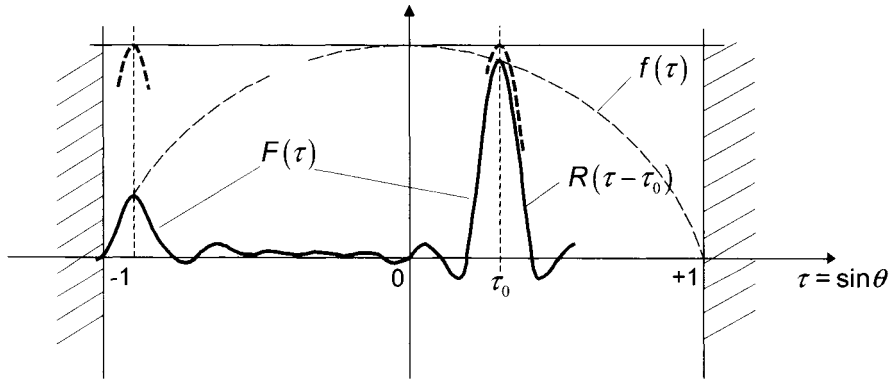

Fig. 11.13 Effect of the directivity of the element pattern.

11.4 VARIATION OF GAIN AS A FUNCTION OF POINTING DIRECTION[2, 3, 4]

11.4.1 Array operating on transmission

Consider a large planar array, of area S, fed by a matched feed network (§2.1.1) according to an illumination of uniform amplitude and a linear phase function which produces a beam pointing in the direction **u** (Fig. 11.14).
The element spacing of the array is assumed sufficiently small that only a single lobe is present in the angular range under consideration. Under these conditions it has been shown (§11.3.3; equation (11.22)) that the useful lobe width increases as $1/\cos\theta_0$. This means that the array directivity decreases as $\cos\theta_0$. This result can be confirmed by imagining the field transmitted by the array in the near field region. Due to the stationary phase conditions, the beam radiates a portion of plane wave tilted by an angle θ_0, of extent S', which is the projection of the array area S onto the pointing direction θ_0

$$S' = S\cos\theta_0 \tag{11.27}$$

The array directivity (or gain, when no loss is present) is of the form

$$D(\theta_0) = D_0\cos\theta_0 \tag{11.28}$$

where

$$D_0 = \frac{4\pi S}{\lambda^2} \tag{11.29}$$

is the array directivity when $\theta_0 = 0$. The concept of directivity is related to the 'shape' of the radiated pattern, particularly its 3 dB beamwidth. To evaluate the gain we should take into account the mismatch losses due to mutual coupling. If the array is assumed very large and the illumination uniform, the geometrical and electrical environment of an element does not depend on the particular element, to within the excitation phase gradient. Thus, in each of them we observe a reflected wave,

---

[2] Parad, L.I., 'Some mutual coupling effects in phased arrays', *Microwave Journal*, Vol. 5, No. 2, pp87-89, June 1962.

[3] Hannan, P.W., 'The element gain paradox for a phased array antenna', *IEEE Trans. Antennas & Propagation*, Vol. AP-12, pp423-433, July 1964.

[4] Allen, J.L., 'Gain and impedance variations in scanned dipole arrays', *IRE Trans. Antennas & Propagation*, Vol. AP-10, pp566-572, Sept 1962.

measured by an active reflection coefficient $\rho(\mathbf{u})$ which varies with the imposed phase gradient, but which is identical for all elements. Thus, the maximum array gain for the pointing angle θ_0 is deduced from the directivity (equation (11.28)) by multiplication by the transfer coefficient: $1-|\rho(\mathbf{u})|^2$. This gives

$$G(\mathbf{u}) = D_0 \cos\theta_0 \left[1-|\rho(\mathbf{u})|^2\right] \tag{11.30}$$

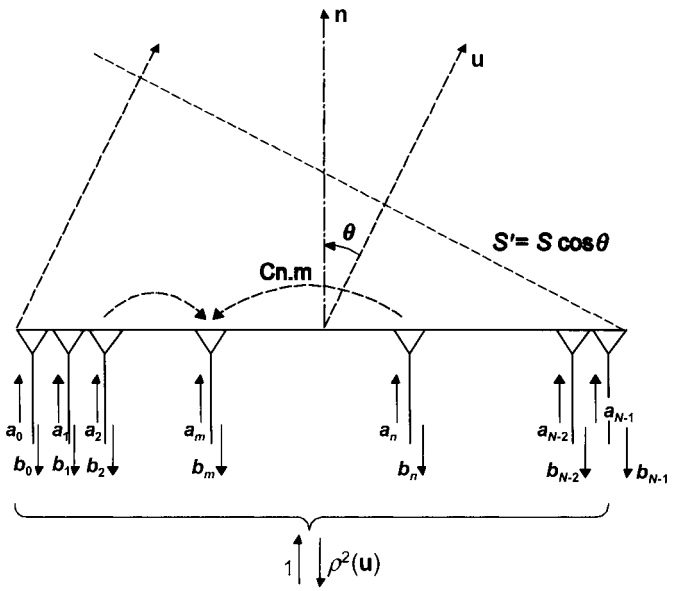

Fig. 11.14 Gain variations vs. pointing directions **u**, in the presence of mutual coupling.

If now we consider the gain $g(\mathbf{u})$ of an element, in the presence of the other elements assumed to be terminated with matched loads, we can write, according to the principle of superposition

$$G(\mathbf{u}) = Ng(\mathbf{u}) \tag{11.31}$$

and

$$g(\mathbf{u}) = g_0 \cos\theta\left(1-|\rho(\mathbf{u})|^2\right) \tag{11.32}$$

where

$$g_0 = \frac{D_0}{N} \tag{11.33}$$

is the element directivity, in the normal direction. Let us point out that in these expressions, $\rho(\mathbf{u})$ is the active reflection coefficient observed when all elements are excited with the phase gradient in the direction **u**. The modulus of the pattern $f(\mathbf{u})$ which is involved in equations (11.6) and (11.7) is proportional to the square root of the gain $g(\mathbf{u})$. It is thus strictly related to the active reflection coefficient $\rho(\mathbf{u})$.

11.4.2 Array on receive

Consider an incident plane wave, coming from the direction **u**. We observe a specularly reflected wave, one or several evanescent waves, and a transmitted wave. In each element, we observe the *same* transmitted wave to within a constant phase gradient corresponding to the tilt of the incident wave.

The variations of power received at any element as a function of the incidence angle **u,** allow us, in comparison with a standard element, to evaluate the gain $g(\mathbf{u})$ of an element in the presence of the others. Equations (11.31) and (11.32) lead then to the gain $G(\mathbf{u})$ and to the modulus $|\rho(\mathbf{u})|$ of the active reflection coefficient. This measurement allows us to use a simple prototype since *phase shifter and feed network are not involved.* On the other hand, $\rho(\mathbf{u})$ can be calculated from measurements of the coupling coefficients between elements, as we shall see later.

11.4.3 Array active reflection coefficient - mutual coupling[5]

Active reflection coefficient

If N elements of the array are excited in transmission by a set of emerging waves (Fig. 11.14), a_1, a_2, ..., a_n..., a_N, we observe, due to mutual coupling, N reflected waves b_1, b_2, ... , ... b_N, linearly related to the first ones, of the form

$$b_m = \sum_{n=1}^{N} C_{m,n} a_n \tag{11.34}$$

where the coefficients $C_{n,m}$ characterize the matrix of the coupling coefficients.

In the case of a uniform linear array excited with a constant phase gradient (see equations (11.14) and (11.15)) corresponding to the pointing angle $\tau_0 = \sin\theta$, we have

[5]Amitay, N., Galindo, V. and Wu, C.P., *Theory and Analysis of Phased Array Antennas*, Wiley-Interscience, London, 1972.

$$\varphi = 2\pi\Delta\nu\tau_0 = kd\tau_0, \quad \left(k = \frac{2\pi}{\lambda}\right) \tag{11.35}$$

and after equation (11.10)

$$a_n = a_0 \exp(-jknd\tau_c) \tag{11.36}$$

We observe at element m the reflected wave

$$b_m = a_c \sum_{n=1}^{N} C_{m,n} \exp(-jknd\tau_0) \tag{11.37}$$

which characterizes an 'active reflection coefficient'

$$\rho_m(\tau_0) = \frac{b_m}{a_m} = \sum_{n=1}^{N} C_{m,n} \exp\left[-jk(n-m)d\tau_0\right] \tag{11.38}$$

Form of the coupling coefficients

The coupling coefficients depend here only on the interelement spacing $d|n-m|$. They take the following form

$$C_{m,n} = \gamma(d|n-m|)\exp\left[-j\beta_S d|n-m|\right] \tag{11.39}$$

where γ is a decreasing positive function of the interelement spacing and β_S is close to k.

Under these conditions, the coefficient ρ takes the form

$$\rho_m(\tau_0) = \sum_{n=1}^{N} \gamma(d|n-m|)\exp\left\{-jd\left[\beta_S|n-m| + k\tau_0(n-m)\right]\right\} \tag{11.40}$$

The measurement of the coupling coefficients $C_{n,m}$ allows us to derive the active reflection coefficient of the array, and hence its radiation characteristics.

11.4.4 Blind angle phenomenon[5, 6, 7]

Mutual coupling

In some cases, we observe that for certain pointing directions τ_0 close to those corresponding to the appearance of the grating lobe in the visible domain, the active reflection coefficient becomes close to unity: almost all the transmitted power is reflected. This causes the appearance of a null in the radiation pattern of an element in the presence of the others and then the array gain becomes zero in the corresponding direction. Several theories have been proposed to explain this phenomenon. All concern the existence of a surface wave whose coupling phenomena are the effects and whose propagation constant is precisely the coefficient β_S.

This phenomenon may be explained by considering the form of the active reflection coefficient (equation (11.40)). If we apply the method of stationary phase to this expression, we see that $|\rho_m(\tau_0)|$ is maximum for pointing directions τ_0 such that

$$d\left[\beta_S|n-m|+k\tau_0(n-m)\right]=2\pi K \qquad (K=1,2,...) \qquad (11.41)$$

For the elements of rank $n > m$, this is obtained for

$$d(\beta_S+k\tau_0)=2\pi \qquad (11.42)$$

and for the elements of rank $n < m$, for

$$d(-\beta_S+k\tau_0')=-2\pi \qquad (11.43)$$

Consequently

$$\tau_0=\frac{\lambda}{d}-1-\left(\frac{\beta_S}{k}-1\right), \quad \tau_0'=-\tau_0 \qquad (11.44)$$

We obtain a pair of symmetrical directions $\pm\tau_0$ for which the reflection coefficient is maximum, thus the minimum gain. Since β_S is close to k or slightly greater (slow wave) equation (11.44) shows that the pointing angle τ_0 giving the maximum for ||,

---

[6] Knittel, H., Hessel, A. and Oliner, A., 'Element pattern nulls in phased arrays and their relations to guided waves', *Proc. IEEE*, Vol. 56, No. 11, pp1822-1836, December 1968.

[7] Lee, S.W., 'On the suppression of radiation nulls and broadband impedance matching of rectangular waveguide phased arrays', *IEEE Trans. Antennas & Propagation*, Vol. AP-19, No. 1, pp 41-51, January 1971.

is close or slightly less than τ_M for which the first grating lobe of the array appears (§11.3.4, equation (11.24)).

Remark: In equation (11.41) we have not chosen other values for K besides $K = 1$. This is because in the rather frequent case of a slow wave the corresponding directions are not in the real domain.

Expression for $\rho(\tau)$ in a simple theoretical model

In the case of a uniform infinite array the coefficient $\rho(\tau)$ is the same for all elements. If we number them from $-\infty$ to $+\infty$, we have for the elements of rank zero

$$\rho(\tau) = \sum_{-\infty}^{+\infty} \gamma(d|n|) \exp\left[-jd\left(\beta_S |n| + k\tau n\right)\right] \tag{11.45}$$

Since the blind angle direction τ_0 is given by equation (11.41), in the vicinity of $\tau = \tau_0$ only the elements of rank $n > 0$ play a significant role and we can write

$$\rho(\tau) = \sum_{0}^{+\infty} \gamma(dn) \exp\left[-jdnk\left(\tau - \tau_0\right)\right] \tag{11.46}$$

Let us assume for the mutual coupling coefficients an exponentially-decreasing function such as

$$\gamma(dn) = \gamma_0 \exp(-\alpha dn) \tag{11.47}$$

where α characterizes the reduction of the coupling from one element to the next. Let us set

$$y = \exp\left\{-d\left[\alpha + jk\left(\tau - \tau_0\right)\right]\right\} \tag{11.48}$$

then

$$\rho(\tau) = \gamma_0 \sum_{0}^{\infty} y^n = \frac{\gamma_0}{1 - y} \tag{11.49}$$

and

$$\left|\rho(\tau)\right|^2 = \frac{\gamma_0^2}{1 + \exp(-2\alpha d) - 2\exp(-\alpha d)\cos\left[kd\left(\tau - \tau_0\right)\right]} \tag{11.50}$$

We see that for $\tau = \tau_0$ $\left|\rho(\tau)\right|$ takes a maximum value

$$\rho_M = \frac{\gamma_0}{1 - \exp(-\alpha d)} \leq 1 \tag{11.51}$$

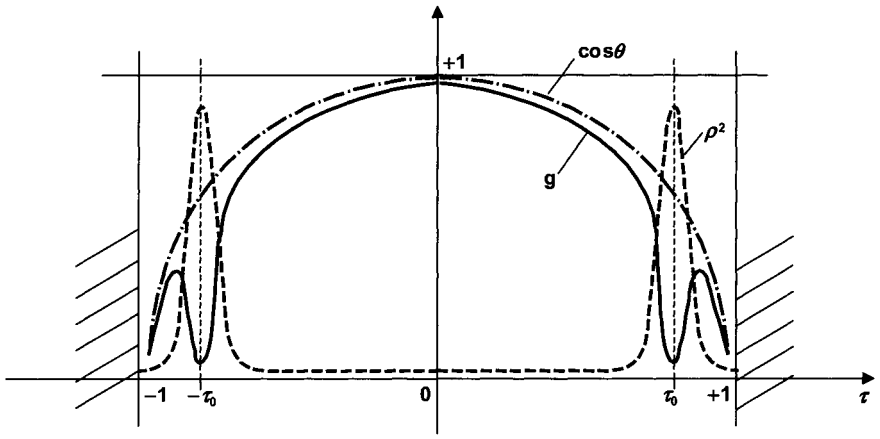

Fig. 11.15 Active reflection coefficient; blind angle phenomenon.

With this notation, we obtain

$$|\rho(\tau)|^2 = \frac{\rho_M^2}{1+\left[\dfrac{\sin\left(kd\dfrac{\tau-\tau_0}{2}\right)}{\sinh\left(\dfrac{\alpha d}{2}\right)}\right]^2} \tag{11.52}$$

If the interelement spacing d is small, we have

$$|\rho(\tau)|^2 = \frac{\rho_M^2}{1+\dfrac{k^2}{\alpha^2}(\tau-\tau_0)^2} \tag{11.53}$$

We obtain an analogous form in the vicinity of the symmetrical direction $\tau_0' = \tau_0$.

These expressions show that the maximum for $|\rho|^2$ in the direction τ_0 (minimum of radiation) is greater as α becomes smaller, that is to say as the fall-off of interelement coupling is reduced. The variations of $|\rho(\tau)|^2$ and of the corresponding element gain $g(\tau)$ given by equation (11.30) are represented in Fig. 11.15.

In the case of a small array, we obtain a result analogous to that of the case of a rapid decrease of α, namely the minimum of radiation in the blind angle directions becomes blunter.

11.4.5 Case where the element spacing is relatively large

In this case, mutual coupling is small and the element pattern is principally defined by the type of element chosen. Nevertheless, the pattern of such an element may be particularly distorted by the presence of neighbouring elements without the appearance of significant coupling coefficients $C_{m,n}$. This is due to the fact that the neighbouring elements can be excited by coupling in a high-order mode that does not propagate at the input but radiates and modifies the pattern of the element which is fed. This phenomenon is observed in the case of large horns whose aperture may locally propagate an antisymmetrical mode, for instance, of the $TE_{2,0}$ type. This is also observed in the case of longitudinal radiation elements.

11.4.6 Study of an array of open-ended guides considered as a periodic structure

An array can be considered as a periodic structure separating two media: the external medium ($z > 0$) is the semi-infinite space of free propagation (with its visible and invisible domains - see §11.3.1), and the internal medium ($z < 0$) composed of the guides feeding the array.

Consider a plane wave incident upon a receiving array. The main problem is to determine the transfer coefficient of the array, which is generally measured by the amplitude of the principal mode excited in the guides. We can deduce by reciprocity other characteristics corresponding to various conditions of excitation of the array, for example, active reflection coefficients, element pattern, etc.

To solve this problem, a method consists of expressing the transverse electromagnetic field in the plane of discontinuity $z = 0$ in two forms both as external field and internal field.

The external field comprises the incident wave and the field diffracted by the array. The latter, due to the periodic structure of the array, can be expressed in the form of a spectrum of a set of visible and invisible plane waves (that is to say, propagating and evanescent). The internal field, in an arbitrary guide, consists of the set of propagating and evanescent modes which propagate in this guide (towards the negative z). This gives a doubly-infinite set of linear equations whose coefficients are the transfer or reflection coefficients. They can be solved by limiting the number of modes to a certain rank[8]. Sometimes an angle of incidence is found for which the transfer coefficient is zero, which corresponds to a blind angle.

---

[8] Roederer, M.A., 'Etudes des reseaux finis de guides rectangulaires à parois épaisses', *L'Onde Electrique*, November 1971.

11.5 EFFECTS OF PHASE QUANTIZATION

11.5.1 Case where all phase shifters are fed in phase

To understand the effect of the phase quantization, we shall assume that the element spacing is small so that the array can be treated as a continuous aperture. If such an array points in the direction $\tau = \sin\theta$, we know that the phase at a point M has a constant gradient (§11.3.2), and thus varies linearly as a function of the abscissa x of M. In fact, this follows from equation (11.15) by substituting the element spacing d by the abscissa x, as follows.

$$\varphi(x) = 2\pi \frac{x}{\lambda} \tau \tag{11.54}$$

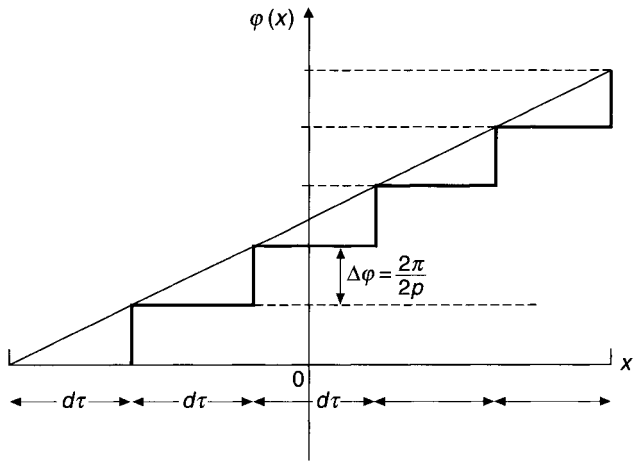

Fig. 11.16 Phase quantization (constant phase origin).

As the phase is quantized in increments $\Delta\varphi = 2\pi/2^p$, in fact we apply a scale variation to the array whose steps have a height of $\Delta\varphi$ and a length of d_τ such that the mean phase slope is maintained (Fig. 11.16)

$$\Delta\varphi = \frac{2\pi}{2^p} = 2\pi \frac{d_\tau}{\lambda} \tau \tag{11.55}$$

then

$$d_\tau = \frac{\lambda}{\tau} \frac{1}{2^p} \tag{11.56}$$

The illumination obtained has a constant phase in the intervals d_τ. This corresponds to an array of element spacing d_τ pointing in the direction τ. This array has a grating lobe in the direction τ_1 such that (eqn. 11.17)

$$\tau - \tau_1 = \frac{\lambda}{d_\tau} = \tau^p \tag{11.57}$$

The angular deviation of the quantization lobe is thus proportional to the pointing error τ. The array lobes are weighted by the pattern $f'(\tau)$ of the element of aperture d_τ, that is to say

$$f'(\tau) = \frac{\sin\left(\pi \frac{d_\tau}{\lambda} \tau\right)}{\pi \frac{d_\tau}{\lambda} \tau} \tag{11.58}$$

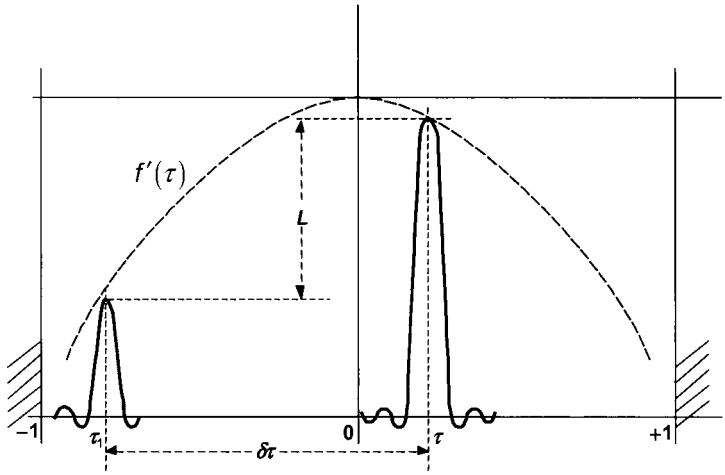

Fig. 11.17 Effect of phase quantization (constant phase origin).

The relative level of the useful lobe of direction τ and of the quantization lobe of direction τ_1 is then (Fig. 11.17)

$$L = \frac{f'(\tau_1)}{f'(\tau)} = \frac{1}{2^p - 1} \tag{11.59}$$

This level is independent of the pointing angle. It only depends on the accuracy of the phase shifters, for example, $p = 3$ bits, $L = 1/7$, that is to say approximately -17 dB.

11.5.2 Effects of quantization when the phase origin varies from one phase shifter to another

From the preceding, the stepwise phase functions give a periodic character to the phase errors, which lead to localized parasitic lobes of relatively high levels, particularly for phase shifters of just a few bits. If we now assume that the phase displayed for each phase shifter involves a constant of 'origin' depending on the number of bits of the phase shifter (Fig. 11.18), this phase is of the form

$$\Phi_n = \varphi_n + k\Delta\varphi \qquad (k = 1, 2, \ldots) \tag{11.60}$$

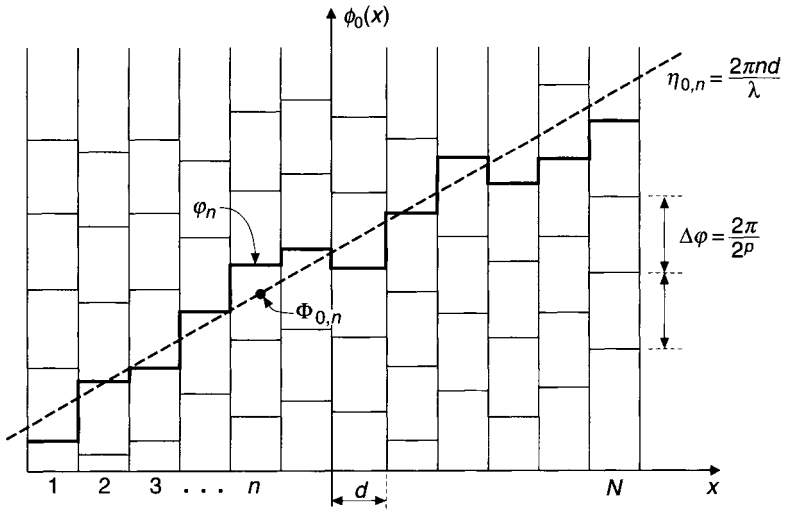

Fig. 11.18 Phase quantization (random phase origin).

Under these conditions, the periodic character of the phase errors along the array disappears. If the theoretical phase of the phase shifter n is $\varphi_{0,n}$, the phase error is

$$\Psi_n = \Phi_{0,n} - (\varphi_n + k\Delta\varphi) \tag{11.61}$$

k is chosen so that this error is minimum. It never exceeds $\Delta\phi/2$ but its exact value depends on the difference $\phi_{0,n} - \varphi_n$. If the origin phases φ_n are randomly distributed, we see that there is no correlation between the errors of the different elements. The probability density of the phase error Ψ_n of a element is uniform over $-\Delta\phi/2$ to $+\Delta\phi/2$. The illumination function of an uniformly illuminated array is thus of the form (to first order)

$$a_n = \exp\left[j\left(\Phi_{0,n} - \Psi_n\right)\right] \approx \exp\left(j\Phi_{0,n}\right)\left(1 - j\Psi_n\right) \tag{11.62}$$

The phase error introduces a parasitic illumination

$$\Delta a_n = j\Psi_n \exp\left(j\varphi_{0,n}\right) \tag{11.63}$$

and a parasitic pattern

$$\Delta R(\tau) = \sum_0^{N-1} \Psi_n \exp\left(j\Phi_{0,n}\right)\exp\left(j2\pi n\Delta\nu\tau\right) \tag{11.64}$$

which is superimposed on the desired pattern

$$R(\tau) = \sum_0^{N-1} \exp\left(j\Phi_{0,n}\right)\exp\left(j2\pi n\Delta\nu\tau\right) \tag{11.65}$$

In the direction of maximum radiation θ_0, we have

$$R(\tau_0) = N \tag{11.66}$$

The relative mean energy of the parasitic radiation (Fig. 11.19) is the mean square value

$$\overline{L} = \left|\frac{\overline{\Delta R(\tau)}}{R(\tau)}\right|^2 = \frac{1}{N^2}\overline{\Delta R(\tau)\Delta R(\tau)^*}$$

$$\overline{L} = \left|\frac{\overline{\Delta R(\tau)}}{R(\tau)}\right|^2 = \frac{1}{N^2}\sum_0^{N-1}\sum_0^{N-1}\overline{\Psi_n\Psi_m}\exp\left[j\left(\Phi_{0,n} - \Phi_{0,m}\right)\right]\exp\left[j2\pi\Delta\nu\tau(n-m)\right] \tag{11.67}$$

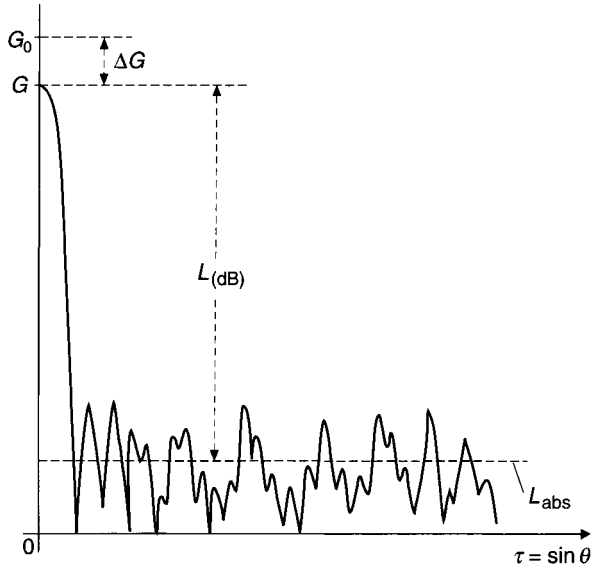

Fig. 11.19 Mean phase quantization sidelobe energy level.

By hypothesis

$$\overline{\Psi_n \Psi_m} = 0$$

except for $n = m$, in which case

$$\overline{|\Psi_n|^2} = \frac{1}{3}\left(\frac{\Delta\varphi}{2}\right)^2 \tag{11.68}$$

Then

$$\overline{L} = \frac{\left(\frac{\Delta\varphi}{2}\right)^2}{3N} = \frac{\pi^2}{3N2^{2p}} \tag{11.69}$$

or in decibels

$$\overline{L_{\text{dB}}} = -(10\log N + 6p - 5) \tag{11.70}$$

This is plotted in Fig. 11.20. The rms quantization sidelobe level decreases by 6 dB for each additional bit and by 10 dB for each ten-fold increase in the number of antenna elements.

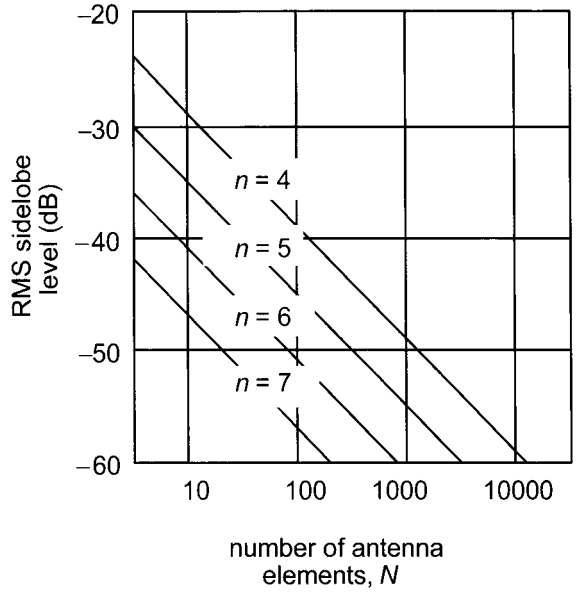

Fig. 11.20 Quantization sidelobe level as a function of number of bits n and number of elements N.

Influence on accuracy on-axis

The mean level of diffused radiation is found again in the null depth of the difference channel. If the slope of the null is $1/\theta_{3\text{dB}}$ (see §10.4.2), the standard deviation of the position of the axis in a plane, taking into account the fact that only the component in phase with the difference of this radiation produces a deviation, is given by

$$\frac{\sigma_e}{\theta_{3\text{dB}}} = \frac{\pi}{2^p\sqrt{6N}} \tag{11.71}$$

Numerical example

With a relative level of –40 dB the standard deviation is of the order of $\theta_{3\text{dB}}/100$.

Influence of the gain

The energy lost in the parasitic lobes involves a relative loss of gain

$$\frac{\Delta G}{G_0} = \frac{\sum_0^{N-1}\overline{|\Delta a_n|^2}}{\sum_0^{N-1}\overline{|a_n|^2}} = \overline{|\Psi_n|^2} = \frac{1}{3}\left(\frac{\Delta\varphi}{2}\right)^2 \tag{11.72}$$

and in decibels

$$10\log\frac{G}{G_0} \approx -\frac{14}{2^{2p}} \tag{11.73}$$

Remark: The mean 'absolute' level of the quantization lobes is obtained by multiplication of the relative level by the principal gain

$$G = Ng_0(\mathbf{u})$$

where $g_0(\mathbf{u})$ is the element gain in the presence of the other elements. Thus we have

$$\overline{L_{\text{ABS}}} = G\bar{L} = \frac{\pi^2}{3.2^{2p}} g_0(\mathbf{u})$$

and in decibels

$$\bar{L}_{\text{ABS}}(\text{dB}) = g_0(\mathbf{u})_{\text{dB}} - 6p + 5 \tag{11.74}$$

Thus, the *absolute* level *depends only on the accuracy of the phase shifters* (number of bits) and not on the number of elements.

Numerical example
We desire an absolute level of less than –7 dB with respect to isotropic. Assuming a typical element gain of 6 dB, the number of bits should be greater than 3.

Note: If phase shifters with random phase origins φ_n are used, then their values must be stored in a memory and used in the calculation of the displayed phases.

11.6 FREQUENCY-SCANNED ARRAYS

An electronically scanned antenna can be realized in a simple way by using a frequency-scanned array. Scanning is then obtained by varying the frequency. A simple means to obtain such an array is to use a length of transmission line to feed the array by means of directional couplers. Two adjacent elements of the array, spaced by a, are fed by two couplers separated in the transmission line by a length b. The array and transmission line properties allow us to show that a frequency deviation df about the central frequency f_0 produces an angular scanning $d\tau$ given in radians, to first order, by the following equation:

$$d\tau = \frac{b}{a}\frac{\lambda_g}{\lambda}\frac{df}{f_0}$$

where λ_g is the guide wavelength. We know that the phase shift produced by a length b of the transmission line is given by

$$\Delta\varphi = \frac{2\pi b}{\lambda_g} \tag{11.75}$$

This causes a deviation θ of the beam with respect to the normal, such that (equation (11.15))

$$2\pi \frac{a}{\lambda} \sin\theta = \Delta\varphi - 2K\pi \tag{11.76}$$

the integer K being chosen so that $|\sin\theta| \leq 1$.

Setting, as usual, $\tau = \sin\theta$, and taking the differential of this equation

$$ad\left(\frac{\tau}{\lambda}\right) = d\left(\frac{b}{\lambda_g}\right)$$

or

$$a\frac{\lambda d\tau - \tau d\lambda}{\lambda^2} = -b\frac{d\lambda_g}{\lambda_g^2} \tag{11.77}$$

In the vicinity of the normal ($\tau \approx 0$)

$$d\tau = -\frac{b}{a}\frac{\lambda}{\lambda_g}\frac{d\lambda_g}{\lambda_g} \tag{11.78}$$

If the transmission line has no frequency cut-off (coaxial line filled with a dielectric of dielectric constant ε), we have

$$\lambda_g = \frac{\lambda}{\sqrt{\varepsilon}}$$

Then

$$d\tau = -\frac{b}{a}\sqrt{\varepsilon}\frac{d\lambda}{\lambda} = +\frac{b}{a}\sqrt{\varepsilon}\frac{df}{f} \tag{11.79}$$

If the transmission line (waveguide) has a cut-off wavelength λ_c, we have the classical relationship

$$\frac{1}{\lambda_g^2}+\frac{1}{\lambda_c^2}=\frac{1}{\lambda^2} \tag{11.80}$$

which gives, upon differentiation

$$-\frac{d\lambda_g}{\lambda_g^3}=-\frac{d\lambda}{\lambda^3}$$

and finally we obtain

$$d\tau=\frac{b}{a}\frac{\lambda_g}{\lambda}\frac{df}{f} \tag{11.81}$$

The deviation in radians is proportional to the relative length (b/a) of the waveguide, to the ratio of guide and free-space wavelengths, and to the relative frequency deviation.

Exercise: Repeat the calculation of the two preceding cases by generalizing when the pointing direction is not close to the array normal ($\tau_0 \neq 0$).

11.7 ANALOGUE BEAMFORMING MATRICES

11.7.1 Introduction

We have seen (§7.2.2, §9.7.1) that multiple-beam antennas are sometimes used in radar and sonar applications, as an alternative to electronic scanning, to improve the range and the angular resolution of equipment. On the other hand, multiple beams and electronic scanning can be combined, since the angular scanning of a group of several beams allows us to increase the duration of the illumination of targets (this improves velocity measurements by the Doppler effect). In addition, it allows us to perform interpolations and combinations between signals received from multiple beams (this improves the angular accuracy and allows techniques to reduce the effect of jamming (§14.3, §14.4)).

Such antennas can be realized by using a kind of *retina* of multiple primary elements on the focal surface of a reflector or a lens. If we desire to combine multiple beams with electronic scanning we might use a reflectarray or an active lens (§11.2.2).

This technique is valid as long as the angular domain covered by the multiple beams is not too large (about 5 to 6 degrees). Beyond that, even using a long focal length and aplanatic systems, we are limited by geometrical aberrations which distort the beams (§9.7)

The use of array antennas combined with beamforming matrices allows us to avoid these limitations.

In general, these matrices are microwave structures known as 'reciprocal passive multipoles', in principle without losses, since their properties rule those of the multiple-beams that they fed.

Other types of matrices are used, e.g. analogue and digital matrices (§11.8) which frequently require a frequency shift of the received signals.

11.7.2 General properties of multi-port networks

'S' matrix

A multi-port network is composed of N ports in the form of waveguides, numbered from 1 to N. On each of them we define a reference plane π_n where we observe:

- an incident wave of complex amplitude a_n;
- a reflected or emerging wave of amplitude b_n;

The coefficients a_n and b_n are assumed to be normalized so that the transmitted powers are measured (in watts) by $|a_n|^2$ and $|b_n|^2$.

Assume that an single incident wave (a_p) is sent to the port (p), the other ports being terminated in matched loads. We observe emerging waves of the form

$$b_1 = S_{1,p}a_p, \quad \ldots \quad b_n = S_{n,p}a_p, \quad \ldots \quad b_p = S_{p,p}a_p, \quad \ldots \tag{11.82}$$

Thus the elements $S_{n,p}$ are *transfer coefficients*. They can be arranged in the form of a matrix which is *symmetric* if the network is reciprocal. The elements of the principal diagonal (S_{pp}) are the reflection coefficients

$$[\mathbf{S}] = \begin{bmatrix} S_{11} & S_{12} & \ldots. & S_{1N} \\ S_{21} & S_{22} & \ldots. & S_{2N} \\ & & & \\ S_{N1} & S_{N2} & \ldots. & S_{NN} \end{bmatrix} \tag{11.83}$$

In general, the set of incident and emerging waves may be represented by column matrices

$$[\mathbf{A}] = \begin{bmatrix} a_1 \\ a_2 \\ \vdots \\ a_N \end{bmatrix} \text{ and } [\mathbf{B}] = \begin{bmatrix} b_1 \\ b_2 \\ \vdots \\ b_N \end{bmatrix} \tag{11.84}$$

So we have the matrix relation

$$[\mathbf{B}] = [\mathbf{S}][\mathbf{A}] \tag{11.85}$$

Case of a lossless matrix

Consider again the case where we inject a wave (a_p) at the single port (p). The net emerging power must be equal to the incident power

$$|b_1|^2 + \ldots + |b_N|^2 = |a_p|^2$$

then

$$|S_{1,p}|^2 + |S_{2,p}|^2 + \ldots + |S_{N,p}|^2 = 1 \tag{11.86}$$

Thus, the sum of the squares of the transfer coefficient magnitudes of a row or a column is equal to unity.

Orthogonality of a lossless matrix

Consider again the case of an excitation of the single port (p) by an incident wave (a_p). We have seen that the emerging waves are expressed by

$$b_1 = S_{1,p}a_p, \ \ldots \quad b_n = S_{n,p}a_p, \ \ldots \quad b_N = S_{N,p}a_p$$

Now reverse the sense of propagation of the emerging waves; they become incident waves of same amplitude but of *conjugate phases* in order to take into account the reversal of the direction of propagation

$$a_1' = b_1^*, \ a_2' = b_2^*, \ \ldots \ a_N' = b_N^* \tag{11.87}$$

By reciprocity all the power contained in these incident waves returns to the *single port* (p). Thus, the power transmitted to any other arbitrary port (n) is zero. Let us calculate this power. From the foregoing, the emerging signal at (n) is

$$b_n = S_{n,1}a'_1 + S_{n,2}a'_2 + \ \ldots\ + S_{n,p}a'_p + \ \ldots\ + S_{n,N}a'_N = 0$$

Taking into account relations (11.87), we obtain

$$S_{n,1}S^*_{1,p} + S_{n,2}S^*_{2,p} + \ \ldots\ + S_{n,N}S^*_{N,p} = 0$$

or still, by symmetry

$$S_{n,1}S^*_{p,1} + S_{n,2}S^*_{p,2} + \ \ldots\ + S_{n,N}S^*_{p,N} = 0 \qquad (11.88)$$

This relation yields the property of orthogonality: the hermitian product of two single rows or two single columns is zero.

11.7.3 Beamforming applications

Orthogonality of the illuminations of an array (Fig. 11.21)

An array of N radiating elements is fed by a multi-port network comprising $N+M$ ports: N 'outputs' feeding the radiating elements of the array and M 'inputs' among which we consider two denoted A and B. The latter are assumed matched and independent, that is to say isolated.

$$S_{AA} = S_{BB} = S_{AB} = S_{BA} = 0$$

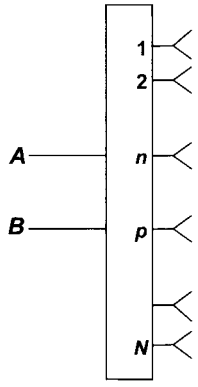

Fig. 11.21 Orthogonality of the array illuminations.

This gives the following results:

Conservation of energy:

$$\begin{aligned} |S_{A,1}|^2 + |S_{A,2}|^2 + \ \ldots\ + |S_{A,N}|^2 &= 1 \\ |S_{B,1}|^2 + |S_{B,2}|^2 + \ \ldots\ + |S_{B,N}|^2 &= 1 \end{aligned} \tag{11.89}$$

Orthogonality:

$$S_{A,1}S^*_{B,1} + S_{A,2}S^*_{B,2} + \ \ldots\ + S_{A,N}S^*_{B,N} = 0 \tag{11.90}$$

Interpretation: The illuminations of the array produced by excitation of the inputs A and B are respectively

$$S_{A,1}, S_{A,2}, \ \ldots\ S_{A,N}$$

$$S_{B,1}, S_{B,2}, \ \ldots\ S_{B,N}$$

from which we can conclude

Theorem: *In a lossless distribution the illuminations produced from two arbitrary isolated inputs are orthogonal.*

Orthogonality of the characteristic functions

We know that the characteristic functions of radiation are obtained by Fourier transformation of illuminations. The conservation of the hermitian product (Parseval's theorem) leads to the orthogonality of the characteristic functions. If (α, β, γ) are the direction cosines of the unit vector $\mathbf{u}$ $\left(|\alpha^2| + |\beta|^2 + |\gamma|^2 = 1\right)$, we have

$$\int_{-\infty}^{\infty}\int_{-\infty}^{\infty} \mathbf{F}_A(\alpha,\beta)\mathbf{F}^*_B(\alpha,\beta)\,d\alpha d\beta = 0 \tag{11.91}$$

In the case of a rectilinear array, if θ is the angle of $\mathbf{u}$ to the normal of the array (see notations of §11.3.1), we have

$$\int_{-\infty}^{\infty} \mathbf{F}_A(\tau)\mathbf{F}^*_B(\tau)\,d\tau = 0 \quad (\tau = \sin\theta) \tag{11.92}$$

In practice, orthogonality is often verified in the real domain ('visible') that is to say for $-1 \leq \tau \leq 1$. In particular, this is the case of point elements of one half-wavelength spacing; the characteristic functions are periodic with period $\lambda/d = 2$. In this case it is sufficient to limit the integral to this domain

$$\int_{-1}^{1} \mathbf{F}_{\mathrm{A}}(\tau)\, \mathbf{F}_{\mathrm{B}}^{*} d\tau = 0 \tag{11.93}$$

Directional beams

Consider a regular rectilinear array of an element spacing d and length $D = Nd$ with uniform amplitude illumination. A matrix with M inputs $(A_0, \ldots A_m, \ldots A_{M-1})$ can create M orthogonal directional beams if the illuminations corresponding to each of these inputs $(S_{m,0}, S_{m,1}, \ldots S_{m,N-1})$ possess a phase illumination $(\varphi_{m,1}, \varphi_{m,2}, \ldots \varphi_{m,N})$ which varies linearly along the array, and if the phase shift relative to two decoupled inputs varies by an integer multiple of 2π along the array.

These conditions are satisfied if the transfer coefficient from an input port (m) to an output (n) is of the form

$$S_{m,n} = \frac{1}{\sqrt{N}} \exp\left(-j2\pi \frac{nm}{N}\right) \tag{11.94}$$

Comment: Discrete Fourier transform
If the input ports are excited with complex amplitudes $(a_1, \ldots a_m, \ldots a_M)$, the resulting output illumination is of the form

$$b_n = \frac{1}{\sqrt{N}} \sum_{m=0}^{N-1} a_m \exp\left(-j2\pi \frac{nm}{N}\right) \tag{11.95}$$

Conversely, on receive, if the signals collected by the N elements of the array are defined by the distribution b_n $(0 \leq n \leq N-1)$, the signals received at the M output ports are given by

$$a_m = \frac{1}{\sqrt{N}} \sum_{n=0}^{N-1} b_n \exp\left(j2\pi \frac{nm}{N}\right) \tag{11.96}$$

We observe that the two distributions (a_m) and (b_n) are related by a discrete Fourier transform.

Radiated patterns: These follow from the radiation characteristic functions which are the Fourier transforms of the illuminations. The array factors, which are the

characteristics functions assuming that the elements are isotropic, are obtained from the transfer coefficients $S_{m,n}$ in the form of a Fourier series

$$R_m(\tau) = \frac{1}{N}\sum_{n=0}^{N-1} S_{m,n} \exp(j2\pi\Delta\nu\tau) = \frac{\sin\left[N\pi\Delta\nu(\tau-\tau_m)\right]}{N\sin\left[\pi\Delta\nu(\tau-\tau_m)\right]} \qquad (11.97)$$

The τ_m define the sampled pointing directions

$$\tau_m = m\Delta\tau \qquad (11.98)$$

$\Delta\tau$ is the pointing deviation of two adjacent beams

$$\Delta\tau = \frac{1}{2\nu_0} = \frac{1}{N\Delta\nu} = \frac{\lambda}{Nd} = \frac{\lambda}{D} \qquad (11.99)$$

The patterns $R_m(\tau)$ are periodic orthogonal functions of period $1/\Delta\nu = \lambda/d$. The maximum of each pattern coincides with the nulls of the others. If the element spacing is small, of the order of $\lambda/2$, we can neglect the periodic character and represent the array factors in the form

$$R_m(\tau) = \frac{\sin\left[N\pi\Delta\nu(\tau-\tau_m)\right]}{N\pi\Delta\nu(\tau-\tau_m)} = \frac{\sin(N\pi\Delta\nu\tau - m\pi)}{N\pi\Delta\nu\tau - m\pi} \qquad (11.100)$$

We shall encounter these functions again in Chapter 12.

11.7.4 Examples of matrices

Butler matrix[9]

This matrix is based on the use of 3 dB directional couplers.

[9] Butler, J. and Lowe, R., 'Beam forming matrix simplifies design of electronically scanned antennas', *Electronic Design*, Vol. 9, April 1961, pp170-173.

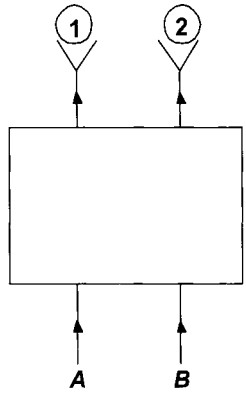

Fig. 11.22 Two-element array fed by a 3 dB directional coupler.

Two-element array: A 3 dB coupler can feed a two-element array and form two decoupled orthogonal beams (Fig. 11.22). If we consider the two ports A and B and the outputs 1 and 2 which excite the two elements of the array, the transfer coefficients characterizing the two illuminations are

$$S_{A,1} = \frac{1}{\sqrt{2}}, \qquad S_{A,2} = \frac{1}{\sqrt{2}} \exp\left[-\left(j\frac{\pi}{2}\right)\right]$$
$$S_{B,1} = \frac{1}{\sqrt{2}} \exp\left[-\left(j\frac{\pi}{2}\right)\right], \qquad S_{B,2} = \frac{1}{\sqrt{2}} \tag{11.101}$$

We verify the conservation of energy and the orthogonality of the matrix.

The array factors obtained (in a planar space) are of the form

$$F_A(\tau) = \cos\left(\pi\tau + \frac{\pi}{4}\right), \quad F_B(\tau) = \cos\left(\pi\tau - \frac{\pi}{4}\right) \tag{11.102}$$

Four-element arrays: The matrix has four inputs and can generate four orthogonal beams. It is composed of four 3 dB couplers connected through two $\pi/4$ phase shifters (Fig 11.23). The transfer coefficients obtained are represented below on a trigonometric circle.

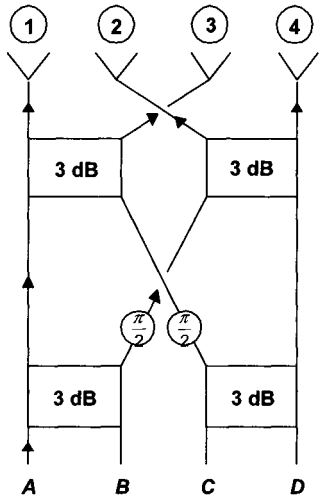

Fig. 11.23 Four-element array fed by a 4×4 Butler matrix.

The four patterns have the form indicated above, with an angular spacing between the beams (for a spacing $d = \lambda/2$): $\Delta\tau = 1/2$.

Generalization: To form N beams, the number C of couplers required is given by the function

$$C = \frac{N}{2}\log N \qquad (11.103)$$

The drawback of Butler matrices is in the complexity of their interconnection, particularly for large matrices. For large arrays it is better to use other types such as Blass matrices or quasi-optical matrices.

Comment: The Butler matrix is of didactic interest, since it is the circuit equivalent of the FFT (Fast Fourier Transform) where the 'Butterflies' are replaced by 3 dB couplers[10]. An application of the Butler matrix to circular arrays is given in §11.8.4.

---

[10] Ueno, M., 'A systematic design formulation for Butler matrix applied FFT algorithm', *IEEE Trans. Antennas & Propagation*, Vol.29, No.3, pp496-501, May 1981; see also correction in *IEEE Trans. Antennas & Propagation*, Vol.29, No.5, p825, September 1981.

Blass matrix

The M excitation guides (1, 2, ... m, ... M) are connected to the N guides feeding the elements of the array (1, ... n, ... N) through directional couplers. The coupling coefficients are chosen so that the transfer coefficients $S_{m,n}$ follow the desired illumination functions (Fig. 11.24). The guides are terminated with matched loads. An application of the Blass matrix is given in §11.2.2, Fig. 11.9.

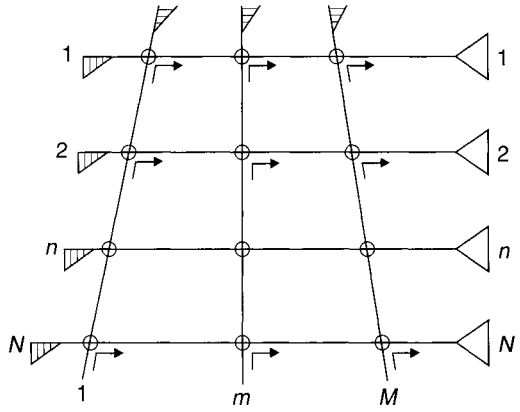

Fig. 11.24 Blass matrix.

Orthogonality: Since the couplers are directional, and the elements are assumed to be matched, the inputs are isolated, and the corresponding patterns are orthogonal.

Phase functions: The phases vary linearly along the array with an increment which deviates from the tilt angle of the excitation guide with respect to the feeding guides. This increment can be corrected by introducing a constant phase shift in front of each element. With circular polarization an easy solution consists of using 'helical' antennas: an axial rotation of the helix allows to create the necessary constant phase shift.

Electronic scanning: By inserting programmable phase shifters in front of the antenna elements it is possible to combine multiple beams and electronic scanning.

Advantage of the Blass matrix: The number C of couplers necessary to form M beams is

$$C = MN \tag{11.104}$$

Thus, this system is particularly attractive for large arrays with a small number of beams. The number of couplers may be rather large, but the interconnection layout is simple and does not require overlapping or multilayer technologies.

Disadvantage: The phase increment depends on the wavelength and equally on the direction of the beams. Thus, the system is not well suited to large arrays if the bandwidth of the transmitted signals is very wide.

Application exercise: We wish to synthesize a passive antenna possessing a null in a fixed direction independent of the form or direction of the useful beam.

Such a characteristic is useful in radar applications; a null in the direction of the horizon can suppress clutter and occasional jamming.

To solve this problem, we can use a two port Blass matrix. One port (A) is associated with a uniformly illuminated beam with maximum gain in the horizontal direction. The other port (B) creates a steerable beam by means of phase shifters (Fig. 11.25).

Consider an incident plane wave from the horizontal direction. By reciprocity it can be shown that all the power is absorbed at A in the load. Therefore, no energy is sent to the port B; its pattern has a null in the horizontal direction.

More precisely, an incident wave of direction θ (with respect to the normal to the array) generates a signal in the channel n

$$a_n = \exp(jn\pi\tau) \quad \text{where } \tau = \sin\theta, \quad d = \frac{\lambda}{a} \tag{11.105}$$

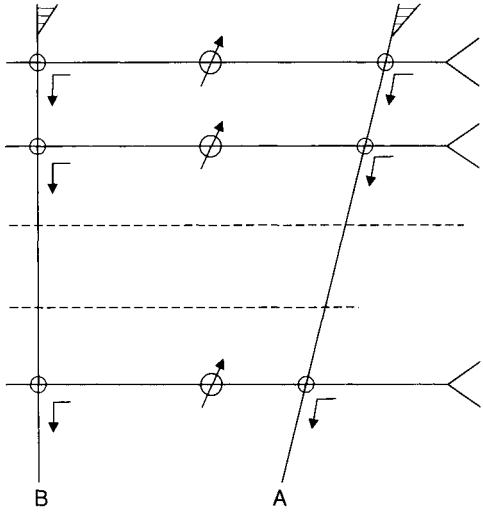

Fig. 11.25 Phased array radiating a pattern with a fixed null.

This can be separated into

- a constant illumination $\alpha_n = \alpha_0$ (which provides a signal at A);
- and a residual illumination β_n orthogonal to α_n

$$a_n = \exp(jn\pi\tau) = \alpha_0 + \beta_n$$

From which we obtain the residual incident wave

$$a_n' = \beta_n = \exp(jn\pi\tau) - \alpha_0$$

Since the latter is orthogonal to the distribution α_0, we have

$$\sum_{n=0}^{N-1} \alpha_0 \left[\left(\exp(jn\pi\tau) - \alpha_0 \right) \right] = 0$$

from which we obtain

$$\alpha_n = \operatorname{sinc}\left(\frac{N\pi\tau}{2} \right) \exp\left(j\pi \frac{N-1}{2} \right)$$

Then

$$\alpha_0' = \exp(jn\pi\tau) - \exp\left(j\pi\frac{N-1}{2}\right)\operatorname{sinc}\left(\frac{N\pi\tau}{2}\right) \tag{11.106}$$

Let us form a pattern pointing in a direction τ_0. We sum these signals (a_n') in a direction τ_0 with a phase shift $(-n\tau_0)$, i.e.

$$F_{\tau_0}(\tau) = \sum_0^{N-1} a_n' \exp(-jn\pi\pi_0)$$

$$= \left\{\operatorname{sinc}\left[\frac{N\pi(\tau-\tau_0)}{2}\right] - \operatorname{sinc}\left(\frac{N\pi\tau}{2}\right)\operatorname{sinc}\left(\frac{N\pi\tau_0}{2}\right)\right\}\exp\left(j\pi\frac{N-1}{2}\right) \tag{11.107}$$

↑	↑	↑
pointing in direction τ_0	pointing in direction $\tau_0 = 0$ (horizon)	weighted by the sidelobe of the preceding pattern

Thus, we obtain a pattern pointing in direction τ_0 but slightly distorted in order to generate a null in the direction ($\tau = 0$).

11.7.5 Non-orthogonal directional beams

Problem of multiple-beam angular coverage

We have seen that orthogonal adjacent directional beams of the form sinc(x) crossover at a relative level of $2/\pi$, i.e. approximately –4 dB. If an illumination taper is used in order to reduce the sidelobes of the orthogonal beams, the crossovers occur at an even lower level. This means a hole in the radar coverage may occur in the corresponding direction, and a lower detection probability will result.

A solution to this problem is to bring the beams closer to one another. If the chosen angular spacing $\Delta\tau'$ is lower than the spacing resulting from the orthogonality condition $(\Delta\tau = 1/2\nu_0 = \lambda/Nd)$, the relative overlap level becomes

$$L' = \operatorname{sinc}\left(\frac{\pi}{2}\frac{\Delta\tau'}{\Delta\tau}\right) \approx 1 - \frac{\pi^2}{24}\left(\frac{\Delta\tau'}{\Delta\tau}\right)^2 \tag{11.108}$$

and in dB

$$L_{\text{dB}} \approx 4\left(\frac{\Delta\tau'}{\Delta\tau}\right)^2 \tag{11.109}$$

If for instance the angular spacing is reduced by half, the loss is approximately one dB.

However, the problem still remains of decoupling the corresponding ports. This problem may be solved, in the case of passive matrices, at the expense of some losses. This reduces the real gain but the improvement of the relative gain in the critical direction allows us to obtain an optimum solution.

Quasi optical matrix: Rotman lens

Description (§11.2.2: electronic phased lens): The Rotman lens is enclosed between two parallel conducting plates (Fig. 11.26). Its external face is a regular linear array, its internal face an array arranged along a curve constituting the 'principal surface' (§9.3) of the system. These two arrays are connected by two fixed-phase shifters ensuring focusing, and occasionally variable phase shifters if we want to combine electronic scanning with beam forming.

Multiple beams are created by means of a 'retina' of primary elements placed on the focal surface of the lens, which approximates to the arc of a circle of radius equal to the focal length F.

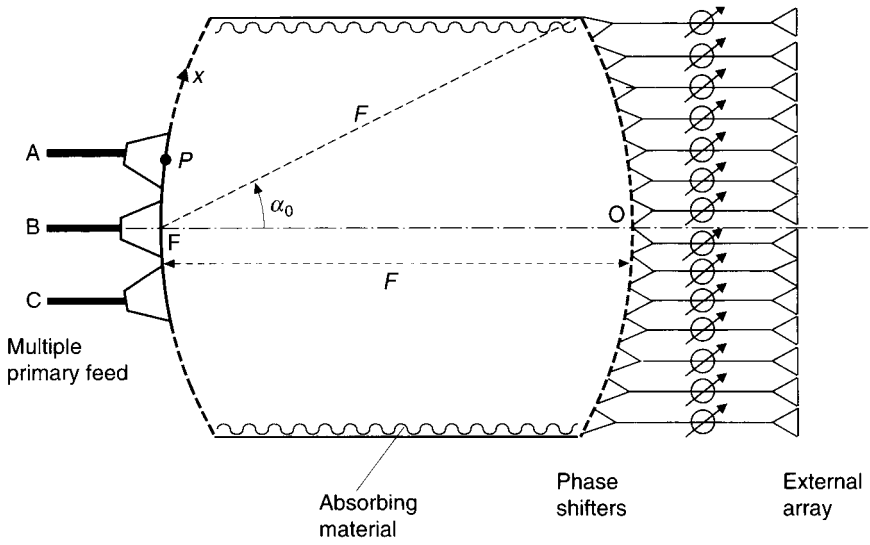

Fig. 11.26 Array with Rotman lens.

The shape of the principal surface (the internal face) is chosen in order to minimize the geometrical aberrations. One of the most troublesome is the *coma* aberration (§9.7.3) which creates a cubic distortion of the wavefront. To cancel it the Abbe condition means that the principal surface should be a sphere (or a circle in this case) centred at the focus. The inputs of the matrix are the primary sources, which in general have some small degree of mutual coupling. The radiated beams are not in general perfectly orthogonal, since part of the primary pattern is not intercepted by the lens and the undesirable spillover is generally absorbed by an appropriate material.

Diffraction spot: An axial incident wave produces, through the lens, a circular wave converging at the focus. At a point P in the vicinity of the focus F, the diffraction spot is obtained from the Huygens-Fresnel formula. If D is the lens length (array length), x the abscissa along the focal curve and α_0 the semi-angle subtended by the lens, seen from the focus, we obtain (§9.9.3, eqn. 9.113)

$$\Psi(x) = \operatorname{sinc}\left(\frac{2\pi x}{\lambda}\sin\alpha_0\right) \approx \operatorname{sinc}\left(\frac{\pi D x}{\lambda F}\right) \tag{11.110}$$

The distance δ between nulls of this spot is given by (eqn. 9.114)

$$\delta = \frac{\lambda}{\sin\alpha_0} \approx \frac{2\lambda F}{D} \tag{11.111}$$

Imaging and multiple beams: A multiple point 'object' configuration of radiating elements, at infinity, may be defined by a distribution $A(x)$, each point M of abscissa x defining a direction MO. These elements produce an image $B(x)$ in the focal plane through the system, which is the convolution of the distribution $A(x)$ with the diffraction spot $\Psi(x)$ (§13.5). Assuming negligible distortions, we find

$$B(x) = A(x) \otimes \Psi(x)$$

This image can be sampled with the maximum spacing Δx by applying the sampling theorem.

$$\Delta x = \frac{\lambda}{2\sin\alpha_0} \approx \frac{\lambda F}{D} \tag{11.112}$$

that is to say $\Delta x = \delta/2$.

This is half the size of the diffraction spot. There is therefore a tradeoff between the antenna gain that we can obtain from a primary element and the spacing sampling: the first is optimized for a primary aperture close to δ, the second for an aperture smaller than $\lambda/2$ (§9.9.3).

It is theoretically possible to reconcile these two requirements. In effect, we know how to realize primary elements whose illuminations are functions of the orthogonal sinc(x) type. These would produce sector primary patterns without spillover, and would lead to a uniform illumination of the lens, thus the maximum gain. Nevertheless, this solution gives high sidelobes. That is why, in practice, we can fit in the primary elements by means of loaded magic-T at the expense of some losses. On the other hand, we observe that these losses are only effective on receive. On transmit, if all the elements are excited in-phase, there are no losses. On receive we obtain an overlap rate of 50% between the elements. The patterns are optimized, but there is a loss of gain (Fig. 11.27).

In the operational systems where *external* noise is significant (this is frequently the case when low noise temperature receivers are used) this drawback is acceptable. It disappears to a large extent if each primary element comprises an *active module* that amplifies the received signal before it reaches the loaded magic-T.

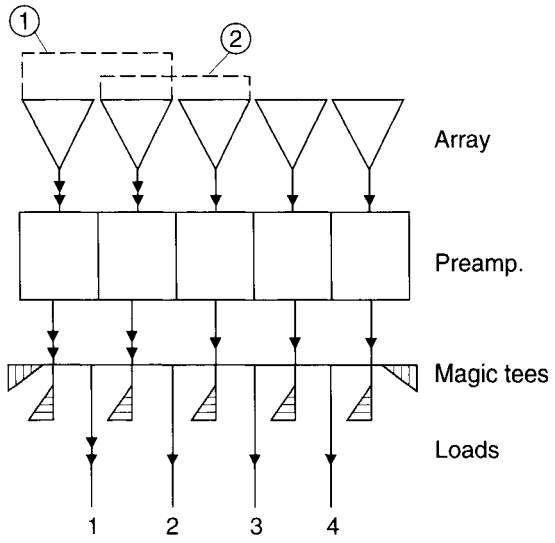

Fig. 11.27 Active multiple-channel primary feed with overlapping illuminations.

11.8 FURTHER TOPICS

11.8.1 Active modules

Passive and active phased arrays - requirements for modules

One of the principal applications of phased array antennas is in radar, offering advantages in respect of beam agility, adaptive pattern control and (ultimately) multiple simultaneous surveillance and tracking functions.

Phased array radars can be divided into two categories: passive phased arrays (Fig. 11.28a) use a single high-power transmitter, distributing the power to the individual array elements via a feed network incorporating phase shifters, and active phased arrays (Fig. 11.28b), in which each element or subarray has its own active module, comprising transmit power amplifier, phase shifter, receive low-noise amplifier, and possibly transmit upconverter/receive downconverter as well. Active phased arrays avoid the losses that occur in the feed network of a passive phased array. They also have reliability advantages, in that a fault in a single module does not cause a catastrophic failure of the whole radar (*graceful degradation*) and in that a failed module can be replaced without taking the entire radar out of commission. The principal disadvantage is that phased array active modules have proved expensive to develop, which probably accounts for the relative slowness of these concepts to find widespread use in practical radars.

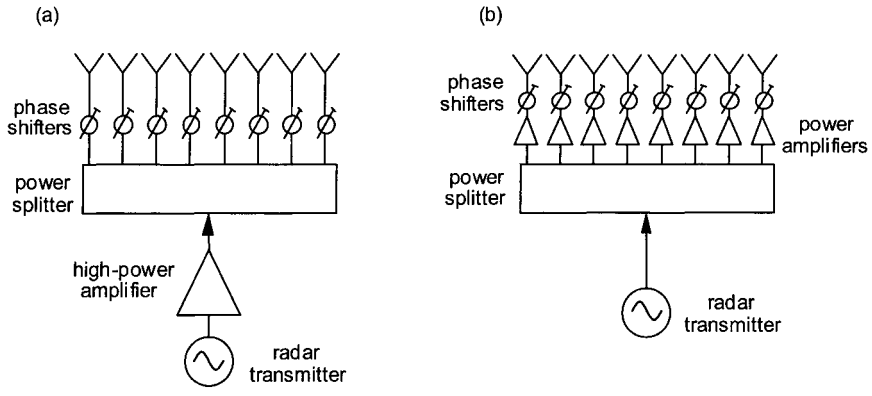

Fig. 11.28 (a) passive, and (b) active phased array antennas (shown in transmit mode).

Figure 11.29 shows a block diagram of a typical active phased array module. The interface and control signals that are needed to each module are: transmit and receive RF signals, phase shifter control, and dc supply. Alternatively, instead of the transmit and receive signals being at RF, these can be at IF, with a microwave local oscillator distributed to each module, or the local oscillator can even be in digital form. Clearly, the distribution of these signals to each module represents a technical challenge, and optical techniques represent an attractive option.

The entire module may be realized as a GaAs MMIC (or a small number of separate MMICs), with potential advantages of low production costs and high unit-to-unit reproducibility. Gallium Arsenide FET technology has advanced over the past decade or two to the point where power outputs of several watts at 10 GHz are achievable, and correspondingly more at lower frequencies. Figure 11.30 shows a typical module for an active phased array radar.

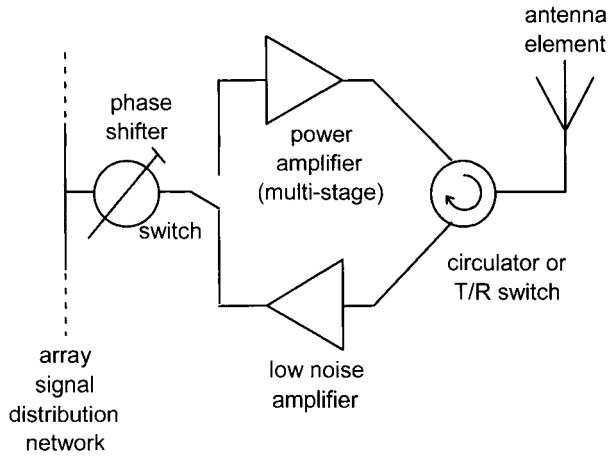

Fig. 11.29 Block diagram of a typical active phased array module.

Due to the finite efficiency of the power amplifiers (typically 40% at best), there will be a considerable amount of heat to be dissipated at the array face. Thus thermal design is also very important, particularly if the infra-red signature must also be minimized. It is also important that the phase and amplitude responses of the modules (for example, variations in power amplifier phase response due to thermal effects) track properly, particularly if low-sidelobe patterns are to be achieved.

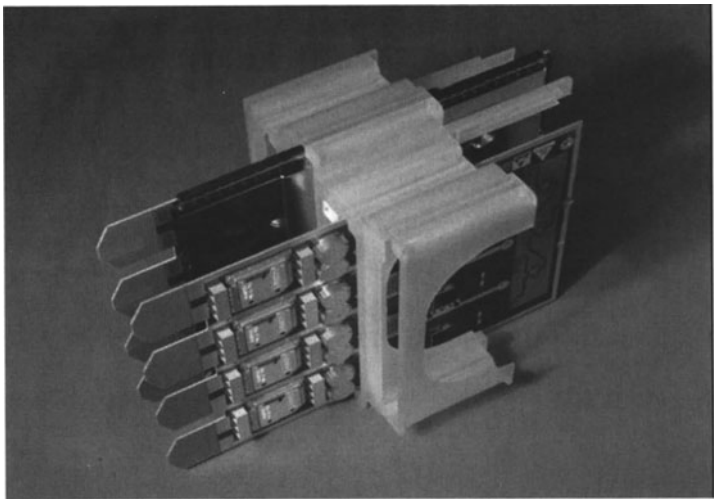

Fig. 11.30 Module for the SAMPSON active phased array radar (photo: AMS).

Optical control of phased arrays

As has already been remarked, the distribution of interface and control signals to the array modules represents a technical challenge, and some years ago[11] it was suggested that the use of optical fibres might provide a solution, avoiding the bulkiness, loss and weight of coaxial cables. In addition optical fibres are immune from electromagnetic interference.

The signals to be fed to each module are[12]:

- a microwave phase reference;
- a lower frequency transmit waveform;
- element control signals.

The corresponding output signals are:

- a received signal;
- element monitoring signals.

---

[11] Forrest, J.R., Richards, F.P., Salles, A.A. and Varnish, P., 'Optical fibre networks for signal distribution and control in phased array radars', *Proc. RADAR'82 Conference*, IEE Conf. Publ. No. 216, pp408-412, October 1982.

[12] Seeds, A.J., 'Optical technologies for phased array antennas'; *IECE Trans. Electronics*, Vol. E76-C, No. 2, pp198-206, February 1993.

Usually the transmit and received signals will be at IF, and the control and monitoring signals will be digital. Consequently, the most demanding signal distribution problem concerns the microwave phase reference.

Single-mode optical fibre is used, since this avoids the introduction of modal noise due to mechanical disturbance of the fibre. The losses of single-mode fibre are approximately 0.3 dB/km at 1.55 μm, and 3 dB/km at 850 nm. The microwave signal is intensity-modulated onto a semiconductor laser, and detected at the module, either using a photodiode, or directly controlling an oscillator device such as an IMPATT, bipolar transistor or MESFET. Modulation bandwidths of over 30 GHz have been reported. The advent of optical amplifiers means that optical transmission factors of greater than unity are possible, and this is important if the optical signal has to be split many ways to distribute the signal to a large number of modules.

It is also possible to use two optical sources phase locked together, such that their frequency difference forms the microwave signal (Fig. 11.31).

A more recent idea is to use direct digital synthesis within each module. This still requires the distribution of a high-frequency clock signal to each module, but gives enormous flexibility with respect to transmit signal generation, spatio-temporal coding (§14.2), and phase or true-delay beamforming.

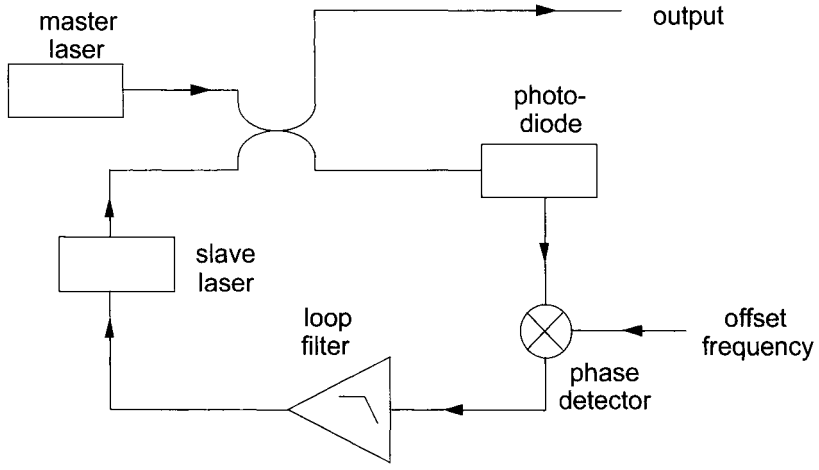

Fig. 11.31 Optical phase-locked loop, used to provide the microwave reference signal to a phased array module.

11.8.2 Digital beamforming

An important development over the past two decades or so has been the use of digital techniques for antenna beamforming, principally (though not exclusively) for receiving applications. Digital technology has obvious advantages in respect of flexibility, reliability and repeatability, and for these reasons there is a continuing trend to work with digital signals as early as possible in a receiving system. Essentially, the signal from each element of the array is digitized, and the phase and amplitude weighting performed by digital multiplication by a complex weight. The signals from all elements are then summed digitally, giving a number in digital form whose directional response is a function of the array geometry and the (digital) weights, in exactly the same way as with analogue beamforming.

The benefits offered by digital beamforming may be summarized as:

- the beam direction and shape may be varied very rapidly, in principle at the full digital clock rate, allowing digital implementations of the adaptive algorithms discussed in §14.4;
- it is possible to form multiple beams from a single array without the usual constraints on orthogonality (§11.7.3);
- the phase and amplitude errors of each receiver channel may be characterized and corrected, giving very accurate control of phase and amplitude, and hence of pattern shape and sidelobe level;
- in radar applications, the increased flexibility allows optimum use of available radar power and dwell time for surveillance and tracking functions, according to the particular scenario.

Implementation

A block diagram of a typical digital beamforming array is shown in Fig. 11.32. Each element (or subarray) feeds a dedicated receiver channel, providing amplification and selectivity. Note that the local oscillators must be coherent from one channel to another, so they are each derived from a single oscillator and distributed to each receive channel. The signal in each channel is digitized, usually in I/Q form at baseband. If the signal bandwidth is B, then the bandwidth of each of the I and Q channels is $B/2$. Hence the minimum (Nyquist) sample rate of the ADCs is B. The frequency and phase responses of the receiver channels must track closely, over the full dynamic range of signals to be handled, though if it can be arranged for calibration signals to be injected into each receive channel sequentially, any errors can be calibrated out. Also, errors in the complex downconverters must be kept to a low level - specifically the gains of the I and Q channels must be identical, they must be in exact phase quadrature, and there should be no dc offsets in the mixers.

Churchill et al.[13] have described a technique by which errors of these kinds may be characterized and corrected.

The desire to avoid such errors, and the advent of faster and faster ADCs, has led to the widespread use of direct digitization at IF (or even, ultimately at RF) with a single ADC per channel. This is helped by realizing that the Sampling Theorem (Nyquist) demands that the sample rate need only be at least twice the bandwidth of the signal to be sampled, rather than twice the highest frequency present. More specifically[14], the sample rate should respect

$$2B\left\{\frac{Q}{n}\right\} \leq f_s \leq 2B\left\{\frac{Q-1}{n-1}\right\} \qquad (11.113)$$

where the signal bandwidth $B = f_H - f_L$, $Q = f_H/B$, n is a positive integer and $n \leq Q$. The form of the subsequent digital processing to extract the baseband I and Q signals is described in many books on digital signal processing[15].

---

[13] Churchill, F.E., Ogar, G.W. and Thompson, B.J., 'The correction of I and Q errors in a coherent processor', *IEEE Trans. Aerospace & Electronic Systems*, Vol. AES-17, No. 1, pp131-137, January 1981.

[14] Glover, I.A. and Grant, P.M., *Digital Communications* (second edition), pp173-175, Pearson, Harlow, 2004.

[15] Mulgrew, B., Grant, P.M. and Thompson, J., *Digital Signal Processing - Concepts and Applications* (second edition), Palgrave MacMillan, Basingstoke, 2003.

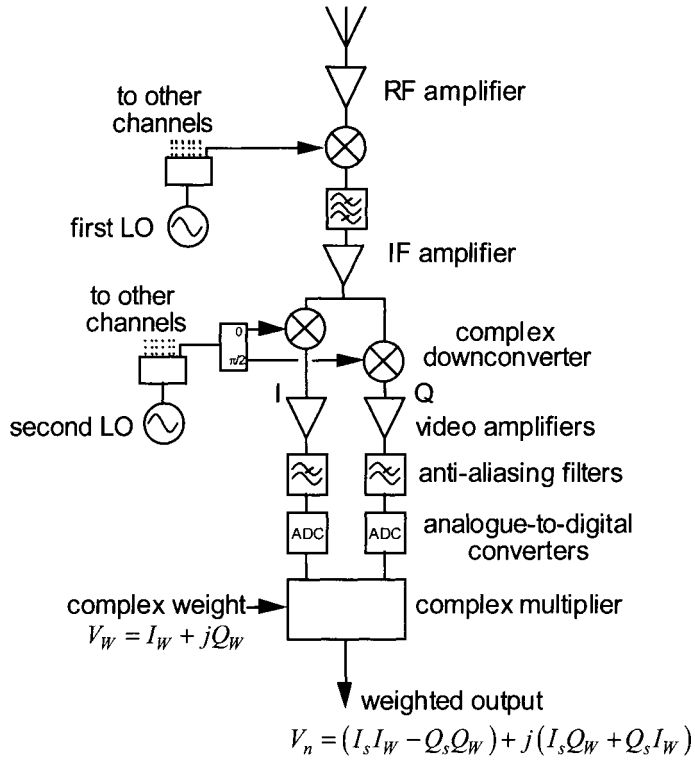

Fig. 11.32 Typical architecture of one channel of a digital beamforming receiver, with baseband digitization.

The weighting of the digitized signal, in amplitude and phase, is achieved as follows. Suppose that the baseband signal is represented by $V_s = I_s + jQ_s$ and the corresponding weight is $V_w = I_w + jQ_w$. The product of these is the weighted output from the nth channel

$$V_n = (I_s I_w - Q_s Q_w) + j(I_s Q_w + Q_s I_w) \tag{11.114}$$

The weighted outputs are then summed digitally to form the beam

$$V_b = \sum_n V_n \tag{11.115}$$

Of course, it is entirely possible to form more than one beam simultaneously from the same set of digitized signals V_s, in different directions and of different shapes.

The dynamic range of V_b depends on the number of receiver channels M of the array and the number of bits N of the ADCs. If the maximum voltage output per channel is A, then the maximum value of V_b is MA, corresponding to a power $(MA)^2/2$. The minimum power corresponds to the least significant bit of one ADC (allowing one bit for the sign), i.e. $\left(A/2^{N-1}\right)^2$. The dynamic range is the ratio of these two power levels, which is $2^{2(N-1)}M$, or

$$\left[6(N-1) + 10\log_{10}M\right] \text{ dB} \qquad (11.116)$$

Array calibration

To obtain the full benefit of a digital beamforming array it is necessary to calibrate out all the errors of the analogue parts of the system. The calibration routine consists of injecting a test signal into each receiving channel in turn, and measuring the amplitude and phase of the received signal. Any departures from the desired amplitude and phase can then be compensated using corrected digital weights. In general, the larger the part of the system that lies within the calibration loop, the better. The interval between calibrations will, of course, depend on the timescale on which the channel responses may be expected to vary.

There are several options:

(i) the calibration signals may be injected into each of the receiver channels, immediately behind the antenna elements. This is relatively simple to implement, but care must be taken in the design of the network that distributes the calibration signals;

(ii) the calibration signals may be obtained by one or more sources in the near field of the array. The different path lengths to the array elements and the difference in their amplitude responses are assumed known. This method requires very precise knowledge of the position of the calibration source, and the calibration source may even cause blockage of the aperture;

(iii) the same technique can be used with a source in the far-field. This avoids the variation in path length and amplitude responses of the array elements.

11.8.3 MEMS technology in phased arrays

MicroElectroMechanical Systems (MEMS) technology is a relatively recent development that has the potential to make a great impact in phased arrays. MEMS components were originally developed in the 1970s for applications such as accelerometers and other sensors, but in the early 1990s the technology began to be applied to RF switches, and eventually to phase shifters and other RF components. Essentially they consist of miniature devices that use mechanical movement to realize a short circuit or open circuit in a transmission line.

MEMS switches

The key MEMS component for phased array applications is the RF switch. The actuation mechanism is usually electrostatic, although thermal, magnetostatic or piezoelectric activation is also possible. They have been demonstrated at frequencies from DC to 120 GHz. Table 11.1, taken from reference [11], summarizes the properties of electrostatic MEMS switches compared to those of FET and PIN diode switches.

From this it can be seen that RF MEMS switches have very low power consumption, very high isolation and low loss, and excellent intermodulation performance. Furthermore, they can be built on glass or low-cost silicon substrates. Switches capable of 1-10 billion switching cycles are already available, and this is likely to be improved upon by a factor of 10 in the near future. However, their switching speed and power handling capability are inferior to PIN and FET switch technology.

Parameter	RF MEMS	PIN	FET
Voltage (V)	20-80	±3-5	3-5
Current (mA)	0	3-20	0
Power consumption (mW)	0.05-0.1	5-100	0.05-0.1
Switching time	1-300 μs	1-100 ns	1-100 ns
C_{up} (series) (fF)	1-6	40-80	70-140
R_s (series) (Ω)	0.5-2	2-4	4-6
Capacitance ratio	40-500	10	n/a
Cutoff frequency (THz)	20-80	1-4	0.5-2
Isolation (1-10 GHz)	very high	high	medium
Isolation (10-40 GHz)	very high	medium	low
Loss (1-100 GHz) (dB)	0.05-0.2	0.3-1.2	0.4-2.5
Power handling (W)	< 1	< 10	< 10
Third-order intercept point (dBm)	+66-80	+27-45	+27-45

Table 11.1. Performance comparison of FET, PIN and RF MEMS electrostatic switches.

There are various configurations of switches. Figure 11.33 shows a photomicrograph of one example, which is a series switch developed by the Rockwell Scientific Company[16]. This has what has been termed a 'clam shell' configuration, and is fabricated on a GaAs substrate, with a 2 μm layer of silicon dioxide deposited using

[16] Mihailovich, R.E., Kim, M., Hacker, J.B., Sovero, E.A., Studer, J., Higgins, J.A. and DeNatale, J.F., 'MEM relay for reconfigurable RF circuits', *Wireless Comp. Letters*, Vol.11, No.2, pp53–55, February 2001.

a low-temperature PECVD process onto the substrate. The top electrodes are 75 × 75 μm and are fabricated using a 250 nm layer of gold over a 1.2 μm thick PECVD silicon dioxide membrane. Quoted performance figures include switching time: 8–10 μs, loss: 0.1 dB (0.1–50 GHz) and isolation: 50 dB (4 GHz), 30 dB (40 GHz) and 20 dB (90 GHz).

RF MEMS phase shifters

Phase shifters can be built using switches to switch lengths of transmission line, in the usual way (§11.2.1). Figure 11.34 shows an example of a 2-bit phase shifter realized by the University of Michigan and Rockwell Scientific. This occupies an area of 9.6 mm^2. Measured performance at 10 GHz gives a phase accuracy of ±2 degrees, an average insertion loss of 0.55 dB, and a return loss of better than 14 dB.

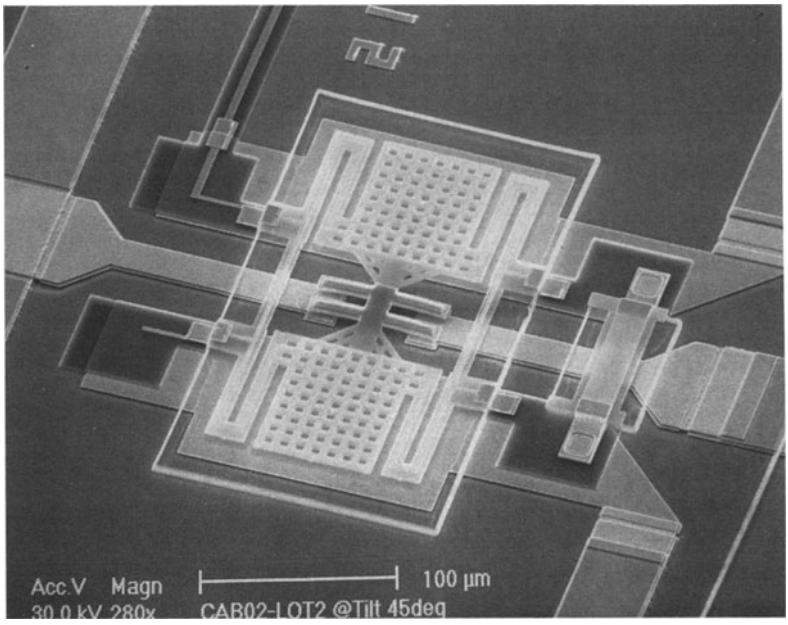

Fig. 11.33 Photomicrograph of a MEMS series switch (photograph: Rockwell Scientific Company).

Other MEMS components

It is also possible to realize other microwave components in MEMS technology, including tunable oscillators, tunable filters, physically movable antennas, and frequency selective surfaces.

There is no doubt that this technology will have a major impact on the development of future antenna array systems.

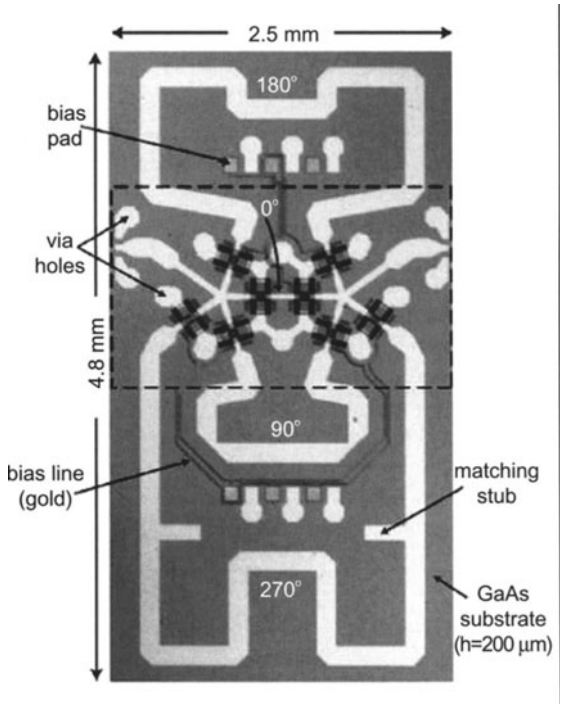

Fig. 11.34 RF MEMS phase shifter (photograph: Dr Gabriel Rebeiz).

11.8.4 Circular, cylindrical, spherical and conformal arrays

Circular and cylindrical arrays are used in applications that require coverage over the full 360° of azimuth. They also have some potentially-useful properties in respect of operation over wide instantaneous bandwidths. It is perhaps interesting to consider that the element density, when the array is viewed sideways-on, is greatest at the edges, effectively giving the array an inverse amplitude taper. Thus we might expect circular arrays to be good for direction-finding applications (where wide-spaced

elements give a high sensitivity of differential phase to signal direction), but not so good for forming low-sidelobe beams.

Beam cophasal excitation

The simplest method of feeding a circular array is simply to arrange for the signals from all the elements to add coherently in the particular direction of interest (Fig. 11.33). For omnidirectional elements, and assuming that the number of elements is large, this gives an azimuth-plane beam of the form

$$D(\theta) = \mathrm{J}_0\left(\frac{4\pi}{\lambda}\sin\frac{\theta}{2}\right) \qquad (11.117)$$

where θ is the azimuth angle, J_0 is the Bessel function of order zero, r is the array radius and λ is the wavelength. This is plotted in Fig. 11.35 for the case of an array of diameter 5λ.

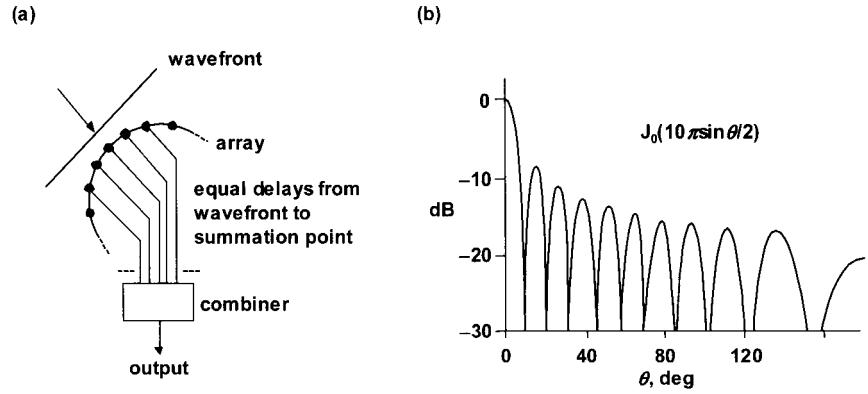

Fig. 11.35 (a) Beam cophasal excitation; (b) resulting radiation pattern (with no amplitude taper).

Whilst this form of excitation may be simple, steering of the beam (beyond limited scan) requires commutation of interlaced array sectors. In contrast with linear arrays, the pointing direction of the generated beam is *not* frequency dependent, but the use of phase shifters makes the beamwidth slightly frequency dependent, with an approximately quadratic variation. Moreover, the phase illumination of the array follows a rather complicated form.

A comparison between linear arrays and beam-cophasal excited circular arrays is given in Appendix A11.

Phase mode excitation

To overcome these limitations the idea of phase mode excitation was developed. Consider firstly a continuous circular array (i.e. one with an infinite number of elements and negligible interelement spacing), and suppose that the elements are omnidirectional. The excitation of the array F can be regarded as a periodic function of azimuth angle θ, of period 2π, and can therefore be expressed as a Fourier series

$$F(\theta) = \sum_{m=-N}^{N} C_m \exp(jm\theta) \tag{11.118}$$

Each term of the series is known as a *phase mode*, and the coefficient C_m (which is in general complex) is a *phase mode coefficient*. It can be seen that the zero-order phase mode ($m=0$) corresponds to an excitation of constant phase as a function of azimuth angle. The first-order phase mode ($m = 1$) corresponds to one cycle of phase over 360° of azimuth; the second-order phase mode ($m = 2$) corresponds to two cycles of phase over 360° of azimuth, and so on. The negative-order phase modes simply correspond to phase variation in the opposite sense.

When an array is excited by a single phase mode, the far-field pattern $D_m(\theta)$ has a similar form

$$\begin{aligned} D_m(\theta) &= C_m j^m \mathrm{J}_m(\beta r)\exp(jm\theta) \\ &= K_m \exp(jm\theta) \end{aligned} \tag{11.119}$$

where $\mathrm{J}_m(.)$ is the Bessel function of order m, $\beta = 2\pi/\lambda$, and r is the array radius.

The far-field phase modes are omnidirectional in azimuth, but each with the same characteristic variation of phase with azimuth angle as the corresponding excitation phase mode. The frequency-dependence of this expression is contained in the Bessel function, so for omnidirectional elements the variation of the phase mode amplitudes with frequency is as shown in the dotted responses of Fig. 11.36. For directional elements the corresponding expression is no longer a single Bessel coefficient, but a series of terms, each corresponding to the Fourier coefficients of the element pattern[17]. For the particular case of an element pattern of the form $(1 + \cos\theta)$, which is a reasonable approximation to many practical elements, the equivalent expression to (11.119) is

$$D_m(\phi) = C_m j^m \left[\mathrm{J}_m(\beta r) - j\mathrm{J}'_m(\beta r)\right]\exp(jm\theta) \tag{11.120}$$

---

[17] Rahim, T. and Davies, D.E.N., 'Effect of directional elements on the directional response of circular antenna arrays', *Proc. IEE*, Vol. 129, Pt. H., No. 1, pp18-22, 1982.

This gives a much flatter variation of phase mode amplitude with frequency, since the maxima of $J_m(\beta r)$ correspond to the zeroes of $J'_m(\beta r)$ (and vice versa), which is much more suitable for broadband operation (Fig. 11.36).

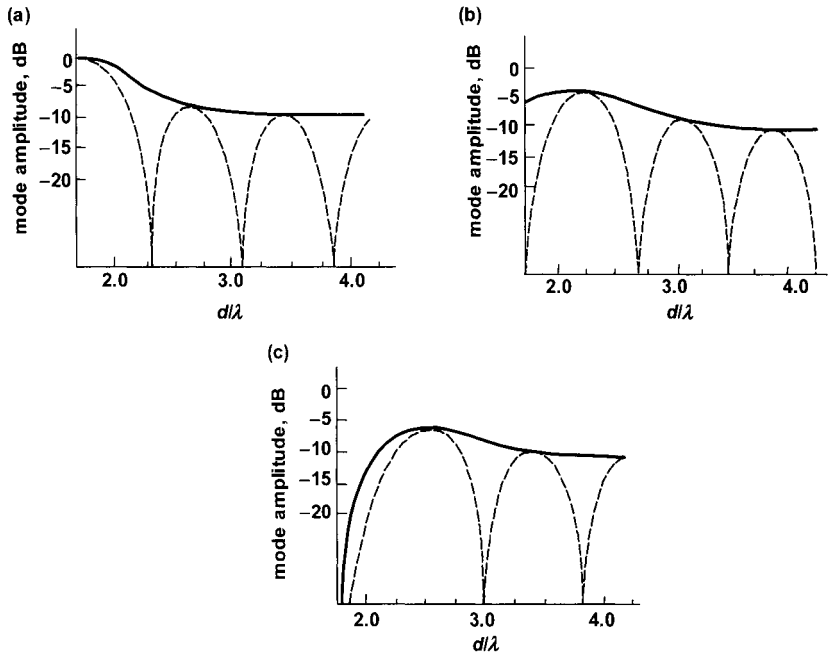

Fig. 11.36 Calculated variation of phase mode amplitude with frequency: (a) zero-order mode; (b) first-order mode; (c) second-order mode: ----- omnidirectional elements; ——— $(1 + \cos\theta)$ directional element patterns (after ref. 14).

When a discrete array is used exactly the same theory applies, but the excitation function $F(\theta)$ is sampled at the element locations by a sampling function $S(\theta)$. For an array of n omnidirectional elements

$$S(\theta) = \sum_{q=-\infty}^{\infty} \exp(jnq\theta) = 1 + \sum_{q=1}^{\infty} \exp(jnq\theta) + \sum_{q=-\infty}^{-1} \exp(jnq\theta) \qquad (11.121)$$

giving

$$D_m(\theta) = C_m j^m J_m(\beta r) \exp(jm\theta)$$

$$+\sum_{q=1}^{\infty} C_m j^{-g} \mathrm{J}_{-g}(\beta r)\exp(-jg\theta)$$
$$+\sum_{q=-\infty}^{-1} C_m j^{h} \mathrm{J}_{h}(\beta r)\exp(jh\theta) \qquad (11.122)$$

where $g = (nq-m)$ and $h = (nq+m)$.

The first part of this expression is identical to that for a continuous array (11.119). The two series represent ripple terms as a function of θ (spatial ripple). As a rule of thumb, to keep the spatial ripple acceptably low, the interelement spacing should be no greater than $\lambda/2$, which in practice provides an upper limit to the frequency of operation.

For an n-element array it is possible to generate $n+1$ phase modes, though the $+n/2$ and $-n/2$ phase modes are actually identical. The discrete Fourier Transform to generate the phase modes from the element signals is conveniently provided by a Butler Matrix. The bandwidth is usually limited to about one octave by that of the quadrature hybrid couplers that form part of the Butler Matrix, though with special-purpose components it is possible to improve upon this[18].

The behaviour of phase modes as a function of elevation angle can be understood by realizing that the zero-order mode is the co-phasal sum of all the element signals, so there is a maximum in the vertical direction, weighted by the element pattern in that direction. For all the other phase modes the element signals are summed with an integer number of cycles of phase, so there is a null in the vertical direction, irrespective of the element pattern.

As an illustration, Fig. 11.37 shows measured phase mode patterns of a 4-element circular array, at a frequency of 900 MHz. The array elements were $\lambda/4$ monopoles, and there was a single central monopole element which acted as a reflector, giving the other elements a more directional pattern and hence improving the bandwidth of operation. The characteristic variation of phase with direction is clearly evident, as well as the spatial ripple due to the discrete nature of the array.

---

[18] Withers, M.J., 'Frequency-insensitive phase-shift networks and their use in a wide-bandwidth Butler matrix', *Electronics Letters*, Vol. 5, No. 20, pp496-497, October 1969.

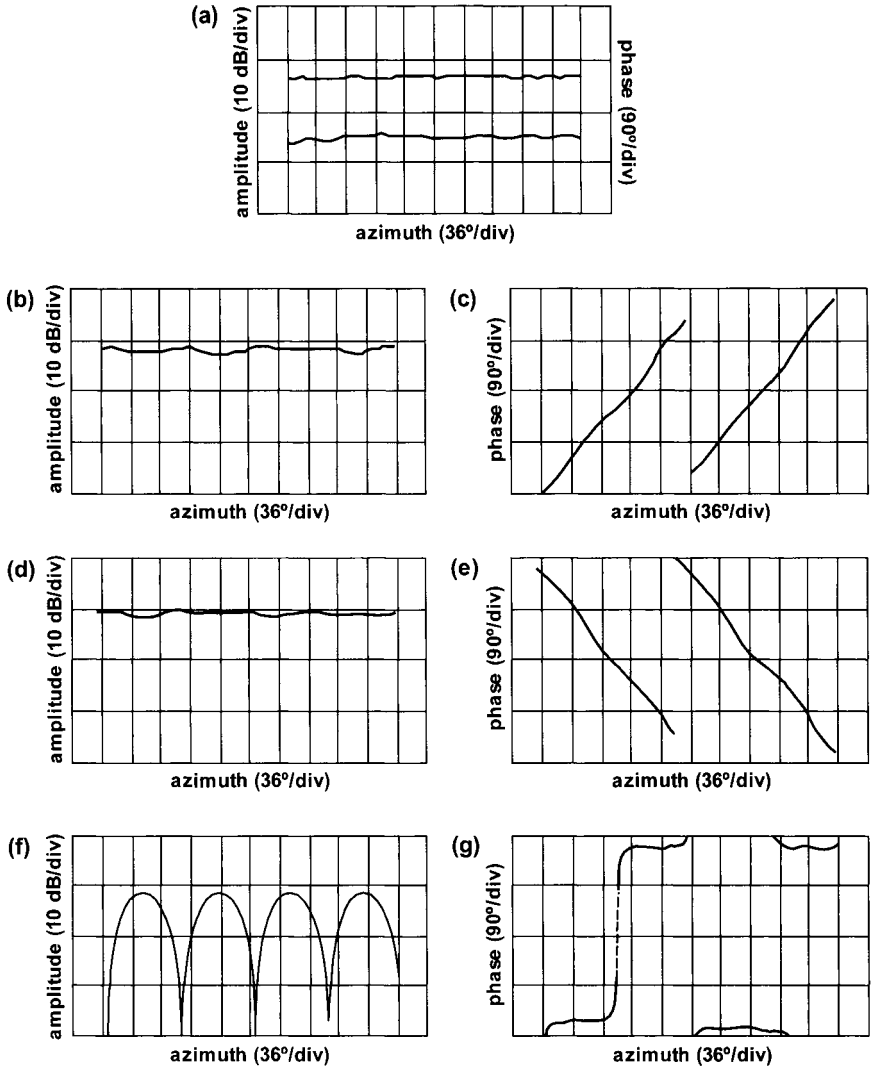

Fig. 11.37 Measured phase mode patterns of a 4-element circular array of monopole elements, at a frequency of 900 MHz, as a function of azimuth angle: (a) zero-order mode amplitude (upper) and phase (lower); (b) +1 order mode amplitude; (c) +1 order mode phase; (d) −1 order mode amplitude; (e) −1 order mode phase; (f) second-order mode amplitude; (g) second-order mode phase. Amplitude: 10 dB/div; phase 90°/div.; horizontal scale (azimuth angle) in each case 36°/div.

Null steering

A plane wave incident on the array will excite all phase modes simultaneously. Suppose that the zero-order phase mode and first-order phase mode are equalized in amplitude and added together (Fig. 11.38). It is easy to see that there is one direction in which they will cancel, giving a single null. The direction of this null can be steered by inserting a phase shifter in one of the paths, and the null direction is given directly by the setting of the phase shifter. Furthermore, if the phase mode coefficients K_m can be characterized and compensated by means of networks with appropriate transfer functions, then the null shape and direction can be maintained over the full instantaneous bandwidth of the array.

These results hold for any two phase modes whose orders differ by one.

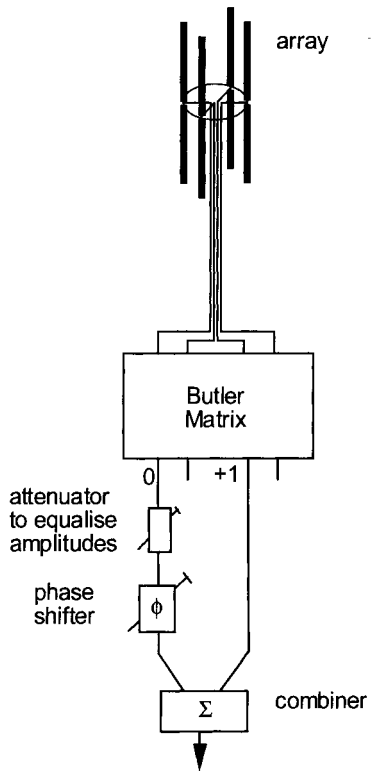

Fig. 11.38 Null-steering with a four-element circular array.

Direction finding

In a rather similar way, if the phase difference is measured between two adjacent phase modes when a plane wave is incident on the array, this phase difference provides a direct reading of the direction of arrival of the signal (Fig. 11.39), and the same comments about broadband operation apply. In fact, if phase modes whose orders differ by two are chosen, then the sensitivity is increased by a factor of two, but at the expense of introducing a 180° ambiguity (which can be resolved by the original measurement). As an example, an experimental system based on this principle has been constructed and demonstrated, operating over the band 2–30 MHz[19], and has been produced commercially.

It is also possible to use superresolution direction finding techniques with phase modes; this is discussed in §14.6.5.

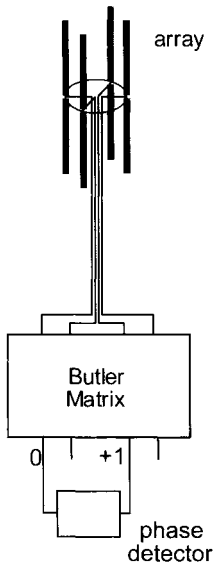

Fig. 11.39 Direction finding: a plane wave incident on the array will excite all phase modes simultaneously. The phase difference between two adjacent phase modes will provide a direct indication of the direction of arrival of the signal. Greater sensitivity (at the expense of ambiguity) can be obtained by using phase modes whose orders differ by more than one, and the ambiguities resolved by lower-order comparisons.

[19] Cvetkovic, M., Davies, D.E.N., Griffiths, H.D. and Collins, B.S., 'An HF direction-finding and null steering system employing a four-element circular array', *Proc. 4th IEE Intl. Conference on HF Radio Systems and Techniques*, London; IEE Conf. Publ. No. 284, pp221-225, April 1988.

Pattern synthesis

The results quoted above for null steering are an example of a much more general application of phase modes to synthesize radiation patterns. Davies[20] showed that phase modes may be treated in the same way as the elements of a uniformly-spaced linear array, and all the techniques developed for linear array pattern synthesis may be applied to circular arrays, subject to the following comments.

- Phase modes are omnidirectional in azimuth, so the 'elements' are also omnidirectional. The radiation pattern of the circular array corresponds to the array factor of the linear array.
- Phase modes are orthogonal (since they are the outputs of a discrete Fourier Transform), so there is no mutual coupling.
- The radiation patterns have the same shape (in θ space) as those formed by a linear array (in $kd\sin\theta$ space) with an interelement spacing of $\lambda/2$, independent of frequency.
- For a discrete array, exciting a single mode port excites a periodic sequence of modes. For example, if the +1 mode is excited on a four element array, the −7, −3, +5, and +9 modes are also excited. These additional harmonics correspond to additional linear array 'elements'.

As an example, Fig. 11.40 shows an example of an instantaneously broadband beam pattern with <−20 dB sidelobes, formed in this way from a four-element array of monopole elements, measured over the frequency band 8–12 GHz.

Isolated omnidirectional patterns

A further property of circular arrays excited by means of phase modes is that there is high isolation between the individual phase mode ports of the Butler Matrix (§11.7.3). This arises because of the orthogonality property of the Discrete Fourier Transform. The phase modes therefore act as isolated omnidirectional patterns, potentially over a broad bandwidth. In practice, imperfections in the Butler Matrix and variations in the impedances presented by the array elements limit the isolation, but it is easy to obtain 20 or 30 dB of isolation without taking any special precautions. The bandwidth is usually limited by that of the Butler Matrix to an octave or so.

A particular application for this idea lies in radiocommunications base stations, where it is desired to multiplex several transmitters to the same antenna, with each

[20] Davies, D.E.N., 'A transformation between the phasing techniques required for linear and circular aerial arrays', *Proc. IEE*, 1965, Vol. 112, No. 11, pp2041-2045.

having an omnidirectional pattern[21]. Each transmitter is fed to one phase mode port of the Butler Matrix feeding the array. This considerably relaxes the specification on any multiplexing filters that are used.

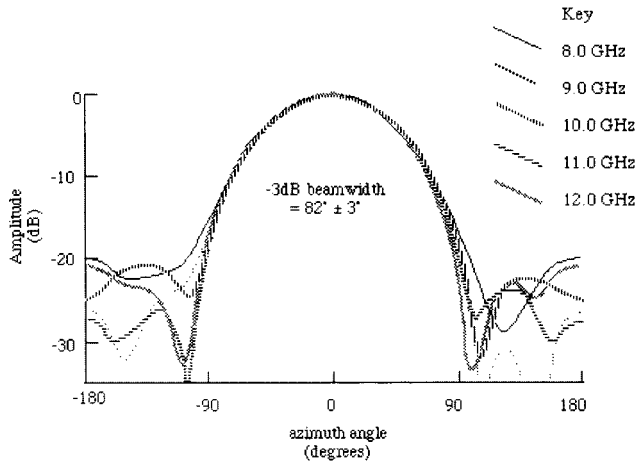

Fig. 11.40 Example of instantaneously broadband beam pattern synthesized over the band 8–12 GHz, using a 4-element array of monopoles.

Sectoral phase modes[22]

Whilst the omnidirectionality property of phase modes is in most cases an attraction, there may be instances where it is a disadvantage, for example in DF applications where there is more than one co-channel signal present. In fact, in the phase-comparison DF scheme of Fig. 11.39, when a 15 dB weaker co-channel signal is also received by the array, the worst-case DOA error is $2\arcsin 10^{-15/20} = 20.5°$.

There is therefore some attraction in the ability to form two sets of multibeam patterns, such that each angular sector is covered by a pair of low-sidelobe beams with linear and opposite phase slopes. Amplitude comparison may then be used to unambiguously determine the angular sector facing the incident signal, while a more accurate bearing is obtained by detecting and comparing the phases of the two directional beams covering that sector, just as with ordinary phase modes, but with a

---

[21] Guy, J.R.F. and Davies, D.E.N., 'Novel method of multiplexing radiocommunication antennas using circular array configuration', *Proc. IEE*, 1983, Vol. 130, Pt. H, No. 6, pp410-414.

[22] Griffiths, H.D. and Eiges, R., 'Sectoral phase modes from circular antenna arrays'; *Electronics Letters*, Vol.28, No.17, pp1581–1582, August 1992.

much-reduced susceptibility to out-of-sector interference. Such patterns are known as sectoral phase modes.

Excitation scheme: A pair of beams in direction $\phi_m = (2\pi/M)m$, $m = 0,...,M-1$ sharing the same directional amplitude pattern and characterized by equal but opposite phase slopes may be approximately synthesized by linearly combining a set of symmetrically-weighted but asymmetrically-numbered phase modes

$$F_{m1}(\phi) = \sum_{\mu=-L}^{L-L_0} a_l + e^{j(2\pi/M)m\mu}\, \Phi_\mu(\phi,\omega)/K_{\mu 0}(\omega) \Lambda A(\phi - 2\pi m/M)\, e^{(L_0/2)(\phi-2\pi m/M)} \tag{11.123}$$

$$F_{m2}(\phi) = \sum_{\mu=-L+L_0}^{L} a_l - e^{j(2\pi/M)m\mu}\, \Phi_\mu(\phi,\omega)/K_{\mu 0}(\omega) \Lambda A(\phi - 2\pi m/M)\, e^{-(L_0/2)(\phi-2\pi m/M)} \tag{11.124}$$

where

$$l^{\pm} = \mathrm{Int}\left(|\mu \pm L_0/2| + 1/2\right) \tag{11.125}$$

$$A(\phi) = a_0 + 2\sum_{l=1}^{L-\mathrm{Int}(L_0/2)} a_l \cos l\phi \tag{11.126}$$

$L < M/2$, $0 < L_0 < 2L$ and for an odd L_0: $a_0 = 0$. Under uniform excitation $A(\phi)$ becomes

$$A(\phi) = \sin\left[(2L - L_0)\phi/2\right]/\sin(\phi/2) \tag{11.127}$$

and its null-to-null beamwidth is $4\pi/(2L - L_0) < 4\pi/M$. A proper coverage of an angular sector of $2\pi/M$ radians is this ensured with a sidelobe level of approximately –13.5 dB. This may of course be improved, at the expense of an increased beamwidth, by applying an amplitude taper to the combined phase modes. Because each pair of synthesized patterns cover one of M angular sectors but otherwise behave as omnidirectional phase modes we have named them 'sectoral phase modes' or SPM beams.

Both the amplitude pattern $A(\phi)$ and the phase slope of SPM beams are affected by the choice of L_0. The larger L_0, the less directional are the beams but the steeper are their phase slopes. At the extreme, $L_0 = 2L$ and the two beams are simply the two omnidirectional phase modes Φ_{-L} and Φ_L. Thus, whereas the highest DF accuracy but poorest immunity is achieved by comparing the phases of the highest-order modes of the set $\Phi_{-L},...,\Phi_0,...,\Phi_L$, best immunity but least accuracy results

from the comparison of two SPM beams with $L_0 = 1$. In the latter case the respective phase slopes of the two compacted beams are 1/2 and –1/2, and

$$\arg F_{m1}(\phi) - \arg F_{m2}(\phi) = \phi - 2\pi m/M \qquad (11.128)$$

Naturally, the viability of the proposed SPM scheme for a wideband DF system depends on wideband alignment of the omnidirectional phase modes. As shown above, this has been demonstrated for a circular array of directional elements with an analogue beamformer, and can also be implemented in a digital beamforming network by appropriate filtering.

Null-steering enhancement: The need for a radiation pattern with a steerable null arises in both communication and DF applications, where the receiving array has to reject unwanted interference or jamming signals. Classically, a circular array pattern null may be synthesized by the subtraction of adjacent phase modes (Fig. 11.38) and steered by an intermediate phase shift β

$$\Phi_\mu / K_{\mu 0} - e^{j\beta}\Phi_{\mu+1} \Big/ K_{(\mu+1)0} \;\Lambda 2e^{-j\mu\phi}e^{-j(\phi-\beta-\pi)/2}\sin(\phi-\beta)/2 \qquad (11.129)$$

The nulled phase modes can then be linearly combined by an inverse DFT to yield a multiple pattern of M directional beams. The pattern formed at $\phi = \beta$ is, however, shared by all the directional beams, which for some applications may be somewhat restrictive. Additional independently-steered nulls may be incorporated in the system (at the expense of wider beams) but they too will be shared by all the beams.

Here we consider an alternative multibeam nulling scheme. Instead of combining adjacent phase modes, the same nulling concept is applied to M pairs of SPM beams characterized by $L_0 = 1$

$$F_m = F_{m1} - e^{j\beta_m}F_{m2} \;\Lambda 2e^{j(\beta_m+\pi)/2}A(\phi - 2\pi m/M)\sin(\phi - \beta_m - 2\pi m/M)/2 \qquad (11.130)$$

where $A(\phi)$, F_{m1} and F_{m2} $(0 \le m \le M-1)$ are given by eqns. (11.126), (11.123) and (11.124) respectively. By controlling the M phase shifts $\{\beta_m\}_{m=0}^{M-1}$ the proposed modified configuration allows each directional beam to independently steer its own null.

Simulated examples: Fig. 11.41 displays the two amplitude plots and the comparative phase response for a pair of SPM beams, formed from a 16-element circular array by combining two sets of 14 phase modes each with low-sidelobe weighting. The comparative phase response is nearly linear with a slope of approximately unity over an angular sector larger than $\pm 360^\circ/32 = 11.25^\circ$.

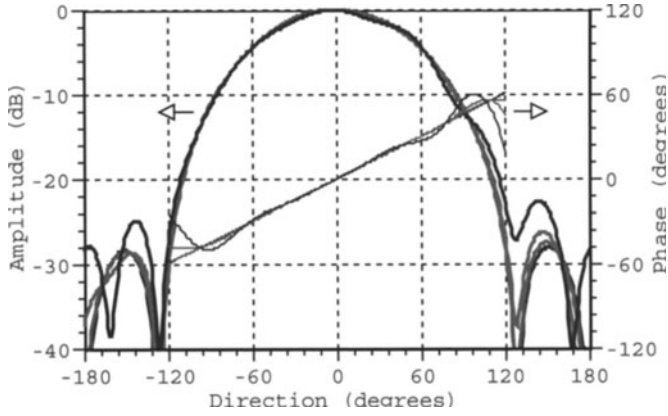

Fig. 11.41 Comparative phase plot and amplitude patterns for a pair of SPM beams formed by aligning and combining phase mode sets $\{\Phi_{-7}/K_{(-7)0},...,\Phi_6/K_{(6)0}\}$ and $\{\Phi_{-6}/K_{(-6)0},...,\Phi_6/K_{(7)0}\}$ in a 16-element array with interelement spacing of 0.4 wavelengths and element power pattern of $\cos^2\phi/2$. Mode weighting (in dB): { −15.5 −12.8 −8.3 −4.7 −2.3 −0.7 0 −0.7 −2.3 −4.7 −8.3 −12.8 −15.5}.

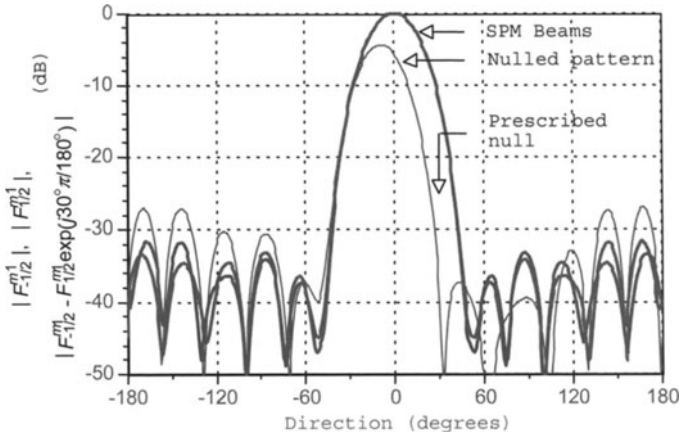

Fig. 11.42 Directional beam with prescribed pattern null at close to 30° formed by phased subtraction of two SPM beams.

The amplitude patterns, which are almost identical, both drop to a peak sidelobe level less than –31 dB outside an angular region of ±43°. A directional beam with a

pattern null is shown in Fig. 11.42. This pattern is synthesized by applying a phase shift of 30° to one of the SPM beams and subtracting it from the other. The result is a $\sin\phi/2$-type null at $\phi = 32.3°$.

Conclusions: A simple circular array scheme for synthesizing broadband directional beams with phase-mode-like phase behaviour has been presented. Such beams may be formed by linearly combining a set of aligned phase modes, and it has been shown that they may be beneficially applied to modally-based DF and null-steering systems.

Spherical phase modes[23]

The preceding sections have demonstrated a wide range of applications of circular arrays (and by extension, of cylindrical arrays). It is interesting to consider whether the same properties may be shown by spherical arrays, considering their excitation in terms of spherical harmonics.

Consider an excitation function $E(\theta',\phi')$ on the surface of a sphere (Fig. 11.43), and consider one spherical harmonic term (spherical phase mode) $Y_{l'}^{m'}$ of this excitation, with $Y_l^m(\theta,\phi)$ defined as

$$Y_l^m(\theta,\phi) = \sqrt{\frac{(2l+1)(l-m)!}{4\pi(l+m)!}} P_l^m(\cos\theta) e^{jm\phi} \tag{11.131}$$

where the associated Legendre functions P_l^m mean that the amplitude of the spherical harmonics are a function of direction. The directional dependence of phase is given by the exponential term, and the name 'spherical phase mode' is justified by analogy with their circular array counterparts.

The far-field radiation pattern is given by

$$D(\theta,\phi) = \frac{1}{4\pi} \iint_{s'} Y_{l'}^{m'}(\theta',\phi') e^{j\beta a\cos\psi} ds' \tag{11.132}$$

where a is the radius of the sphere, $\beta = 2\pi/\lambda$ and λ is the wavelength. The plane waves in the far field can be expanded into a sum of partial waves using Bauer's formula:

$$e^{j\beta a\cos\psi} = \sum_{l=0}^{\infty} (2l+1) j^l \hat{\mathrm{J}}_l(\beta a) \mathrm{P}_l(\cos\psi) \tag{11.133}$$

---

[23] De Witte, E. Griffiths, H.D. and Brennan, P.V., 'Phase mode processing for spherical antenna arrays', *Electronics Letters*, Vol.39, No.20, pp1430-1431, 2 October 2003.

where $\hat{\mathrm{J}}_l$ is a spherical Bessel function of the first kind and P_l a Legendre polynomial, both of order l[24]. Also, using the addition theorem to expand the Legendre zonal harmonics into spherical harmonics

$$\mathrm{P}_l(\cos\psi) = \frac{4\pi}{2l+1}\sum_{m=-l}^{l} Y_{l'}^{m'*}(\theta',\phi')Y_l^m(\theta,\phi) \tag{11.134}$$

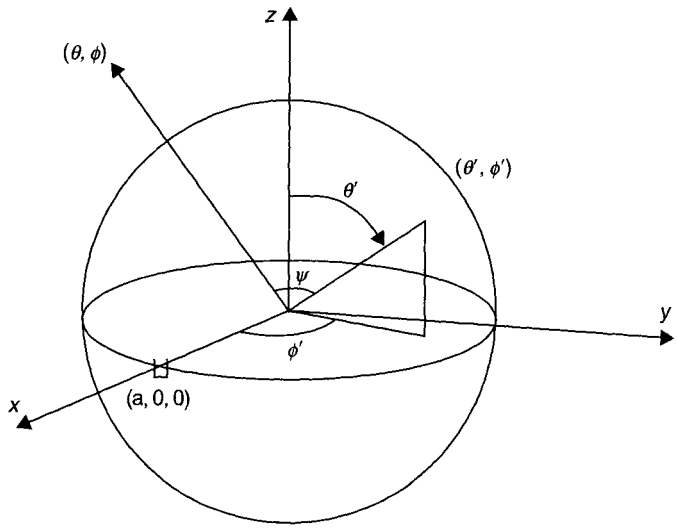

Fig. 11.43 Spherical array geometry.

The far field becomes:

$$D(\theta,\phi) = \sum_{l=0}^{m}\sum_{m=-l}^{l} j^l \hat{\mathrm{J}}_l(\beta a) Y_l^m(\theta,\phi) \underbrace{\iint_{s'} Y_{l'}^{m'*}(\theta',\phi')Y_l^m(\theta,\phi)ds'}_{\delta_{ll'}\delta_{mm'}} \tag{11.135}$$

where we have used the orthogonality property of spherical harmonics over the sphere. Finally, we obtain the far field

---

[24] Gradshteyn, I.S. and Ryzhik, I.M., *Tables of Integrals, Series and Products*, Academic Press, 1980.

$$D(\theta,\phi) = j^{l'}\hat{\mathrm{J}}_{l'}(\beta a)Y_{l'}^{m'}(\theta,\phi) \qquad (11.136)$$

In this result we recognise the same spherical harmonic $Y_{l'}^{m'}$ of the excitation, which shows that a spherical phase mode of the excitation function results in a far field radiation pattern with the same spherical phase mode form, just as with circular arrays.

Discrete spherical arrays: A practical array will consist of discrete elements whose effect can be represented as the product of the spherical harmonic Y_l^m with a sampling function $S(\theta,\phi)$. The sampling function can take various forms; one example is a weighted equiangular sampling grid of spatial bandwidth B, which has an azimuthal angle between elements of π/B and an elevation angle between elements of $\pi/2B$. For an equiangular topology of $2B \times 2B$ elements it has been shown[25] that any function of spatial bandwidth $l_{\max} \le B$ can be perfectly reconstructed from its $4B^2$ samples. Furthermore, for this element distribution, the far field can be evaluated analytically. It can be shown that this element distribution, when excited according to a particular harmonic, radiates a far field that consists of the same harmonic, together with higher order harmonics (perturbation states). The latter are heavily attenuated by the spherical Bessel factor from equation (11.136), which in turn depends on the ratio of the wavelength to the radius of the sphere.

Fig. 11.44 shows an example to verify the preceding theory. Figure 11.44(a) shows a spherical harmonic of a continuous excitation, corresponding to $l = 3$, $m = 2$ in equation (11.136), with $a = 0.5$ m and $\lambda = 0.15$ m. Figure 11.44(b) shows the calculated far field pattern from a discrete set of elements on the same sphere. Each element radiates a weighted sample of the continuous function Y_3^2. The sample grid has a spatial bandwidth $B = 32$. The far field is calculated with the equivalent Riemann sum of equation (11.132):

$$D(\theta,\phi) = \frac{\sqrt{2}}{4B}\sum_{j=0}^{2B-1}\sum_{k=0}^{2B-1} a_j^{(B)} Y_l^m(\theta_j,\phi_k)\, e^{j\beta a\cos\psi} \qquad (11.137)$$

where the sample points are taken on the weighted equiangular grid $\theta_j = \pi j/2B$, $\phi_k = \pi k/B$, and the weights $a_j^{(B)}$ account for the $\sin\theta$ factor in the continuous integral formulation $(ds' = \sin\theta d\theta d\phi)$.

---

[25] Driscoll, J.R. and Healy, D.M. Jr., 'Computing Fourier transforms and convolutions on the 2-sphere', *Adv. Appl. Math.*, Vol.15, pp202-250, 1994.

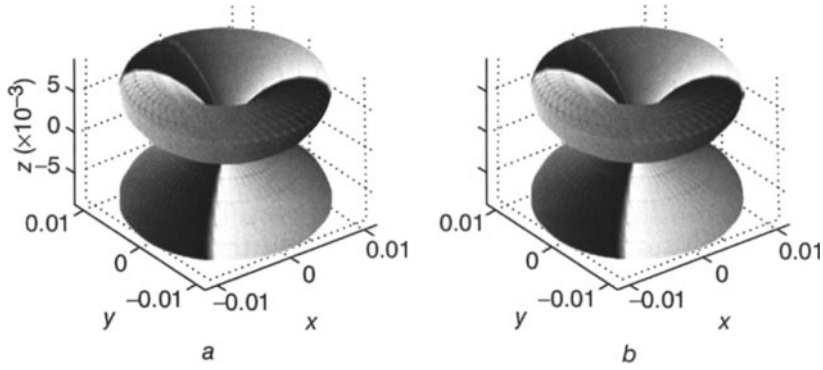

Fig. 11.44 Spherical harmonic Y_3^2 and corresponding far field pattern from sampled array. In both cases phase is represented on grey scale. (a) theoretical spherical harmonic; (b) calculated far field.

Practical implementations and applications: In a practical implementation the spherical phase modes may be generated by a stage of discrete Fourier transforms followed by a Legendre transform. The latter projects the sample vectors onto the associated Legendre functions. A bank of Butler matrices can implement the first stage. The output is a set of sample vectors for every value of m. The second stage can be implemented partially in the digital domain by first projecting the sample vector onto a cosine or sine base, depending on m, with Discrete Cosine and Discrete Sine transforms. The rest of the processing can be done digitally. As the number of nonzero terms in this projection is equal to the order l of the associated Legendre functions, this technique would minimise the number of A/D converters for a given spherical bandwidth.

In[17] it was shown how the use of directional element patterns improves the bandwidth of planar circular arrays. A similar observation is made for spherical arrays. Here the raised cosine patterns are rotated around the normal axis of the elements on the sphere. Since these patterns can be achieved by the mismatch with direction of circularly-polarised radiation and circularly-polarised elements, it can be anticipated that such elements will be optimum with spherical phase mode excitations.

Spherical phase modes generated in this way should be usable in all of the direction finding, null steering and pattern synthesis applications described earlier, in azimuth and elevation rather than just in azimuth. It is suggested that one of the more immediate applications might be to broadband beamforming and superresolution direction finding.

Conformal arrays

Conformal arrays are the most general type of phased array, and can be defined as an array whose elements are mounted flush on a non-planar surface. They have particular applications in arrays for missiles or high-speed aircraft, and also in systems that require wide-angle coverage. Some of their properties, advantages and disadvantages may be summarized as:

- because the elements are mounted flush on the surface, there is no aerodynamic drag;
- the error in scan angle that occurs with a radome in a linear or planar array is eliminated or reduced;
- since the array is three-dimensional it can be difficult to ensure that all elements radiate the same polarization. It is possible to use circular polarization, but it is not easy to obtain an element pattern that remains perfectly circularly polarized over a wide angle;
- it is difficult to etch elements on singly- or doubly-curved surfaces.

The techniques used in the design of conformal arrays are described in detail by Borgiotti[26]. A modern concept for the use of conformal arrays is the so-called 'smart skin', in which the surface of a platform is covered with antenna elements which form an array which can be used for a variety of applications in radar, communications, etc. The concept has some synergy with the waveform diversity techniques described in §14.7.11.

11.8.5 Sparse and random arrays

Introduction

The interelement spacing in a conventional array is constant. In these so-called 'regular' arrays the spacing should be of the order of $\lambda/2$, to avoid grating lobes (§11.3.4). This means that their various properties, such as the number N_0 of elements, the 3 dB beamwidth $\theta_{3\text{dB}}$, the maximum gain G, are closely interrelated. For example, for a uniformly illuminated planar circular array with diameter D and N_0 elements each of gain g, we have the following approximate relationships.

---

[26] Borgiotti, G., 'Conformal arrays', Chapter 11 in *The Handbook of Antenna Design*, Vol.II, A.W. Rudge, K. Milne, A.D. Olver and P. Knight eds, Peter Peregrinus, Stevenage, 1983.

$$N_0 = \pi \frac{D^2}{\lambda^2} \quad , \quad \theta_{3dB} = \frac{\lambda}{D} = \sqrt{\frac{\pi}{N_0}} \quad , \quad G = N_0 g \qquad (11.138)$$

On the other hand, in order to lower the close-in sidelobes, it is necessary to apply an amplitude weighting function.

Several practical considerations lead us to seek a means of choosing these parameters more independently of each other. One reason results from the use of active modules on transmission. Such amplifiers are usually used in class C for maximum output power, so that amplitude weighting of the array is not practicable. To reduce the level of close-in sidelobes we can vary the *density* of elements, i.e. the number of elements per unit area, so that the density is reduced towards the periphery of the array.

A second reason is that of economy; the cost of an array depends on the number of radiating elements. This fixes the maximum gain G of the antenna. If the number of elements N is fixed, what is the optimum spatial arrangement of the modules ? By spreading the elements in this way the dimension D of the antenna is increased. This results in an increase in the main lobe directivity and hence in the resolving power (§13.2.2)

In some systems, such as bistatic radars or telecommunications systems, it is useful to optimize independently the transmitting and receiving antenna characteristics. In transmission, *gain* is an essential characteristic., On receive, an array is immersed in a complex environment of wanted signals and parasitic signals. The most important characteristic is then *the angular resolution*; this can be improved by use of *sparse arrays*.

In Chapter 14 (Signal Processing Antennas), we define the concept of *non-redundant* array which, although irregular, cannot be considered as 'sparse'. We will also see that, in certain cases, *multiplicative arrays* allow great savings to be made in the number of elements, whilst still giving good directivity.

All these examples show that the quality criteria for the transmit antenna pattern cannot simply be transposed to the case of the receiving antenna.

Synthesis techniques for irregular arrays

An irregular array is, by definition, sparse, because it is ineffective to use an interelement spacing of less than $\lambda/2$. The array is characterized by two factors: the dispersion rate Δ and the spatial distribution function of the elements.

The dispersion rate is the ratio $\Delta = N_0/N$, where N is the number of elements, and N_0 the number that the array would have if it were fully-populated (non-sparse), with an interelement spacing of $\lambda/2$. In the case of an array occupying an area S, we have

$$N_0 = \frac{4S}{\lambda^2} \quad \text{and} \quad \Delta = \frac{4S}{N\lambda^2} \qquad (11.139)$$

The spatial distribution function is chosen from an enormous number of possible functions, equal to the number of combinations of N elements in N_0 possible positions

$$C_{N_0}^{N} = \frac{N_0!}{N!\ (N_0 - N)!} \tag{11.140}$$

Example: $N_0 = 20$, $N = 10$, $\Delta = 2$, $C_{N_0}^{N} = \dfrac{20!}{(10!)^2} = 184{,}756$

To help make this choice we can start from the idea explained in the introduction, i.e. to vary the element density according to a weighting function chosen at the outset. In this case the position of the elements can, in principle, be fixed deterministically. This method was originally reserved for 'small' arrays. We will now consider statistical (or probabilistic) methods.

Statistical methods

There exist several types of statistical method. We present here one inspired by that due to Skolnik, Sherman and Ogg[27].

Principle: Consider an array which, if it were fully populated, would have N elements. The thinned array is obtained by 'turning off' or 'leaving on' the elements (of equal amplitude), following a random process. We arrange that the average value of the illumination function follows a reference taper function chosen at the beginning.

Let a_n $(0 \le a_n \le 1)$ be the amplitude taper of the fully populated array. We choose a random binary amplitude excitation $\tilde{a}_n$ with the following probability distribution

$$\begin{aligned} \tilde{a}_n &= 1 \quad \text{with probability } a_n \\ \tilde{a}_n &= 0 \quad \text{with probability } 1 - a_n \end{aligned} \tag{11.141}$$

The random variable $\tilde{a}_n$ therefore has an average value

$$\langle \tilde{a}_n \rangle = 1 \times a_n + 0 \times (1 - a_n) = a_n \tag{11.142}$$

and second order moment

$$\langle \tilde{a}_n^2 \rangle = 1^2 \times a_n + 0^2 \times (1 - a_n) = a_n \tag{11.143}$$

---

[27] Skolnik, M.I., Nemhauser, G. and Shermann, J.W., 'Dynamic programming applied to unequally spaced arrays, *IEEE Trans. Antennas & Propagation*, Vol. AP-12, 1964.

Dispersion rate Δ: The number $\tilde{N}$ of elements turned on is also a random variable

$$\tilde{N} = \sum_{n=1}^{n=N_0} \tilde{a}_n \tag{11.144}$$

whose average value is

$$N = \langle \tilde{N} \rangle = \sum_{1}^{N_0} a_n \tag{11.145}$$

The dispersion rate is defined by $\Delta = N_0/N$.

Example: for uniform excitation a_n = const. = a; $\Delta = 1/a$

We see that the choice of a_n allows the illumination function and the dispersion rate to be chosen at the same time.

Average radiation pattern

The array factor can be written in the form:

$$\tilde{F} = \sum_{n=1}^{N_0} \tilde{a}_n \exp ju_n \tag{11.146}$$

where u_n contains the direction of radiation.

The average radiation pattern is identified with the pattern F_0 of the fully-populated array with a reference illumination function a_n

$$\langle \tilde{F} \rangle = \sum_{n=1}^{N_0} a_n \exp(ju_n) = F_0 \tag{11.147}$$

In general, the function a_n will be symmetric in the cardinal planes of the array, and the function F_0 is in general purely real in the direction of radiation.

Average gain (or average power pattern)

This is obtained by taking the average of the square modulus of $\tilde{F}$

$$\langle |F|^2 \rangle = \sum_n \sum_m \langle \tilde{a}_n \tilde{a}_m \rangle \exp j(u_n - u_m) \tag{11.148}$$

Separating out terms of the same order and of different order, the random variables $\tilde{a}_n$, $\tilde{a}_m$ being independent:

$$\left\langle |F|^2 \right\rangle = \sum_n \left\langle \tilde{a}_n^{\,2} \right\rangle + \sum_{n \neq m} \sum \left\langle \tilde{a}_n \right\rangle \left\langle \tilde{a}_m \right\rangle \exp j(u_n - u_m) \tag{11.149}$$

Taking into account equations (11.142) and (11.143)

$$\left\langle |F|^2 \right\rangle = \sum_n a_n + \sum_{n \neq m} \sum a_n a_m \exp j(u_n - u_m) \tag{11.150}$$

which, by reintroducing the term a_n^2 into the double summation, can also be written

$$\left\langle |F|^2 \right\rangle = \sum_n a_n + \sum \sum a_n a_m \exp j(u_n - u_m) - \sum a_n^2 \tag{11.151}$$

$$\left\langle |F|^2 \right\rangle = \left| \sum_{n=1}^{N_0} a_n \exp j u_n \right|^2 + \sum_1^{N_0} a_n (1 - a_n) \tag{11.152}$$

or

$$\left\langle |F|^2 \right\rangle = F_0^2 + \sum_1^{N_0} a_n (1 - a_n) \tag{11.153}$$

So the average power pattern appears as the superposition of

- the ideal reference pattern F_0^2, which is dominant in the main lobe region and in the close-in sidelobes, and
- an isotropic pattern, which is dominant in the far-out sidelobe region (diffuse sidelobes).

Relative level of diffuse sidelobes

On axis, $u_n = 0$, and $|F_0(0)|^2 = \left| \sum_1^{N_0} a_n \right|^2 = \left(\frac{N_0}{\Delta} \right)^2 = N^2$ (11.154)

The relative average level of the diffuse sidelobes is defined as

$$L_0 = \frac{\left\langle |F|^2 \right\rangle}{|F_0|^2} = \frac{1}{N^2} \sum_1^{N_0} a_n (1 - a_n) \tag{11.155}$$

Example: The illumination function affects the diffuse sidelobes rather less than the dispersion rate Δ.

Consider a constant illumination

$$a_n = \text{const.} = a = \frac{1}{\Delta} = \frac{N}{N_0} \tag{11.156}$$

We find that

$$L_0 = \frac{1-a}{N} = \frac{1-N/N_0}{N} = \frac{1-1/\Delta}{N} \tag{11.157}$$

- If $N = N_0$: no dispersion, no diffuse sidelobes;
- If $N << N_0$: large dispersion, $L \approx 1/N$.

In moving from a dispersion rate of 2 to 4, with the same number of elements, the average sidelobe level is increased by a factor 3/2. This comes from the fact that with a constant gain (N), the main lobe narrows; part of the energy of the main lobe moves into the sidelobes.

Probability function of diffuse sidelobes

We can set $\tilde{F} = F_0 + x + jy$, where x and y are zero-mean Gaussian random variables with the same variance. This gives the result that far from the main lobe, in the diffuse sidelobe region, $\left|\tilde{F}\right|$ follows a Rayleigh function, and $\left(\frac{\left\langle\left|\tilde{F}\right|^2\right\rangle}{F_0^2}\right)$ follows an exponential function, with average value L_0. It is therefore completely defined. The probability that the relative level L exceeds kL_0 is given by

$$\text{Prob}\{L>kL_0\} = \exp(-k) \tag{11.158}$$

11.8.6 Retrodirective and self-phasing arrays[28]

Retrodirective arrays

In some applications there is a requirement to reflect an incident signal back in the direction from which it has come, for example to enhance the radar detectability of a target. It may be desirable to do this over a broad range of angles and over a broad bandwidth, and in some cases it may be desired to impose modulation on the reflected signal.

The reflectivity of such an arrangement is characterized by the radar cross section, σ (§4.3.2), so the signal power P_r received by a radar at a range r is given by the radar equation

$$P_r = \frac{P_t G}{4\pi r^2} . \sigma . \frac{1}{4\pi r^2} . \frac{G\lambda^2}{4\pi} \qquad (11.159)$$

There are several means of realizing a retroreflector. A conducting sphere of radius a much greater than the wavelength will provide an omnidirectional reflection corresponding to its physical cross-sectional area A_e, thus $\sigma = A_e = \pi a^2$. A physically-smaller retroreflector can be achieved by a Luneburg lens (§7.3.5) with a metallic coating on the rear face, which gives a radar cross section $\sigma = 4\pi A_e^2 / \lambda^2$, and the same order of performance is achieved with a dihedral or trihedral corner reflector (§12.4).

Another approach is provided by the Van Atta array[29], which is shown in its basic linear array form in Figure 11.45(a). This may be regarded as the passive array equivalent of the corner reflector. Elements equally displaced from the centre of the array are connected by equal length transmission lines; thus the signal received at each element is reradiated from its counterpart with a phase such that a beam is formed in the direction of the incident signal. The retrodirective array will work over a range of directions determined by the beamwidths of the individual elements, which can in principle cover a broad range of angles. The basic idea can readily be extended to a planar array.

An n-element Van Atta array has a maximum RCS (in the absence of losses) of

$$\sigma = \frac{n^2 G_e^2 \lambda^2}{4\pi} \qquad (11.160)$$

---

[28] Margerum, D.L., 'Self-phased arrays', Chapter 5 in Hansen, R.C. (ed), *Microwave Scanning Antennas*, Vol.III, pp341-407, Academic Press, New York, 1964, (reprinted in a single volume by Peninsula Publishing, Los Altos, USA, 1985).

[29] Van Atta, L.C., Electromagnetic Reflectors, US patent No. 2,908,002, October 6 1959.

where G_e is the gain of an individual element, which will be close to unity to give broad angular coverage. Since the retrodirective beam is formed by delays, the performance is broadband, and in practice is limited by the bandwidth of the elements.

The effective RCS can be increased by including bidirectional amplifiers in each path[30], as shown in Fig. 11.45(b); however, the gain of the amplifiers must not exceed the combined isolation of the circulators (or, indeed, the coupling between corresponding elements) or instability will result. For the same reason, it is important that the elements present a good impedance match. The maximum RCS of the arrangement of Fig. 11.45(b) is

$$\sigma = \frac{n^2 G_e^2 G_a \lambda^2}{4\pi} \tag{11.161}$$

where G_a is the amplifier gain, taking into account the losses of the circulators.

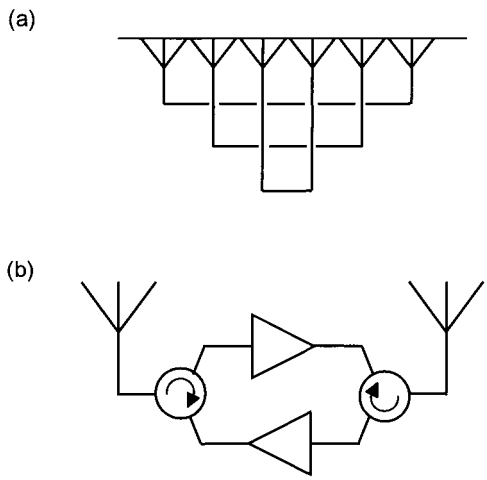

Fig. 11.45 (a) Basic passive form of Van Atta array; (b) the RCS can be increased significantly by using bidirectional amplifiers between pairs of elements.

It can be appreciated that Van Atta arrays are capable of giving very high RCS, particularly in their active form, over a broad range of angles and over a broad bandwidth, from a very compact configuration. It is also possible to modulate or

[30] Davies, D.E.N., 'Some properties of Van Atta arrays and the use of 2-way amplification in the delay paths', *Proc. IEEE*, Vol.110, p507, 1963.

switch the retrodirected signal by including modulators or switches in the signal paths of the arrangement of Fig. 11.45(b).

Self-phasing arrays

In other applications there may be a requirement to receive a signal with an antenna exhibiting gain, over a wide range of directions where the direction is not known *a priori*. This is sometimes known as 'omnidirectional gain'.

This effect can be achieved using a so-called self-phasing array[31]. It is necessary that the signal to be received contains a separate carrier, which may be in the centre of the signal band or at one edge. The basic arrangement is shown in Figure 11.46. At each element of the array the carrier is extracted, by a filter or a phase-locked loop, and used to downconvert the signal to baseband. The signals from all the array elements are then added together.

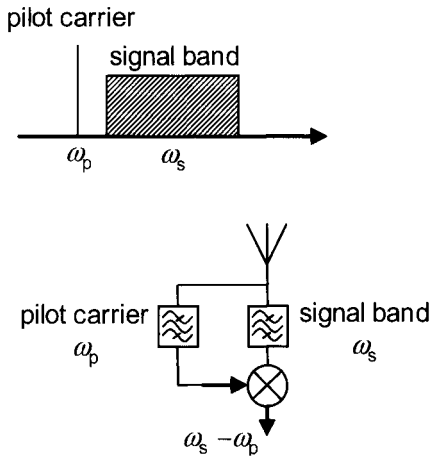

Fig. 11.46 Basic principle of self-phasing array. At each element the pilot carrier is extracted and used to downconvert the signal band.

The bandwidth is limited by the physical size of the array[32]. Considering a linear array of length L, the phases of the output signals at the extreme ends of the array are $(\omega_s - \omega_p)t$ and $(\omega_s - \omega_p)t + \psi_p - \psi_s$, where ψ_p and ψ_s are the phase shifts of the

[31] Cutler, C.C., Kompfner, R. and Tillotson, L.C., 'A self-steering array repeater', *Bell Syst. Tech. J.*, p2013, Sept. 1963.

[32] Brennan, P.V., 'An experimental and theoretical study of self-phased arrays in mobile satellite communications', *IEEE Trans. Antennas & Propagation*, Vol.37, No.11, pp1370-1376, November 1989.

pilot and signal wavefronts due to the difference in path lengths between the elements. If the array is small (or conversely, the overall bandwidth is small), the phase error $\psi_p - \psi_s$ is negligible. More precisely, the phase error is

$$\psi_s - \psi_p = \frac{L(\omega_s - \omega_p)\sin\theta}{c} = \frac{2\pi \sin\theta}{\lambda_{IF}} \tag{11.161}$$

A practical implementation, in which the pilot carrier is extracted by means of a phase-locked loop, and the output is produced at a convenient IF rather than at baseband, is shown in Figure 11.47.

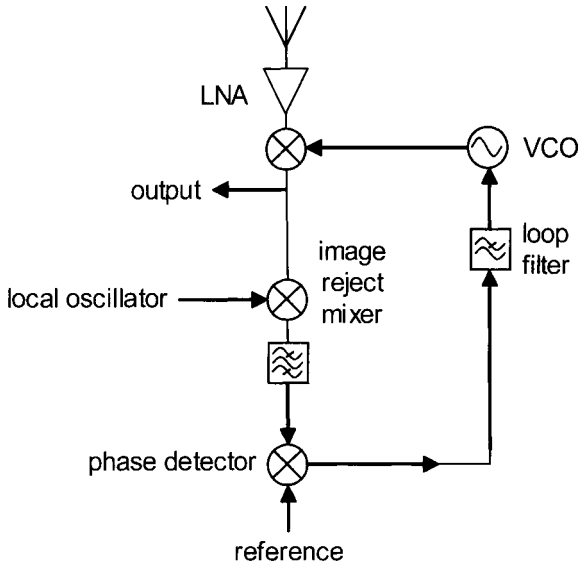

Fig. 11.47 Self-phasing array scheme using a phase-locked loop (after Brennan[32]).

Having extracted the pilot carrier at each element, it is then possible to phase the array on transmit by using the pilot carriers as local oscillators to upconvert the signal to be transmitted. The phases of the pilot carriers contain the phase information to form the transmit beam in the correct direction, without needing to know what that direction is. This may be useful for applications such as terrestrial mobile communications, or communications with satellites in low earth orbit.

Fusco and co-workers at Queen's University Belfast have developed integrated printed antennas with self-phasing receivers to use in these applications, and have

demonstrated an elegant retrodirective duplex communication link based on these principles[33].

Random symmetrical pair arrays

A related scheme is the so-called random symmetrical pair array[34]. The array is formed of pairs of elements, each pair with a random spacing and random orientation.

Fig. 11.48 shows one such pair, of element spacing d and with a signal incident from an angle θ with respect to the normal to the axis of the pair. The signals from the two elements are combined in a hybrid coupler via equal length lines. We assume for the moment that the elements are omnidirectional, and that the signals received at each element are of unit amplitude.

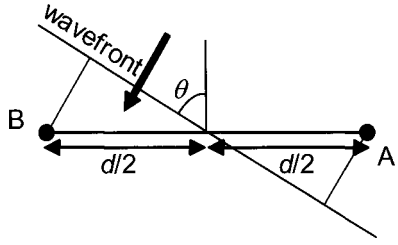

Fig. 11.48 One pair of a random symmetrical pair array.

The wavefront encounters the first element (A) with a phase lead of $\phi = \frac{\pi d}{\lambda}\cos\theta$, and the second element (B) with an equivalent phase lag.

The sum (S) and difference (D) of the two element signals are therefore

$$S = \frac{1}{\sqrt{2}}\left(e^{j\phi} + e^{-j\phi}\right) = \sqrt{2}\cos\phi \qquad D = \frac{1}{\sqrt{2}}\left(e^{j\phi} + e^{-j\phi}\right) = j\sqrt{2}\sin\phi \qquad (11.162)$$

It is evident that, for a signal of a given incidence angle, the sum signals from all such pairs will be purely real and either positive or negative, and the difference signals will be purely imaginary and either positive or negative.

---

[33] Karode, S. and Fusco, V.F., 'Self-tracking duplex communication link using planar retrodirective antennas', *Proc. 1998 Microwave Symposium*, Baltimore, USA, pp977-1000, June 1998.

[34] Benjamin, R., Titze, W.A.U., Brennan, P.V. and Griffiths, H.D., 'Symmetric-pair antennas for beam steering, direction finding or isotropic-reception gain'; *IEE Proc.*, Vol.138, Pt.H, No.4, pp368-374, August 1991.

This suggests a number of applications. Firstly, if the negative sum signals are inverted and all the sum signals added, the result is a beam in the direction of the incident signal. The inversion of polarity, where necessary, could automatically be achieved by squaring the signals, followed by filtering to remove unwanted products. It can be shown that the gain of such a scheme is only 0.91 dB less than that achieved with fully-cophasal addition.

Secondly, the scheme can be used in direction finding: the patterns of the polarities of the signals from each pair can be used to determine the direction of arrival of a signal. The polarities can be measured simply by one-bit phase comparators.

APPENDIX 11A: COMPARISON OF LINEAR AND CIRCULAR ARRAYS

11A.1 Gain of an arbitrary array

Condition for maximum gain

We know that the gain of a linear radiating aperture is maximum when the illumination function is constant, and the same result holds for a planar array. In the case of an *arbitrary* array, what is the condition for maximum gain ?

Consider an array made up of N arbitrary elements oriented in an arbitrary manner, and whose phase centres are located at the points A_n ($n = 0, 1, 2, \ldots N-1$)[35].

We suppose that their characteristic radiation functions $f_n(\mathbf{u})$, which we assume are real, are normalized such that their individual gains are

$$g_n(\mathbf{u}) = \left| f_n(\mathbf{u}) \right|^2$$

Each element is fed with a complex amplitude a_n, normalized in such a way that the feedpoint powers are

$$W_n = \left| a_n \right|^2$$

We can therefore write

$$a_n = \sqrt{W_n} \exp(j\varphi_n)$$

where φ_n are the feedpoint phases.

The total power is the sum of the individual feedpoint powers

$$W = \sum_{n=0}^{N-1} W_n$$

If O is taken as a reference point, the field radiated by the array is the sum

---

[35] If the elements do not possess a defined phase centre, the points A_n are just reference points and $f_n(\mathbf{u})$ are complex. However, the same conclusions hold.

$$F_R(\mathbf{u}) = \sum_{n=0}^{N-1} \sqrt{W_n} \exp(j\varphi_n) f_n(\mathbf{u}) \exp(-jk\mathbf{OA}_n.\mathbf{u})$$

A single omnidirectional element (of unity gain) fed with the total power W gives, under the same conditions, a field

$$F_0(\mathbf{u}) = \sqrt{W}$$

The gain is therefore

$$G_R(\mathbf{u}) = \left| \frac{F_R(\mathbf{u})}{F_0(\mathbf{u})} \right|^2$$

which can be written in the form

$$G_R(\mathbf{u}) = \frac{\left| \sum_{n=0}^{N-1} \left(\sqrt{W_n} \exp(j\varphi_n) \right) \left(f_n(\mathbf{u}) \exp(-jk\mathbf{OA}_n.\mathbf{u}) \right) \right|^2}{\sum_{n=0}^{N-1} \left| \sqrt{W_n} \exp(j\varphi_n) \right|^2 \sum_{n=0}^{N-1} \left| f_n(\mathbf{u}) \exp(-jk\mathbf{OA}_n.\mathbf{u}) \right|^2} \sum_{n=0}^{N-1} \left| f_n(\mathbf{u}) \right|^2$$

Making use of Schwartz's inequality, the gain is maximum if

$$\sqrt{W_n} \exp(j\varphi_n) = A f_n(\mathbf{u}) \exp(-jk\mathbf{OA}_n.\mathbf{u})$$

where A is an arbitrary scalar. We therefore have

(1) $\varphi_n = -k\mathbf{OA}_n.\mathbf{u}$

(2) $W_n = B g_n(\mathbf{u})$ (where B is an arbitrary positive scalar)

In this case the gain is maximum, and of value

$$G_R(\mathbf{u})_{\max} = \sum_{0}^{N-1} g_n(\mathbf{u})$$

Conclusion

THEOREM: *If the feedpoint powers are proportional to the gains of the individual elements in the direction considered, the total gain is maximum and equal to the sum of the individual gains.*

It can be verified that if the elements are identical and oriented in the same direction, the illumination should be uniform and the resulting gain is N times the gain of an individual element. However, for an arbitrary array it is necessary to adjust both the phase *and the amplitude*. This problem can be solved by using *phase mode excitation* (§11.8.3)

Remark: Direct adjustment of the amplitude is difficult in the case of a passive array, since it results in losses. On the other hand, with an array composed of active modules this can be done without losses, by controlling each amplifier, at the same time as adjusting the phase.

11A.2 Gain of a beam cophasal circular array

It can be shown that the gain of an arbitrary circular array does not depend on the *directivity* of the elements, nor the array diameter, but only on the number N of elements and their directivity in the plane perpendicular to the array.

Suppose we have a circular array of diameter $D = 2R$, consisting of N elements with phase centres A_n (with polar coordinates R, α_n) spaced regularly around the circumference of the array. Thus

$$\alpha_n = n\Delta\alpha \quad \text{with} \quad \Delta\alpha = 2\pi/N$$

In an arbitrary direction θ in the plane of the array, the gain of an element is of the form

$$g_n(\theta) = g(\alpha_n - \theta)$$

The maximum resulting gain of the array is therefore

$$G_{\max} = \sum_{n=0}^{N-1} g(\alpha_n - \theta) = N\frac{1}{2\pi}\sum_{0}^{N-1} g(\alpha_n - \theta)\Delta\alpha$$

If the element spacing is small, the summation can be replaced by an integral in terms of the average of the gains in the plane of the array

$$G_{\max} = N\overline{g_n}$$

with

$$\overline{g_n} = \frac{1}{2\pi}\int_0^{2\pi} g_n(\alpha)\, d\alpha$$

This average, which is independent of n, only depends on the element directivity in the plane perpendicular to the array (equation (7.3)).

11A.3 Radiation pattern of a beam cophasal circular array

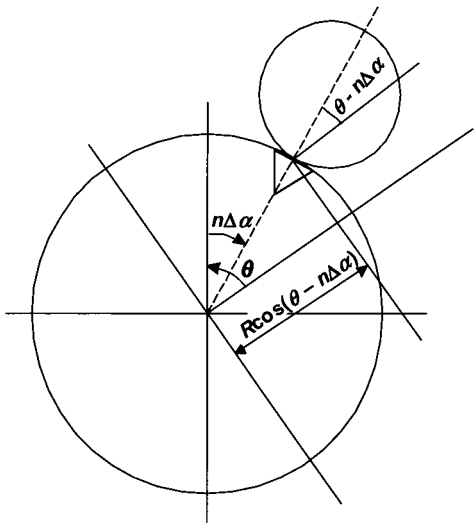

Fig. 11.49 Geometry of circular array.

Let $u_n = a_n \exp(j\varphi_n)$ be the illumination function of an antenna element of phase centre A_n, oriented radially outwards. Its characteristic function, with respect to this point, is real and of the form

$$f_n(\theta) = f(\theta - n\Delta\alpha) \qquad \text{with} \quad \Delta\alpha = d/R$$

The total field in the far field in direction θ is the sum

$$F(\theta) = \sum_{n=0}^{N-1} u_n f(\theta - n\Delta\alpha) \exp\left[jkR\cos(\theta - n\Delta\alpha) \right]$$

If we wish to point a beam in a direction θ_0, for example, $\theta_0 = 0$, we choose the feedpoint phases

$$\varphi_n = -kR\cos n\Delta\alpha$$

We have

$$F(\theta)=\sum_{0}^{N-1}a_n f(\theta-n\Delta\alpha)\exp\left\{jkR\left[\cos(\theta-n\Delta\alpha)-\cos n\Delta\alpha\right]\right\}$$

Condition for maximum gain

For this, the excitation amplitude a_n should be proportional to the amplitude of the element pattern in the desired direction θ_0, i.e.

$$a_n = f(-n\Delta\alpha)$$

We have therefore

$$F(\theta)=\sum_{0}^{N-1}f(\theta-n\Delta\alpha)\,f(-n\Delta\alpha)\exp\left[2jkR\sin\left(\frac{\theta}{2}\right)\sin\left(\frac{\theta}{2}-n\Delta\alpha\right)\right]$$

Array with a large number N of elements

In this case we can replace the above summation by an integral. Setting $\alpha=-n\Delta\alpha$, we have

$$F(\theta)=\int_{0}^{2\pi}f(\alpha+\theta)\,f(\alpha)\exp\left[2jkR\sin\left(\frac{\theta}{2}\right)\sin\left(\frac{\theta}{2}+\alpha\right)\right]d\alpha$$

11A.4 Example: $\cos\alpha$ element patterns

Consider the case of a directional element pattern of the form $f(\alpha)=\cos\alpha$. Setting

$$\beta=\frac{\theta}{2}+\alpha$$

We can separate the radiation pattern into two parts

$$F(\theta)=\int_{0}^{2\pi}\cos^2\beta\exp(jz\sin\beta)\,d\beta\;-\;\int_{0}^{2\pi}\sin^2\beta\exp(-jz\sin\beta)\,d\beta$$

where $z=2kR\sin\left(\frac{\theta}{2}\right)$

This gives explicitly

$$\frac{F(\theta)}{F(0)} = \Lambda_1(z) - \sin^2\left(\frac{\theta}{2}\right) J_0(z)$$

Close to the axis the first term is dominant:

$$\frac{F(\theta)}{F(0)} \cong \Lambda_1(z) = \frac{2J_1(2kR\sin\theta/2)}{2kR\sin\theta/2}$$

The Λ_1 function is plotted in Fig. 9.14.

Note that:

- the 3 dB beamwidth $\theta_{3\text{dB}} \cong \frac{\lambda}{2R} = \frac{\lambda}{D}$;
- level of first sidelobe $L_1 = 0.13$, which is approximately −17 dB.

Further out, it is the second term which dominates. This is a consequence of radiation from the outermost elements, which point away from the axis.

Example: For $\theta = \pi/2$ the following relative levels L_2 are obtained:

- For $D/\lambda = 5$ $L_2 = 0.07$, i.e. approximately −23 dB
- For $D/\lambda = 30$ $L_2 = 0.03$, i.e. approximately −31 dB

11A.5 Comparison of linear and circular arrays

In beam-cophasal circular arrays, the *phase* of the excitation follows a sinusoidal function which is relatively complicated, and the amplitude has to be varied. However, this allows a pointing direction θ_0 which is independent of frequency, depending only on the symmetry of the excitation function with respect to the direction θ_0. This is not the case with linear arrays (§11.3.2, equation (11.19)). The −3 dB beamwidth of a circular array is independent of the pointing direction, but depends slightly on frequency (in a quadratic manner). This is the opposite of the case with linear arrays, where the −3 dB beamwidth does depend on the pointing direction (equation (11.22)), but very little on frequency.

Circular arrays do not suffer from localized grating lobes, such as can occur with linear arrays. They also do not suffer from the blindness phenomenon (§11.4.3). All these advantages should be taken into consideration when making tradeoffs.

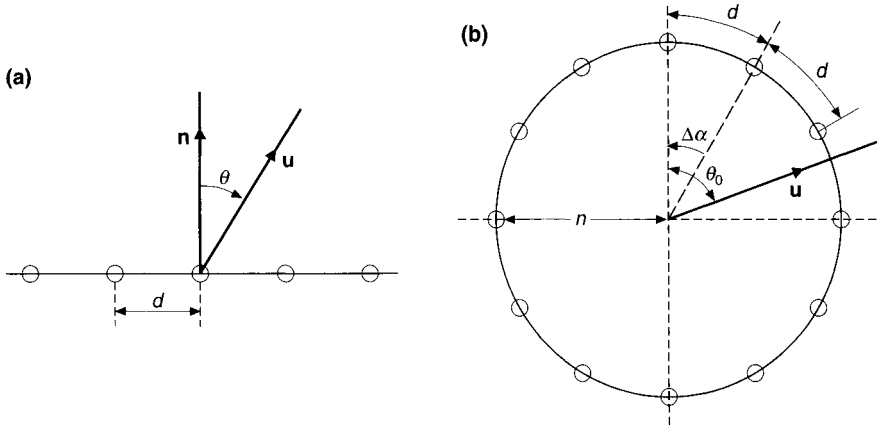

Fig. 11.50 (a) Linear array, and (b) circular array geometry.

FURTHER READING

1. Amitay, N., Galindo, V. and Wu, C.P., *Theory and Analysis of Phased Array Antennas*, Wiley-Interscience, London, 1972.
2. Barton, P., 'Digital beam forming for radar', *Proc. IEE*, Vol. 127, Pt. F, No. 4, pp266-277, August 1980.
3. Benjamin, R. and Seeds, A.J., 'Optical beam forming techniques for phased array antennas', *IEE Proc.*, Vol. 139, Pt. H, No. 6, pp526-534, December 1992.
4. Borgiotti, G., 'Conformal arrays', Chapter 11 in *The Handbook of Antenna Design*, Vol.II, A.W. Rudge, K. Milne, A.D. Olver and P. Knight (eds), Peter Peregrinus, Stevenage, 1983.
5. Brookner, E., 'Phased-array radars', *Scientific American*, pp94-102, February 1985.
6. Cohen, E.D., 'Trends in the development of MMICs and packages for active electronically scanned arrays (AESA)', 1996 IEEE International Symposium on Phased-Array Systems and Technology, Boston, MA, pp1-4, October 1996.
7. Davies, D.E.N., 'Circular arrays', Chapter 12 in *The Handbook of Antenna Design*, Vol.II, A.W. Rudge, K. Milne, A.D. Olver and P. Knight (eds), Peter Peregrinus, Stevenage, 1983.
8. Hansen, R.C. (ed), *Microwave Scanning Antennas*, Vols I-III, Academic Press, New York, 1964, (reprinted in a single volume by Peninsula Publishing, Los Altos, USA, 1985).
9. Mailloux, R., 'Phased array theory and technology', *Proc. IEEE*, Vol. 70, No. 3, March 1982.
10. Mailloux, R., *Phased Array Antenna Handbook* (second edition), Artech House, 2005.
11. Rebeiz, G.M., *RF MEMS: Theory, Design and Technology*, Wiley, 2003.
12. Schelkunoff, S.A., 'A mathematical theory of linear arrays', *Bell System Technical Journal*, Vol. 22, pp80-107, 1943.
13. Shenoy, R.P., 'Phased array antennas - Part 3: active aperture arrays', in *Advanced Radar Techniques and Systems*, G. Galati (ed), Peter Peregrinus, Stevenage, 1993.
14. Steinberg, B.D., *Principles of Aperture and Array Systems Design*, Wiley-Interscience, London, 1976.
15. Steyskal, H., 'Digital beamforming antennas: an introduction', *Microwave Journal*, pp107-124, January 1987.
16. Tsunoda, Y. and Goto, N., 'Sidelobe suppression of planar array antennas by the multistage decision method', *IEEE Trans. Antennas & Propagation*, September 1987.

EXERCISES

11.1 Design of an electronically-scanned array antenna

It is required to define the geometric and electric parameters of a planar array with the following external characteristics.

- wavelength: $\lambda = 10$ cm
- scan angle: in azimuth ±45° either side of the normal to the array
  in elevation –5°, +55° with respect to the horizon
- sidelobes: close-in $L < -23$ dB
  far-out (quantization lobes) - consider two cases $L < -43$ dB
  $L < -49$ dB
- maximum on-axis gain: 37 dB
  taking into account ohmic losses K_1 of the phase shifters
  diode phase shifters 1.3 dB
  ferrite phase shifters 0.7 dB
  taking into account the loss K_2 due to the illumination taper
  taking into account the quantization loss K_3 of the phase shifters
  $p = 2$ bits
  $p = 3$ bits
- 3 dB elevation beamwidth θ_s equal to half the azimuth beamwidth θ_g:
  $\theta_s = \theta_g/2$

The goal of the exercise is to define the internal characteristics of the antenna, starting from the external characteristics stated above.

Q1 After a first-cut estimate of the illumination and quantization losses K_2 and K_3 (for example, $K_1 + K_2 + K_3 = 3$ dB), evaluate the area of the antenna, the horizontal and vertical dimensions H and V, the horizontal and vertical element spacing a_H and a_V (suppose that the array is inclined so as to equalize the phase shifts in elevation), and the number of elements N. Hence deduce the beamwidths θ_s and θ_g.

Q2 Evaluate the number of bits for the phase shifters, in order to meet the specification for the average far-out sidelobes. Evaluate the corresponding losses K_3, for the cases $p = 2$ and $p = 3$.

Q3 Evaluate the loss K_2 in gain due to the aperture weighting function, for the two cases:

(a) a cosine weighting (without 'pedestal') both vertically and horizontally;

(b) a cosine weighting both vertically and horizontally, with the largest pedestal compatible with the specified *close-in* sidelobe level (an attenuation at the edge of −12 dB is suitable).

ANSWERS

Q1 *Antenna area*: With $K_1 + K_2 + K_3 = 3$ dB, the required directivity is 40 dB. Thus:

$$\frac{4\pi S}{\lambda^2} = 10^4$$

which gives approximately $S = 8$ m^2.

Dimensions: We have $\theta_s \approx \dfrac{\lambda}{\mathrm{V}}$; $\theta_g \approx \dfrac{\lambda}{\mathrm{H}}$

It follows that $V = 2H$ and $S = VH = 8$
Thus: $H = 2$m, $V = 4$m

Horizontal and vertical element spacing: These result from equation (11.25). In elevation, a tilt of the plane of the array with respect to the vertical of 25° gives a maximum scan angle of ±30°. We therefore choose

$$a_{\mathrm{H}} = \frac{2}{3}\lambda \approx 6.6 \text{ cm} \qquad a_{\mathrm{V}} = \frac{\lambda}{1+\sqrt{2}/2} \approx 5.8 \text{ cm}$$

Number of elements:

$$N = \frac{H.V}{a_{\mathrm{H}} a_{\mathrm{V}}} = 2050$$

Beamwidths:

$$\theta_s \approx \frac{\lambda}{V} \approx 1.43° \qquad \theta_g \approx \frac{\lambda}{H} \approx 2.86°$$

Q2 *Number of bits for phase shifters*: We make use of equation (11.70). Since the number of bits must be an integer, we choose respectively the following values:

L_{max}	$p_{theoretical}$	p_{actual}	L_{actual}
–43 dB	2.5	3	–46 dB
–49 dB	3.5	4	–52 dB

Quantization loss: due to K_3.
Using equation (11.74), for $p = 3$ $K_3 = -0.22$ dB
$p = 4$ $K_3 = -0.055$ dB

Q3 *Loss due to aperture weighting function* K_2: We find (exercise 7.4)

$$K_2 = \left[\frac{1}{1 + \dfrac{A}{(1+\beta)^2}} \right]^2$$

with $A = \dfrac{\pi^2}{8} - 1$, $\beta = \dfrac{\pi}{2} \dfrac{a}{(1-a)}$

With a pedestal of –12 dB:

$a = 0.063$, $\beta = 0.104$, $K_2 \approx 0.70$, i.e –1.52 dB

11.2 Grating lobes produced by use of phased subarrays fed by delay lines

An array of this kind of length L can be considered as an array where the interelement spacing is equal to the length L' of a subarray.

Q1: For uniform illumination law and for a pointing direction θ_0, show that the array factor is of the form

$$R\left(\frac{\sin\theta}{\lambda}\right) = \frac{\sin\left[N\pi \dfrac{L'}{\lambda}(\sin\theta - \sin\theta_0)\right]}{N \sin \pi \dfrac{L'}{\lambda}(\sin\theta - \sin\theta_0)}$$

Obviously, the grating lobes are in the directions $\theta_{R,k}$:

$$\sin\theta_{R,k} - \sin\theta_0 = k\frac{\lambda}{L'}$$

Q2 Show that at a wavelength λ, the radiation function of a *phased* subarray is given by

$$F_{L'}\left(\frac{\sin\theta}{\lambda}\right) = \operatorname{sinc}\pi L'\left(\frac{\sin\theta}{\lambda} - \frac{\sin\theta_0}{\lambda_0}\right)$$

with

$$\operatorname{sinc} x = \frac{\sin x}{x}$$

Q3 With the overall radiation function of the array being given by the product

$$F\left(\frac{\sin\theta}{\lambda}\right) = RF_{L'}$$

show that the relative amplitude level of the grating lobes is given by:

$$M = \sin\theta_0 \frac{L'}{c} df$$

This is independent of the centre frequency; it depends only on the subarray dimension L' and the frequency shift *df*. As a general rule, it is given by the product of the frequency shift and the time required by the signal to traverse one subarray.